

**EXAMINATION OF THE IMPORTANCE OF REACTIVE OXYGEN SPECIES
RELEASE FROM COMPLEX I IN ISCHEMIA-REPERFUSION INJURY**

By: Nidhi Kuksal

A Thesis submitted to the School of Graduate Studies in partial fulfillment of the
requirements for the degree of

Master of Science

**Department of Biochemistry, Faculty of Science
Memorial University of Newfoundland**

October 2018

St. John's, Newfoundland and Labrador

Abstract

Recent work has indicated that respiratory Complex I may be the sole source of reactive oxygen species (ROS) during ischemic-reperfusion (IR) injury. However, evidence collected by several groups, including ours, has demonstrated that Complex III and Krebs cycle enzymes are also high capacity sites for ROS production. Here, the ROS producing capacity of Complex I was examined in hearts subjected to IR injury. Using mice deficient in Complex I (NDUFS4^{+/-}), the respiratory chain was found to be the main source of ROS in cardiac and liver mitochondria. However, Complex III was found to be the major source, producing ~50% of the total ROS, while Complex I accounted for ~30%. Partial deletion of Complex I sensitized hearts towards reperfusion injury, increasing infarct size, which correlated with higher ROS production. Collectively, these results refute the claim that Complex I is the sole source of ROS following IR injury.

Acknowledgements

Hereby, I take this opportunity to humbly express my gratitude to all those concerned with my thesis entitled “**EXAMINATION OF THE IMPORTANCE OF REACTIVE OXYGEN SPECIES RELEASE FROM COMPLEX I IN ISCHEMIA-REPERFUSION INJURY**”. I would like to share the success of my project with the people who have directly and indirectly helped me out to complete this project.

I would foremost like to thank my supervisor, Dr. Ryan Mailloux, for his valuable guidance and continuous support for my project. I am highly grateful to him for providing me his valuable suggestions and remarks to complete this project. I would also like to thank my co-supervisor Dr. Dake Qi and my committee members (Dr. Mark D. Berry and Dr. Sukhinder Kaur Cheema) for their motivation and support. I would also like to thank the QEII Diamond Jubilee Scholarship program for supporting my research.

I would also like to thank the lab members of the Mailloux lab group for their help with this project. Thank you to Danielle Gardiner, Julia Chalker and Adrian Young

Last but not the least, I would like to thank my family for their unconditional love for me and friends for their continuous support.

Table of Contents

Abstract.....	II
Acknowledgements	III
Table of Contents	IV
List of Tables	VII
List of Figures.....	VIII
List of Abbreviations	X
1. Introduction.....	1
1.1 Nutrient metabolism	1
1.1.1 Glycolysis.....	1
1.1.2 Beta-Oxidation.....	5
1.1.3 Citric acid cycle.....	5
1.1.4 Electron transport chain.....	11
1.2 Regulation of reactive oxygen species.....	17
1.2.1 Antioxidant defence systems.....	19
1.2.2 Proton leak.....	20
1.2.3 Supercomplexes.....	22
1.3 NDUFS4 subunit.....	24
1.4 Cardiac anatomy and physiology	27
1.4.1 Pumping of blood from the heart.....	27
1.4.2 Pacemaker regions of the heart	28
1.5 Ischemia reperfusion injury to the myocardium.....	30
1.5.1 ROS production during ischemic-reperfusion injury of the heart.....	32

1.5.2	Problems with the Chouchani model for IR injury to the myocardium	32
1.6	Research objectives.....	38
1.7	Hypothesis.....	38
2.	Materials and Methods.....	39
2.1	Breeding and maintaining mice.....	39
2.2	Mouse genotyping.....	40
2.2.1	DNA isolation.....	40
2.2.2	Polymerase chain reaction (PCR)	40
2.2.3	Polyacrylamide gel electrophoresis	43
2.3	Isolating the mitochondria.....	43
2.3.1	Bradford assay for protein estimation.....	45
2.4	Amplex Ultra Red (AUR) assay.....	47
2.4.1	Measuring rate of $O_2^{\cdot-}/H_2O_2$ production during PDH and 2-OGDH oxidation...	49
2.4.2	Measuring rate of $O_2^{\cdot-}/H_2O_2$ production during succinate oxidation	52
2.4.3	Measuring rate of $O_2^{\cdot-}/H_2O_2$ production during RET from NADH	52
2.4.4	Immunoblot.....	53
2.5	Isolated heart perfusions.....	56
2.5.1	Measurement of mitochondrial NAD(P)H levels following IR injury.....	63
2.6	Data analysis.....	65
3.	Results.....	66
3.1	Mouse genotyping and immunoblotting for NDUFS4.....	66
3.2	Impact of NDUFS4 deficiency on organ and the body weight	69
3.3	Examination of the $O_2^{\cdot-}/H_2O_2$ release potential of NDUFS4 deficient mitochondria.....	73
3.4	Identification of the high capacity sites for $O_2^{\cdot-}/H_2O_2$ in liver and heart	

mitochondria.....	76
3.5 O₂^{•-}/H₂O₂ production by cardiac tissue supplemented with succinate	80
3.6 Assessment of the induction of electrophilic cell signaling pathway	82
3.7 Examination of the effect of IR injury on NDUFS4 deficient mice	84
3.7.1 Impact of NDUFS4 deficiency on contractile recovery from reperfusion injury.....	84
3.7.2 Partial loss of Complex I augments ROS release from NDUFS4 ^{+/-} mitochondria following reperfusion injury.....	87
3.8 Utilization of Complex I knockout mitochondria to assess NADH-driven ROS release by OGDH and PDH.....	90
4. Discussion.....	93
4.1 Summary.....	93
4.2 Complex I is not the sole source of ROS source during myocardial reperfusion injury.....	94
4.3 Can Complex I protect from ischemia-reperfusion injury?.	97
4.4 Impact of the deletion of the <i>Ndufs4</i> gene on mouse and cell physiology	98
4.5 OGDH and PDH as a source of ROS in liver mitochondria.....	101
4.6 Reverse electron transfer from NADH to OGDH and PDH	103
4.7 Conclusions	105
4.8 Future Directions.....	105
5. References	107

List of tables

Table 1.1-The targets of S-glutathionylation	26
Table 2.1-DNA Sequence of primers used for NDUFS4 genotyping.....	41
Table 2.2-Polymerase Chain Reaction (PCR) protocol for NDUFS4 genotyping.....	42
Table 2.3-Detailed recipe of the immunoblot gel	57
Table 2.4-Dilution factor for the antibodies.....	58
Table 2.5-Detailed recipe of the TTC stain.....	62

List of Figures

Figure 1.1-The glycolytic pathway	4
Figure 1.2-The Citric acid cycle.....	9
Figure 1.3-The pyruvate dehydrogenase complex	10
Figure 1.4-The electron transport chain	15
Figure 1.5-The mechanism of IR injury.....	34
Figure 1.6-Sources of ROS in the ETC.....	37
Figure 2.1-Bradford assay standard curve for determination of protein concentration....	46
Figure 2.2-AUR assay standard curve determination of O ₂ ^{•-} /H ₂ O ₂ concentration.....	48
Figure 2.3-Sites of action for the different inhibitors used in the AUR assays	51
Figure 2.4-The Langendorff assembly.....	61
Figure 2.5-NADH standard curve for measuring NAD(P)H levels after IR injury	64
Figure 3.1-Identification of mice heterozygous or homozygous for the <i>Ndufs4</i> gene by PCR and agarose gel electrophoresis.....	67
Figure 3.2-Confirmation of partial or full ablation of NDUF54 protein expression	68
Figure 3.3-Body weight profile for WT and NDUF54 ^{+/-} mice.....	70
Figure 3.4-Cardiac weight profile for WT and NDUF54 ^{+/-} mice.....	71
Figure 3.5-Liver weight profile for WT and NDUF54 ^{+/-} mice.....	72
Figure 3.6-Partial loss of the <i>Ndufs4</i> gene does not alter O ₂ ^{•-} /H ₂ O ₂ release from liver mitochondria	74
Figure 3.7-Partial loss of the <i>Ndufs4</i> gene does not alter O ₂ ^{•-} /H ₂ O ₂ release from cardiac mitochondria	75

Figure 3.8-Assessment of which enzymes serve as high velocity ROS producers in liver mitochondria	78
Figure 3.9-The electron transport is the major source for ROS release in cardiac mitochondria	79
Figure 3.10-Complex III is the major ROS source in cardiac mitochondria	81
Figure 3.11-Parial deletion of the <i>Nudfs4</i> gene increases GPX1 and TRX2 levels... ..	83
Figure 3.12-Comparison of the contractile status between the genotypes	85
Figure 3.13-Comparison of the infarct size in WT and NDUFS4+/- hearts following an IR challenge	86
Figure 3.14-Assessment of the $O_2^{\bullet-}H_2O_2$ production between the genotypes in IR challenged cardiac tissues	88
Figure 3.15-Comparison of the NADH driven ROS production between the genotypes..	89
Figure 3.16-Assessment of $O_2^{\bullet-}H_2O_2$ production in mitochondria supplemented with NADH.....	92

List of Abbreviations

4-HNE	4-Hydroxynonenal
A form	Active form
ADP	Adenosine diphosphate
Ag	Silver
ANOVA	Analysis of variance
ANT	Adenine nucleotide transporter
ATP	Adenosine triphosphate
AUR	Amplex Ultra Red
AV	Atrioventricular node
BCKDHC	Branched chain amino acid dehydrogenase
BCKDH	Branched chain keto acid dehydrogenase
bp	Base pairs
BSA	Bovine serum albumin
CoA	Coenzyme A
CoQ	Coenzyme Q/Ubiquinone
CPT1	Carnitine Palmitoyl transferase 1
CPI-613	6,8-Bis(benzylsulfanyl) oclanoic acid
CuSOD	Copper superoxide dismutase
Cys	Cysteine
Cys P	Peroxidative cysteine
Cys R	Resolving cysteine
Cyt c	Cytochrome c
D form	Deactivate form
DH	Dehydrogenase
DHODH	Dihydrooroate dehydrogenase complex
DNA	Deoxyribonucleic acid
DTT	Dithiothreitol
ETC	Electron transport chain
ETFQO	Electron transfer flavoprotein – ubiquinone oxidoreductase
FAD	Flavin adenine nucleotide
FADH2	Reduced flavin adenine nucleotide
FCCP	Carbonylcyanide- <i>p</i> -trifluoromethoxyphenyl hydrazone
Fe-S	Iron sulfur cluster
FMN	Flavin mononucleotide
g	Grams
GDP	Guanine diphosphate

GPx	Glutathione peroxidase
GPx 1	Glutathione peroxidase 1
GPx 4	Glutathione peroxidase 4
GR	Glutathione reductase
GRX	Glutaredoxin
GRX1	Glutaredoxin-1
GRX2	Glutaredoxin-2
GRX-SS	Glutaredoxin with an intra-disulfide bond
GRX-SSG	Glutaredoxin with bound glutathione
GSH	Glutathione
GSSG	Glutathione disulfide
GST	Glutathione-S-transferase
GTP	Guanine triphosphate
G3PDH	Sn-glycerol-3-phosphate dehydrogenase
H ⁺	Proton
HCl	Hydrochloric acid
H ₂ O	Water
H ₂ O ₂	Hydrogen peroxide
HRP	Horse radish peroxidase
I/R	Ischemia reperfusion
k	Rate of catalysis
KCl	Potassium chloride
KDa	Kilodalton
KJ	Kilojoules
KMV	α -keto- β -methyl-n-valeric acid
LSD	Least significant difference
LVDP	Left ventricular developed pressure
M	Molar
mg	Milligram
min	Minute
mL	Millilitre
mM	Millimolar
MnSOD	Manganese superoxide dismutase
mol	Mole
MPTP	Mitochondrial permeability transition pore
N	Number
NaCl	Sodium chloride
NAD ⁺	Nicotinamide adenine dinucleotide
NADH	Reduced nicotinamide adenine dinucleotide
NADPH	Nicotinamide adenine dinucleotide phosphate
NDUFS4	NADH:Ubiquinone Oxidoreductase, Subunit S4 of mitochondrial Complex I.
NDUFS4+/-	NDUFS4 heterozygous
NDUFS4-/-	NDUFS4 knockout

NaN ₃	Sodium azide
NH ₄ ⁺	Ammonium ion
nm	Nanometer
nM	Nanomolar
Nrf2	Nuclear factor (erythroid-derived 2)-like 2
O ₂	Molecular oxygen
O ₂ ⁻	Superoxide
OADC	2-Oxoadipate dehydrogenase complex
OGDH/OGDHC	2-Oxoglutarate dehydrogenase complex
OH [•]	Hydroxyl radical
P	Phosphate
PCR	Polymerase chain reaction
PDH/PDHC	Pyruvate dehydrogenase complex
pH	Potential of hydrogen
PFK1	Phosphofructokinase 1
pM	Picomolar
PMF	Proton motor force
PRX	Peroxiredoxin
PRODH	Proline dehydrogenase
PSSG	Protein glutathione mixed disulfide
PVDF	Polyvinylidene difluoride
RET	Reverse electron transport
RISP	Rieske iron sulfur protein
ROS	Reactive oxygen species
SDH	Succinate dehydrogenase
SDHA	Succinate dehydrogenase subunit A
SDS	Sodium dodecyl sulfate
SEM	Standard error of mean
SOD	Superoxide dismutase
SOH	Sulfenic acid
SO ₂ H	Sulfinic acid
SO ₃ H	Sulfonic acid
SQR	Sulfide:quinone oxidoreductase
TBE	Tris-borate EDTA
TBS	Tris-buffered saline
TBS-T	Tris-buffered saline + tween-20
TEMED	Tetramethylethylenediamine
TPP	Thiamine pyrophosphate
TR	Thioredoxin reductase
TRX	Thioredoxin
Tyr	Tyrosine
UCP	Uncoupling protein
UQ	Ubiquinone
UQH [•]	Semi ubiquinone radical

UQH ₂	Ubiquinol
V	Volts
v/v	Volume per volume
WT	Wildtype
w/v	Weight per volume
ZnSOD	Zinc superoxide dismutase
° C	Degrees Celsius
μ g	Micrograms
μ L	Microliters
μ M	Micromolar

1. Introduction

1.1 Nutrient Metabolism

Nutrient metabolism is defined as the breakdown or biosynthesis of carbon containing molecules through various pathways to maintain cell function(s). These molecules are either degraded or produced by catabolic and anabolic pathways, respectively (1). Catabolism refers to the breakdown of organic materials for the production of ATP, the universal energy currency required to fulfill most, if not all, cellular and physiological functions (2). Anabolic reactions, on the other hand, divert organic materials from central catabolic cascades towards “cell building” pathways (*e.g.* lipogenesis or the production of nucleotides). These pathways are also vital for the provision of NADPH, a reducing equivalent that serves as the “bed rock” of antioxidant defenses and production of the building blocks of the mammalian cell (2). Carbohydrates, amino acids, and fatty acids derived from dietary sources are the main drivers of nutrient metabolism. These molecules are metabolized by distinct metabolic pathways that yield common intermediates that converge on the Krebs cycle which is the most central metabolic pathway. Upon entry into the Krebs cycle, carbon units are systematically oxidized, and the electrons released from this metabolic cascade are used to drive ATP biosynthesis via a process called oxidative phosphorylation. Krebs cycle intermediates can also be diverted to support other metabolic pathways including the biosynthesis of amino acids, heme groups, small molecule hormones, lipids, and nucleotides (2).

1.1.1 Glycolysis

After food is ingested, carbohydrates are broken down into their constituent monosaccharides (*e.g.* glucose, fructose, and galactose), absorbed by the gut, and then released

into circulation for distribution around the body (2). These monosaccharides are then taken up by cells and used to generate 2 ATP and 2 pyruvate by glycolysis (Figure 1.1). The first five steps of glycolysis are defined as the “*preparatory phase*”, which includes the breakdown of glucose into two three carbon groups, a process that requires ATP. Glucose is first activated through its phosphorylation on the carbon-6 position by hexokinase (EC 2.7.1.1) in the presence of ATP and Mg^{2+} , forming glucose-6-phosphate (1,2). In the liver, this reaction is catalyzed by glucokinase (EC 2.7.1.2), a hexokinase isoenzyme that displays unique catalytic properties that prevent its allosteric deactivation by glucose-6-phosphate, a critical characteristic that is vital for glucose clearance after a meal (3,2). In the next step, phosphohexose isomerase (EC 2.7.1.11) converts glucose-6-phosphate to fructose-6-phosphate (4,2). Phosphofructokinase-1 (PFK-1) (EC 2.7.1.11) phosphorylates fructose-6-phosphate on the C-1 position producing fructose-1,6-bisphosphate (5,2). Aldolase (EC 4.1.2.13) then cleaves fructose-1,6-bisphosphate into dihydroxyacetone phosphate and glyceraldehyde-3-phosphate (2). Triose phosphate isomerase (EC 5.3.1.1) is required to convert dihydroxyacetone phosphate into glyceraldehyde-3-phosphate (2).

The other half of the glycolysis pathway is defined as the “*payoff phase*” since the triose phosphates yielded in the preparatory phase are used to make ATP by substrate level phosphorylation. First, glyceraldehyde-3-phosphate is oxidized and phosphorylated by glyceraldehyde-3-phosphate dehydrogenase (EC 1.2.1.12) in the presence of NAD^+ and inorganic phosphate forming NADH and 1,3-bisphosphoglycerate (6). The phosphate on the one position is used to form ATP, a reaction catalyzed by phosphoglycerate kinase (7). Phosphoglyceromutase (EC 5.3.1.1) then transfers the phosphate from the carbon-3 position to the second carbon and enolase forms the high energy intermediate phosphoenolpyruvate (2). The

last step also involves the substrate level phosphorylation of ADP, by pyruvate kinase (EC 2.7.1.40), producing pyruvate in the process. When mammalian cells are deprived of oxygen, pyruvate is reduced by lactate dehydrogenase (EC 1.1.1.27) in the presence of NADH to replenish NAD^+ for glycolysis (8). When oxygen is available, however, pyruvate is oxidized further by the Krebs cycle in mitochondria (9).

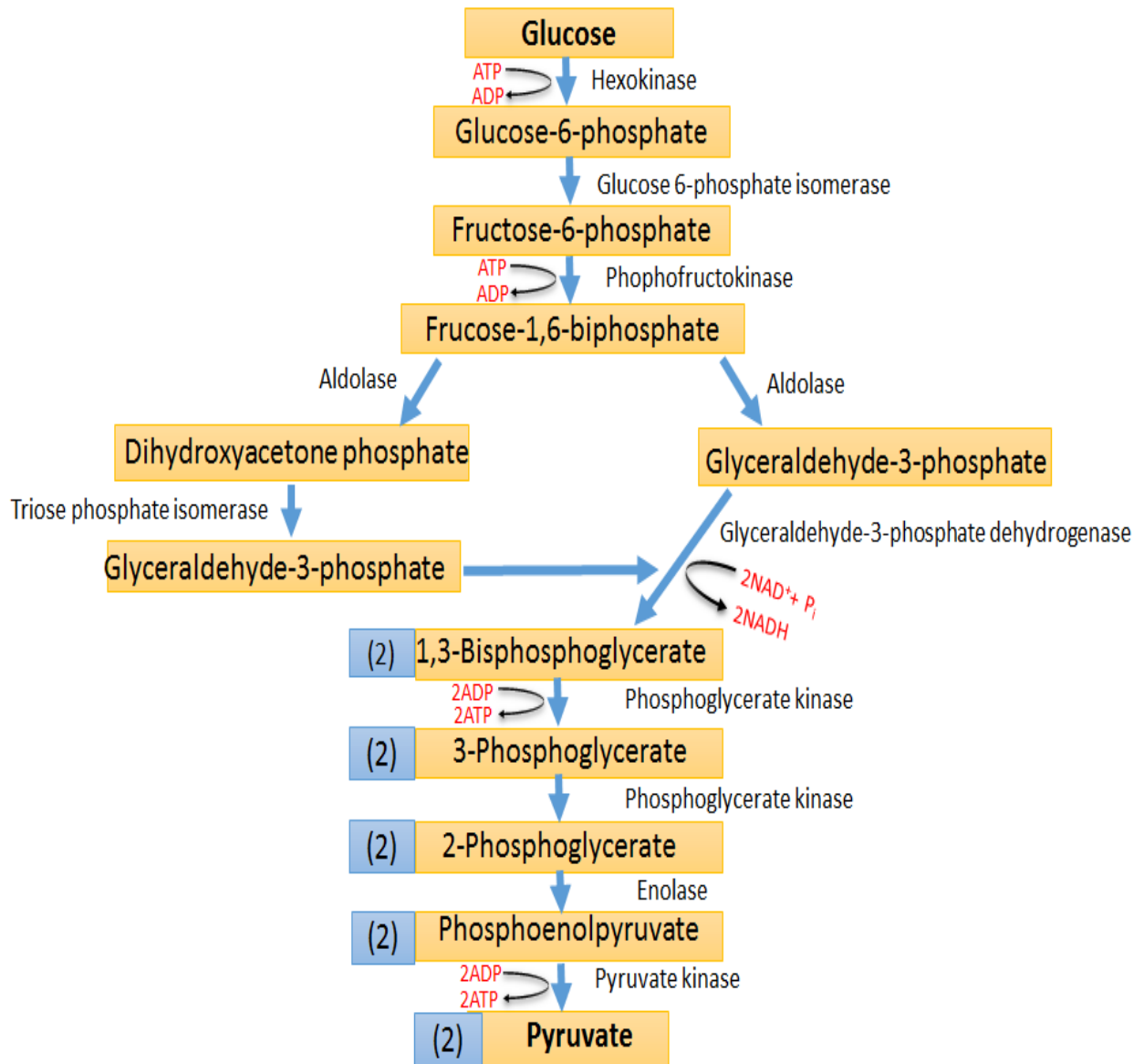


Figure 1.1-The glycolytic pathway

This pathway demonstrates the breakdown of glucose into pyruvate.

1.1.2 *Beta-Oxidation*

Fatty acids constitute an important source of energy, particularly during starvation. In addition, organs like the heart rely heavily on fatty acid oxidation to meet ATP demands. It has been estimated that heart tissue can turn over ~30 kg of ATP a day and ~70-90% of this energy is supplied by the beta-oxidation of fatty acids in mitochondria (10). Beta-oxidation takes place in the matrix of mitochondria and thus fatty acid metabolism relies on the import of fatty acids into the matrix environment. To do so, the CoASH group in fatty acyl-CoA is first replaced with carnitine in the intermembrane space environment by carnitine palmitoyl transferase-1 (CPT-1) (EC 2.3.1.21), which facilitates the entry of fatty acids into the mitochondrial matrix (11). Once the fatty acids enter the matrix, CPT-2 (EC 2.3.1.21), a CPT-1 isozyme, exchanges carnitine for CoASH and β -oxidation is initiated. First, acyl-CoA dehydrogenase (EC 1.3.8.1) oxidizes acyl-CoA forming an enoyl-CoA, which contains an unsaturated region between the alpha and beta carbon. Hydrides yielded from the oxidation are used to reduce FAD to FADH₂ and then these electrons are transferred to the ubiquinone (UQ) pool in the mitochondrial inner membrane (12). The unsaturated region is then hydrated and β -hydroxyacyl-CoA dehydrogenase (EC 1.1.1.35) oxidizes β -hydroxyacyl-CoA producing NADH and β -ketoacyl-CoA. In the last step, the β -ketoacyl-CoA is metabolized by thiolase (EC 2.3.1.16) to facilitate the formation of acetyl-CoA and a fatty acid chain shortened by two carbons (2). Oxidation of fatty acids continues until it is completely broken down to its constituent acetyl-CoA molecules (13). Acetyl-CoA produced from β -oxidation then enters the Krebs cycle where it is broken down further.

1.1.3 *Citric acid cycle*

A complete overview of the Krebs cycle is given in Figure 1.2. Pyruvate yielded from glycolysis or amino acid degradation must first be imported to the mitochondrial matrix by the

symporter pyruvate translocase (also referred to as pyruvate carrier or monocarboxylate transporter), and then converted to acetyl-CoA by the pyruvate dehydrogenase (PDH) (EC 1.2.4.1) complex. Thus, PDH is the important entry point for carbohydrates. PDH is composed of three subunits: 1) the E1 subunit (pyruvate decarboxylase) (EC 6.4.1.1), which decarboxylates pyruvate in the presence of thiamine pyrophosphate (TPP), 2) the E2 subunit (dihydrolipoyl transacetylase), which transfers the acetyl group on TPP to a lipoamide residue. The E2 subunit then catalyzes the transfer of the acetyl group to CoASH forming acetyl-CoA and reduced dihydrolipoamide, and 3) The E3 subunit (dihydrolipoyl dehydrogenase) oxidizes dihydrolipoamide reducing FAD. The hydrides on FADH₂ are then transferred to NAD⁺ producing NADH (15). Figure 1.3 gives a detailed description of the catalytic mechanism for PDH.

Since PDH is the entry point for carbohydrates into the Krebs cycle, it is also an important site for the regulation of metabolism. High ATP/ADP and NADH/NAD⁺ ratios, acetyl-CoA and long chain fatty acids allosterically inhibit PDH (15). Pyruvate dehydrogenase kinase and pyruvate dehydrogenase phosphorylase also play a key role in controlling PDH activity through phosphorylation of the E1 subunit (15). PDH is also regulated by redox signals through reversible oxidation of its E2 subunit by protein S-glutathionylation (10). Pyruvate is also metabolized by pyruvate carboxylase (EC6.4.1.1), which is required to prime the Krebs cycle through the formation of oxaloacetate. Once formed, oxaloacetate condenses with acetyl-CoA and forms citrate through a Claisen condensation reaction, a reaction catalyzed by citrate synthase. Citrate is then isomerized through a *cis*-aconitate intermediate by aconitase forming isocitrate. Next, the first irreversible step of the Krebs cycle is catalyzed by isocitrate dehydrogenase (EC 1.1.1.42) which couples the decarboxylation of isocitrate to the reduction of

NAD⁺. Notably, mitochondria also contain an isozyme for isocitrate dehydrogenase that couples isocitrate oxidation to the production of NADPH, a key moiety required for antioxidant defense and lipogenesis in the matrix. The 2-oxoglutarate generated by isocitrate dehydrogenase is oxidized by 2-oxoglutarate dehydrogenase (OGDH) (EC 1.2.4.2). This is the second irreversible step of the Krebs cycle since 2-oxoglutarate oxidation is coupled to the evolution of CO₂ and formation of NADH. Amino acids can enter the Krebs cycle at the level of 2-oxoglutarate in the Krebs cycle via glutamate metabolism (16). The oxidation of 2-oxoglutarate by OGDH yields succinyl-CoA. OGDH and PDH are homologous in structure and thus have a similar mechanism for forming NADH. The E1 subunit for OGDH also relies on TPP for the decarboxylation of 2-oxoglutarate and is thus called 2-oxoglutarate decarboxylase (17). The E2 subunit is referred to as dihydrolipoyl-succinyltransferase (EC 2.3.1.61) which produces succinyl-CoA (18). The dihydrolipoyl dehydrogenase (EC 1.8.1.4) subunit for OGDH is interchangeable with the E3 subunit of PDH (18). Like PDH, OGDH also plays an important role in the regulation of the Krebs cycle. High ratios of ATP/ADP, NADH/NAD⁺ inhibit the complex. Moreover, high amounts of succinyl-CoA are also responsible for an allosteric inhibition (2). OGDH is also tightly regulated by reversible oxidation of its vicinal thiols on dihydrolipoamide and is also controlled through the S-glutathionylation of the E1 and E2 subunits (10).

After its formation, succinyl-CoA is converted to succinate by succinyl-CoA synthetase (EC 6.2.1.4), which couples the hydrolysis of the thioester bond between CoASH and succinate to the production of ATP (adenosine 5'-triphosphate) or GTP (guanosine 5'-triphosphate) (19). In the next step, succinate dehydrogenase (EC 1.3.5.1), which is a membrane bound enzyme, facilitates the production of fumarate and FADH₂ from succinate. This enzyme is also referred to as Complex II and is considered to be part of the electron transport chain since it couples the

oxidation of succinate directly to the reduction of UQ (ubiquinone) to UQH₂ (ubiquinol) in the electron transport chain (ETC). Fumarase (EC 4.2.1.2) then hydrates fumarate producing malate which is oxidized by malate dehydrogenase (EC 1.1.1.41) forming NADH and oxaloacetate. For every molecule of acetyl-CoA which enters the Krebs cycle, 2 CO₂, 3 NADH, 1 FADH₂ and 1 GTP/ATP molecule are produced (20). The CO₂ formed by carbon oxidation is either converted to carbonic acid by carbonic anhydrase (EC 4.2.1.1) or exhaled from the body. NADH and FADH₂ produced by the Krebs cycle are used to drive oxidative phosphorylation by the electron transport chain.

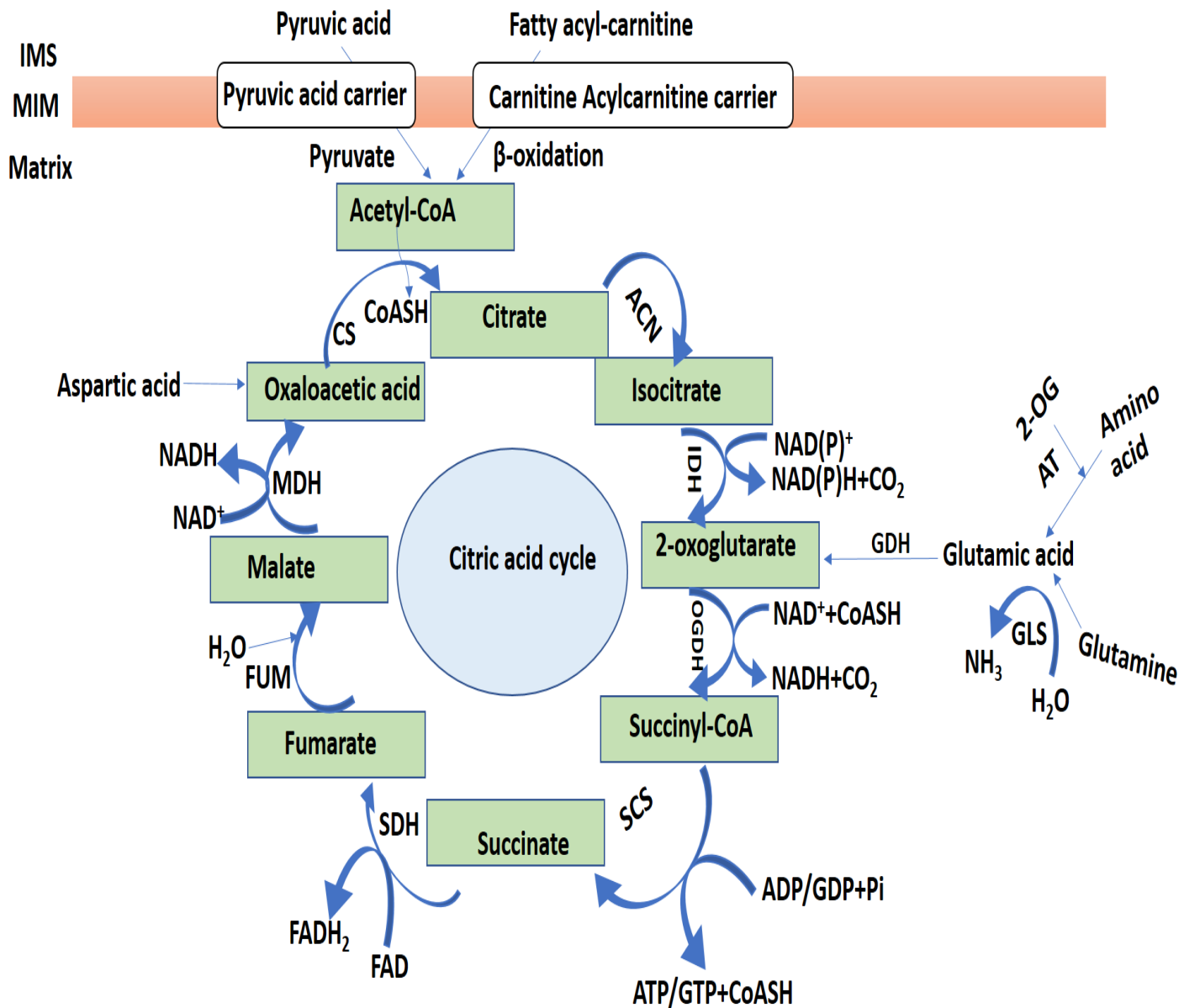


Figure 1.2-The Citric acid cycle

This diagram gives the detailed description of the various steps involved in the Krebs cycle.

ACN (Aconitase), IDH (Isocitrate dehydrogenase), GLS (Glutamine synthetase), AT (Aminotransferase), GDH (Glutamate dehydrogenase), OGDH (2-oxoglutarate dehydrogenase), SCS (Succinyl-CoA synthetase), SDH (Succinate dehydrogenase), FUM (Fumarase), MDH (Malate dehydrogenase), CS (Citrate synthase).

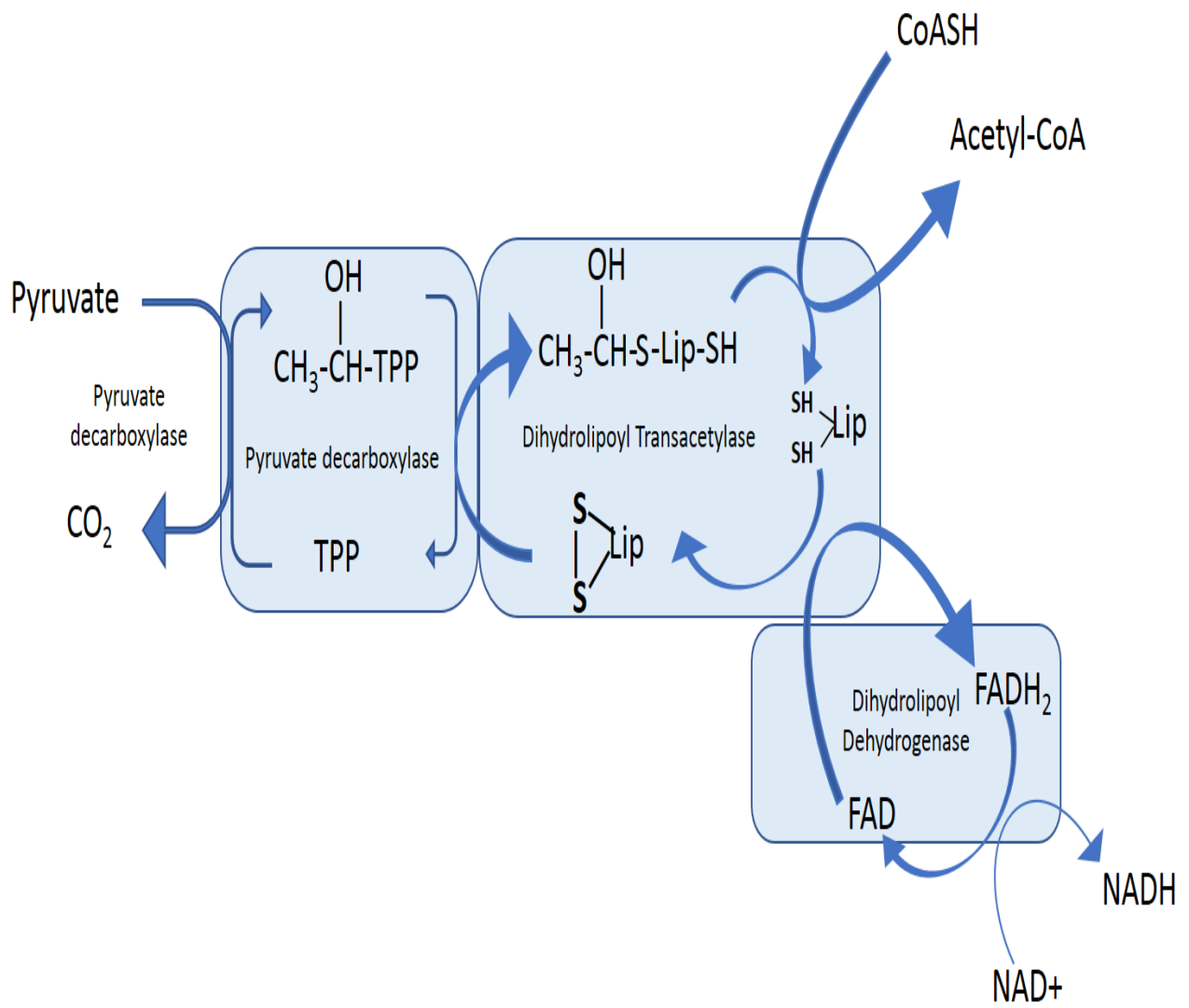


Figure 1.3-Pyruvate dehydrogenase complex

1.1.4 *Electron transport chain*

Mitochondria are double membraned organelles that fulfill many functions in mammalian cells. These organelles play integral roles in calcium buffering and the induction of apoptosis. However, these other roles are often overshadowed by its most important function, the provision of cellular ATP. Mitochondrial ATP production is carried out by the ETC, sometimes just referred to as the respiratory chain, which couples the movement of electrons to the phosphorylation of ADP. Electrons from NADH and FADH₂ travel through respiratory Complexes I-IV to the terminal electron acceptor O₂ at the end of the chain. Energy released from the favorable “downhill” transfer of these electrons is used by Complex V to make ATP. Once formed, ATP is exported into the cytosol to perform useful work. Mitochondria make up ~30-40% of the volume of a cardiomyocyte and are thus vital for heart physiology and function. For example, ATP produced by mitochondria in cardiomyocytes is utilized to maintain the ion gradients and drive the motor proteins required for the pumping of oxygenated blood around the body (10). Mitochondria supply ~90% of the ATP for heart function which is derived from many carbon sources including ketone bodies, lactate, and glucose. However, the main source of ATP in cardiomyocytes is fatty acids, which account for ~70-90% of the ATP formed by heart mitochondria. Figure 1.4 below gives the description of the ETC chain.

The first step of oxidative phosphorylation involves the oxidation of NADH and succinate by Complex I. Complex I (NADH: ubiquinone oxidoreductase) consists of 45 subunits, 7 iron-sulfur (Fe-S) clusters and a flavin mononucleotide (FMN), making it the largest complex in the ETC (19). It is worthy to point out that only 12-13 of these subunits, some of which are encoded by the mitochondrial genome, are required to drive the catalytic activity of Complex I. The other 33 subunits, like NDUF54, are required for the assembly of Complex I, maintenance

of its native conformation, and the formation of supercomplexes. When fully assembled, Complex I takes on an “L” shaped conformation comprised of three separate modules. The N-module makes contact with the matrix environment and couples the oxidation of NADH to the reduction of FMN, which then passes electrons through the 7 Fe-S clusters. The Q-module serves as the interface between the N and P-modules and contains the UQ binding pocket. The reduction of UQ and release of UQH₂ is coupled to the pumping of protons into the intermembrane space by the P-module. Note that the P-module forms the hydrophobic part of Complex I and is thus responsible for the insertion of the respiratory complex into the mitochondrial inner membrane (20). Complex I is an important site for regulation of respiration. It can adopt activated (A-form) and deactivated (D-form) conformations in response to changes in the availability of NADH (21). Complex I activity is also modulated by a variety of redox signals like S-glutathionylation and the assembly/disassembly of supercomplexes (10).

The second complex of the ETC is Complex II (succinate-coenzyme Q reductase or succinate dehydrogenase). This ~120 kDa complex is made up of four subunits designated subunits A – D (22, 23). Subunits A and B are in contact with the matrix. Meanwhile, subunit C, as well as D, are required for partial insertion in the mitochondrial inner membrane. Note that unlike Complexes I, III, and IV, succinate dehydrogenase does not span the inner membrane and is thus not involved proton export. In addition, in contrast to the other complexes, the Gibbs free energy change for succinate oxidation and UQ reduction is ~0 kJ/mol. Therefore, not enough energy is released from Complex II to warrant a conformational change for proton export. The binding sites for succinate and bound FAD are enclosed in subunit A. Succinate from the Krebs cycle binds to Complex II where it gets oxidized to fumarate releasing 2 electrons. These electrons are then transferred to the FAD unit of Complex II, generating FADH₂ (24). Complex

II also contains 3 Fe-S clusters which are required to transfer electrons from FADH₂ to the UQ binding site. During high rates of succinate oxidation, electrons are cycled between a Fe-S cluster and a heme group of subunit C to prevent overflow and electron leaks (24).

Complex III (ubiquinol: cytochrome *c* oxidoreductase) is comprised of 11 subunits and couples the oxidation of UQH₂ to the reduction of cytochrome *c*. (25). The Rieske iron-sulfur protein (RISP) and cytochrome *c*₁ are the two main subunits involved in the passage of electrons to cytochrome *c*. Notably, cytochrome *c* is hydrophilic and found in the interspace where it binds to the outer leaflet of the inner membrane through electrostatic interactions with Complex III. Like Complexes I and II, the Fe-S clusters in RISP and cytochrome *c*₁ can only accept one electron at a time. Therefore, UQH₂ is initially incompletely oxidized to a semi-ubiquinone radical (UQH[•]). This can be dangerous since UQH[•] can form reactive oxygen species (ROS) and loss of these electrons will also diminish ATP output making oxidative phosphorylation inefficient. To deal with this issue, Complex III recycles the second lone electron in UQH[•] through the Q-cycle. This requires two heme groups (cytochrome *b*_L and *b*_H) (26). First, UQH₂ and UQ bind to the Q_O site and the Q_i site of Complex III respectively. The Q_O site is positioned near the outer leaflet of the inner membrane close to RISP, whereas the Q_i is positioned closer to the matrix. Oxidation of UQH₂ in the Q_O site results in the transfer of one electron to RISP while the transfer of the second electron to Q_i is facilitated by cytochrome *b*_L and *b*_H. For complete reduction of ubisemiquinone in Q_i, a second UQH₂ is oxidized in the Q_O site and the second electron is passed to the Q_i binding site. Unlike Complex I and IV, Complex III is not a pump but rather uses a Mitchellian redox loop to move protons into the intermembrane space. In addition, the Gibbs free energy change for electron flow is not as high as Complex I and IV. Therefore, only 2 protons are shuttled out of the matrix instead of four.

Complex IV is composed of 14 subunits, but only three subunits are thought to participate in the transfer of electrons to molecular oxygen (27). These three subunits are: subunit I, subunit II, subunit III (1). Subunit I includes a copper ion (Cu_3) and two heme groups (a and a_3) which combine to form the a_3 : Cu_3 binuclear center (28). When two cytochrome c molecules are reduced, they bind to subunit II. These electrons are then transferred to heme a via the Cu_A center. While heme transports these electrons to the a_3 : Cu_3 center of Complex IV, O_2 binds to the heme groups and is completely reduced to water. In the course of this entire process four protons are released to the intermembrane space (29). The transport of two electrons and the release of four protons from this complex leads to the formation of two H_2O molecules at the end.

The “downhill” movement of electrons from NADH or succinate to O_2 at the end of the chain is thermodynamically favourable and is responsible for the production of the electrochemical gradient of protons across the inner membrane. This proton gradient is produced by Complex I, III and IV and the electrochemical difference in protons across the mitochondrial inner membrane is called the membrane potential or “proton motive force” (PMF) (30). The proton motive force is composed of electrical ($\Delta\Psi_M$) and chemical (ΔpH) components with the former making up ~90% of the overall “force” of

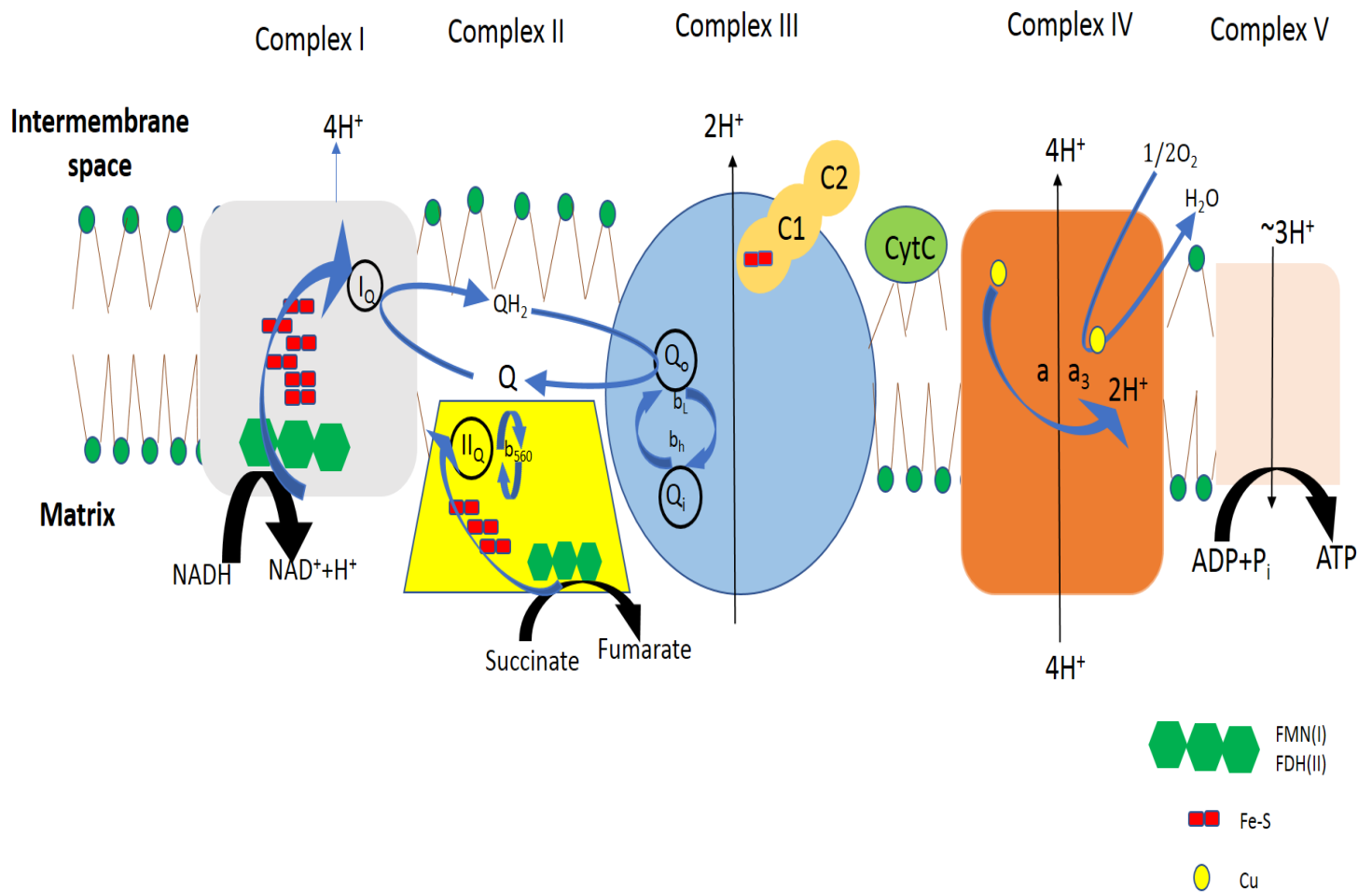


Figure 1.4-The electron transport chain

Transport of electrons from NADH and succinate through the complexes to O₂ at the end of the chain. The protons released into the intermembrane space during the process leads to ATP production.

the gradient. Oxidation of NADH and succinate results in the pumping of 10 and 6 protons into the intermembrane space, respectively.

The overall strength of the proton gradient depends on the rate of proton extrusion and return to the matrix. This invariably depends on the rate of ADP phosphorylation by Complex V and the rate of electron flow to Complex IV. Other factors can be used to enhance proton return to the matrix. The leak of protons by chemical uncouplers or uncoupling proteins, for example, can dissipate the proton gradient. Protons are also used for the transport of solutes or import of proteins into the matrix. Protons can also be return through complexes I and III during reverse electron flow (31). However, a hyperpolarized mitochondrial inner membrane is required to drive reverse flow. Overall, the potential across the mitochondrial inner membrane is ~150-180 mV. When normalized to the diameter of mitochondrial inner membrane, the total force experienced by a mitochondrion is $\sim 300,000 \text{ V cm}^{-1}$ (assuming the inner membrane is 5-7 nm thick) (31).

Complex V (also referred to as ATP synthase) uses the Gibbs free energy stored in the proton gradient to generate chemical energy in the form of ATP. There are two main functional domains in ATP synthase: 1) F_0 domain: found in the inner mitochondrial membrane and is comprised of the channel that facilitates the downhill transport of the protons and 2) F_1 domain: this domain includes the catalytic active sites and is located peripherally to the inner membrane of the matrix (32). The F_1 domain is made up of five subunits: α , β , γ , δ , and ϵ (32). The γ shaft which is coupled to one of the β subunits, is thereby encircled by three α and β subunits. There are three β subunits which have the similar composition but differ in conformation and this difference is likely caused due to their association with the γ subunit. These β subunits can be found in three separate conformations which are directly associated with the binding of ADP and

P_i and the subsequent formation of a γ -phosphodiester bond: 1) β -ADP- which binds to the ADP, 2) β -ATP-which contains the newly formed ATP and 3) β -empty-which does not include any substrates (33). The transport of the protons from the F_o domain triggers the 120° rotation of the γ subunit which is critical for 1) the binding of the next β subunit, 2) causing a change in their conformation. This rotation of the F_1 is referred to as rotational catalysis. Initially a β subunit occurs in the β -ADP conformation state which changes to β -ATP form, when ADP and P_i bind to the β -ADP site (33). This β -ATP form is beneficial to confine the substrates together and hence facilitate phosphorylation. After ATP is generated, the conformation changes to the β -empty state and ATP is liberated. (33). If one β -subunit occurs in the β -ADP form, the other two are found to be in their β -ATP and the β -empty state. The three β subunits rotate through all three conformations, catalyzing the formation of three ATP molecules for one full rotational round of the γ subunits. These ATP molecules thus generated are used in various cellular processes.

1.2 Regulation of reactive oxygen species levels

Reactive oxygen species (ROS) are produced via the incomplete reduction of molecular oxygen. Due to its unique chemical features, O_2 can only accept one electron at a time. Therefore, during the reduction of O_2 to H_2O , several oxygen-containing free radical intermediates are formed, namely, superoxide ($O_2^{\bullet-}$), hydrogen peroxide (H_2O_2), and hydroxyl radical (OH^{\bullet}) (34). Although there are a number of ROS sources in physiology, mitochondria are the main site for production in most mammalian cells. This is due to the high concentration of flavin groups and UQ, which can donate one electron to O_2 generating ROS (34). The proximal ROS formed by mitochondria was once considered to be $O_2^{\bullet-}$ (35). However, it is now accepted that mitochondria directly form a mixture of $O_2^{\bullet-}$ or H_2O_2 , which is dependent on flavin radical

chemistry (35). It has been estimated that 0.02-2% of the total amount of oxygen consumed by mitochondria forms ROS (36, 37). ROS have a bi-functional relationship with mammalian cells where they are required to control various cell programs through signaling at low doses, whereas in excess amounts they can overwhelm antioxidant systems and cause oxidative distress. Use of ROS in signaling has recently been defined as *oxidative eustress* whereas *oxidative distress* occurs when levels are too high, overwhelming antioxidant defenses (42). Oxidative distress is typically associated with ROS accumulation and oxidative damage, which correlates strongly with the development of cardiovascular, inflammatory, and degenerative diseases (38). In cardiac tissue, the over production of ROS is associated with development of a myocardial infarction, ischemia-reperfusion injury, left ventricular hypertrophy, reperfusion arrhythmias, heart failure and fibrosis (38). Superoxide can induce oxidative distress through the rapid disassembly of Fe-S clusters necessary for mitochondrial metabolism (39). Hydrogen peroxide, on the other hand, can induce oxidative damage by irreversibly oxidizing cysteine thiols in low molecular weight molecules and proteins (40). Several essential redox-active metals like Fe and Cu can react with ROS to give rise to OH^\bullet via Fenton and Haber-Weiss reactions. Several nucleotides, lipids, and amino acids are targets for oxidation by OH^\bullet leading to DNA damage, protein and lipid oxidation, and inducing cell death (41).

By contrast, low grade ROS production is required for cell signaling, also called *oxidative eustress*. For instance, low grade ROS production in cardiac tissue has been shown to enhance contractile efficiency, bolster cell stress responses, and protect from reperfusion damage (41). Hydrogen peroxide is the main ROS secondary signaling molecule and regulates protein function through the site specific and reversible oxidation of “*cysteine switches*”. Notably, these switches serve as sensors for overall changes in the cell redox environment and are required for the

induction of stress signaling pathways like Nrf2 activation, T-cell activation (43), adipocyte differentiation (44) and steroidogenesis (45). Hydrogen peroxide is an important secondary messenger and like any other signaling molecule its overall abundance is regulated through its production and degradation. The mitochondria utilize H_2O_2 routinely in cell communication and thus it uses several systems to control its rate of production and overall concentration. Antioxidant systems are required for the degradation of H_2O_2 signals. Mitochondria are enriched with H_2O_2 removing enzymes (45). Production on the other hand, is controlled by regulating electron entry and exit from sites of formation. Electron availability for production is controlled through proton leaks, supercomplex assemblies, and redox signals.

1.2.1 Antioxidant defence systems

Mitochondrial and cellular $\text{O}_2^{\bullet-}$ levels are generally maintained in the picomolar range by the rapid action of superoxide dismutase (SOD), which converts two $\text{O}_2^{\bullet-}$ into one H_2O_2 and one H_2O at a rate of $2.3 \times 10^9 \text{ M}^{-1} \text{ s}^{-1}$ (48). In mitochondria, this reaction is catalyzed by manganese-dependent SOD (SOD2) in the matrix and the Cu/Zn-dependent isozyme (SOD1) in the intermembrane space (48). Once formed H_2O_2 can be degraded by several different enzyme systems. The main H_2O_2 quenching systems in mitochondria are glutathione (GSH) and the thioredoxin (TRX) systems (47). However, catalase can also remove H_2O_2 in the matrix of mitochondria in liver and cardiac cells (46).

Mitochondria do not synthesize GSH and are thus reliant on its uptake from the cytosol (50). The concentration of GSH in the matrix is $\sim 5 \text{ mM}$ (49). Removal of H_2O_2 by the glutathione system is catalyzed by glutathione peroxidase-1 (GPX1) in the matrix of mitochondria. GPX1 removes H_2O_2 by forming a disulfide bridge between two GSH molecules, forming oxidized glutathione (GSSG), also called glutathione disulfide (51, 52, 53). The

concentration of GSSG in the matrix of mitochondria is ~0.01-1 mM due to the action of glutathione reductase (GR), which rapidly reduces GSSG in the presence of NADPH to reform GSH. Mitochondria also contain a second glutathione peroxidase isoform called GPX4 and it couples the degradation of lipid hydroperoxides, an intermediate in lipid peroxidation, to the oxidation of GSH. It is important to note that the GSH/GSSG ratio does display rapid changes in oxidation which is utilized to convey redox signals (53). Oxidation of glutathione pools is accompanied by the protein S-glutathionylation of protein cysteine thiols and serves as an important regulatory device for mitochondrial function (discussed below).

The thioredoxin (TRX) system is the second major H_2O_2 degradation pathway in mitochondria and relies on the catalytic activity of peroxiredoxin (PRX) (54). Mitochondria contain two PRX isozymes, PRX3 and PRX5. PRX3 displays a catalytic preference for the elimination of H_2O_2 whereas PRX5 reacts mostly with lipid hydroperoxides. All PRX enzymes are homodimers that contain two catalytic cysteine thiols on each monomer called the peroxidatic cysteine (Cys_P) and resolving cysteine (Cys_R) (54). Each monomer is also organized in a head-to-tail orientation. First, Cys_P reacts with H_2O_2 forming a sulfenic acid residue (SOH). Next, the SOH is resolved by Cys_R on the neighboring monomer forming a disulfide bridge. Disulfide bridge formation between the monomers deactivates the catalytic activity of PRX3 and PRX5. Reactivation requires reduction by TRX2 (thioredoxin-2) through a disulfide bond exchange reaction. Oxidized TRX2 is then reactivated by thioredoxin reductase-2 (TR2) and NADPH.

1.2.2 Proton leak

The role of proton leaks in quenching $O_2^{\bullet-}/H_2O_2$ production is well documented but also happens to be one of the most contentious issues in the field of mitochondrial bioenergetics.

Proton leak is a physiological process where protons are returned to the matrix of the mitochondria by-passing ATP synthesis (55). Physiological leaks were first found to contribute to non-shivering thermogenesis in brown fat, where the Gibbs free energy released from the leak of protons back into the matrix generates heat to maintain body temperature (55, 56). However, proton leaks in other tissues, like the heart and muscle, have been found to also regulate ROS production. There are two types of leak mechanisms that allow proton reuptake by mitochondria; basal leak and inducible leak. Basal leak involves the unregulated import of protons into the matrix by adenine nucleotide translocase (ANT) (56). Inducible leaks on the other hand represent a regulated form of mitochondrial proton return by uncoupling proteins (UCP) 1-3 (56, 57). ROS production is highly sensitive to the changes in proton leak. Indeed, small increases in the proton motive force correlates with a non-Ohmic increase in mitochondrial ROS release (63). This is associated with the over-reduction of the respiratory chain, increasing the number of electrons available for ROS production. Therefore, proton return can reduce protonic back pressure on the respiratory chain, augmenting electron flow and lowering ROS production.

Overproduction of ROS by the mitochondria and oxidative distress is associated with the loss of UCP2 or UCP3 (58). The end products of lipid peroxidation, 4-hydroxynonenal (4-HNE) and $O_2^{\bullet-}$ have been found to induce proton leak by UCPs (58). Activation of leaks by $O_2^{\bullet-}$ or 4-HNE was suggested to serve as a negative feedback loop for the regulation of ROS release by augmenting leaks (59). UCP1-3 have been found to control ROS release in response to an increase in protonic back pressure in various tissues including heart, skeletal muscle, pancreas, brain, and brown fat (60,61). Overexpression of both UCP2 and UCP3 leads to decreased ROS production while their inhibition has the opposite effect (62).

1.2.3 Supercomplexes

The criteria that dictate electron entry and exit from sites of ROS release include substrate supply and type, access to O₂, and the redox state and concentration of the electron donating site. Thus, factors that can augment electron flow to O₂ at the end of the chain can diminish ROS release by limiting the over reduction of electron donating centers. The individual complexes of the respiratory chain have been found to interact with one another and form what are called “*respirasomes*”. These supercomplexes, which are comprised of Complexes I, III, and IV, UQ, and cytochrome *c*, and sometimes Complex V, have been found to be vital for assuring efficient respiration and electron flow. Assembly of these complexes is also important for controlling ROS release. Indeed, by assembling into a supercomplex, efficient electron flow from Complex I and IV can be assured, limiting the number of electrons that can contribute to ROS production. This is highlighted by studies that have found that supercomplex disassembly, or defects in respirasome formation, correlates strongly with heart disease and neurological disorders (64). The increase in ROS release due to disassembly is thought to occur through the accumulation of electrons in Complex I, but recent work has also found that this also occurs at Complex III (64).

Protein S-glutathionylation is defined as the addition and removal of a glutathione moiety to a protein cysteine thiol residue (65). These reactions are sensitive to changes in the surrounding redox environment through fluctuations in the availability of GSH and GSSG, which is affected by the levels of H₂O₂ and NADPH (65). Unlike other redox modifications, S-glutathionylation reactions are rapid, reversible, and highly specific, since they are mediated by specialized enzymes that sense changes in GSH and GSSG (66). Mitochondria are a hot spot for S-glutathionylation, containing protein targets involved in energy metabolism, ROS release,

mitochondrial shape, and solute import (Table 1.1). In mitochondria, S-glutathionylation reactions are facilitated by the thiol oxidoreductase glutaredoxin-2 (GRX2). GRX2 serves as a GSH /GSSG sensor that S-glutathionylates or deglutathionylates target proteins in response to fluctuations in the matrix redox environment. An increase in GSSG results in GRX2-driven S-glutathionylation of protein targets in mitochondria, whereas restoration of the reductive potential of the glutathione pool has the opposite effect. Recent work by our group, and others, have demonstrated that this reaction mechanism is integral for the negative regulation of ROS release in liver tissue (63,65,66). S-glutathionylation of PDH and OGDH was found to limit ROS release from either enzyme complex which is reversed by GRX2 (66). However, S-glutathionylation has the opposite effect in cardiac mitochondria. Over S-glutathionylation of these complexes for instance has been found to augment ROS production and increase sensitivity to heart disease (66). Loss of GRX2 is associated with left ventricular hypertrophy and recent work has established that variations in GRX2 nucleotide sequence correlates strongly with development of heart disease in humans (66). Therefore, controlled S-glutathionylation through GRX2 is vital for regulating ROS release from mitochondria.

Even though S-glutathionylation could be mediated enzymatically, oxidizing conditions could lead to the spontaneous S-glutathionylation of proteins (67). Oxidative distress could result in higher concentrations of GSSG inducing the non-enzymatic S-glutathionylation of a cysteine through a simple disulfide exchange reaction. These reactions are often associated with oxidative damage and the disabling of protein function due to nonspecific protein S-glutathionylation. However, in some instances, spontaneous protein S-glutathionylation has been shown to protect enzymes from oxidative damage. For instance, Complex I and OGDH have been found to be protected from irreversible oxidative damage by H₂O₂ through the S-glutathionylation of reactive

cysteines required for their enzymatic activity (67). By blocking the thiol residue, H₂O₂ (when at high cellular concentrations) cannot irreversibly form sulfinic and sulfonic acids (67). One more mechanism of spontaneous S-glutathionylation occurs when the protein cysteine thiol residues reacts with GSH to give rise to a thiol radical glutathionyl intermediate, which then gets oxidized to produce protein glutathione mixed disulfide (PSSG) (68). Several enzymes like succinate dehydrogenase exhibited persisted S-glutathionylation under physiological conditions (68). The susceptible nature of proteins and the formation of GSSG possessing microenvironments by the proteins can lead to changes in the criteria which promote S-glutathionylation (68). In addition to oxidative stress S-glutathionylation also plays a major role in energy metabolism. Several processes like mitochondrial shape, protein import, proton leakage and apoptosis have also been found to make use of S-glutathionylation (68).

1.3 NDUFS4 subunit

Complex I is the first component of ETC and is made up of 45 subunits (154,105). One of these subunits includes NDUFS4 (NADH dehydrogenase [ubiquinone] iron-sulfur protein 4 or NADH-ubiquinone oxidoreductase) which is encoded by the *Ndufs4* gene (154,105). NDUFS4 protein occurs in the matrix of the inner mitochondrial membrane of the mitochondria (154,105). Thus, it helps in removal and electrons from NADH and facilitates the transport of these electrons to ubiquinone (154,105). Mutation in this gene leads to several genotypical and phenotypical disorders (105). In our experiments we completely knocked out the NDUFS4 protein which is a subunit of Complex I to form NDUFS4^{-/-} mice. These mice developed severe fatal encephalomyopathy and heart disease by 5-6 weeks of age, which is associated with deficiencies in linear growth (105). Also, these mice homozygous for the *Ndufs4* gene develop alopecia, blindness, and display stunted growth and lethargy (105). Moreover, disorders like

Parkinson disease, neuropathy, liver disease are also caused in humans due mutation in *Ndufs4* gene (154,105).

Table 1.1-The targets of S-glutathionylation

The mitochondrial proteins that are found to be S-glutathionylated since 2013 are listed in this table

Citric acid cycle (CAC)	ETC
Acotinase → Decrease in the activity	Complex I → Increases activity on deglutathionylation → Oxidative stress
2-OGDH → Decreases activity → ROS release is controlled	Complex III → The activity is not yet investigated
Isocitrate dehydrogenase → Decreases activity ROS release is controlled	
Succinate dehydrogenase → ROS release is controlled	Complex V → Decreases activity → Oxidative stress
Pyruvate dehydrogenase → ROS release is controlled	
Succinyl-CoA synthetase → Decreased activity leading to oxidative stress	
Solute carrier proteins (SLC)	Genes controlling mitochondrial fission/fusion
Uncoupling protein 2/3 → Proton leak is controlled due to decrease in activity	Mf1 → Fusion increases on glutathionylation leading to mitochondrial elongation
Adenine nucleotide transporter → MPTP opening is regulated due to decrease in activity	Mf2 → Fusion increases on glutathionylation leading to mitochondrial elongation
Others	
Cyclophilin D → Prevent MPTP opening → controls cell death	
Superoxide dismutase (SOD) → Removes superoxide	

1.4 Cardiac anatomy and physiology

1.4.1 Pumping of blood from the heart

The human heart is a muscular organ found in the thoracic cavity and is protected by a fibrous membrane called the pericardium. The outer layer of the pericardium is attached to the diaphragm whereas the inner layer is known as the epicardium which covers the heart. The cavity between the epicardium and endocardium is known as the pericardial cavity. This cavity contains the pericardium fluid which protects the heart from friction and shock (69). The heart is a four-chambered organ. The upper two chambers are known as the atrium and the lower two chambers are known as the ventricles. There occurs a tricuspid valve between the right atrium and the right ventricle and a bicuspid valve between the left atrium and left ventricle. The vena cava collects the deoxygenated blood from the body and empties it to right atrium which is then pumped into the left ventricle via the tricuspid valve. The function of the valve is to prevent the backflow of the blood. Then from the right ventricle the blood is taken to the lungs for oxygenation by the pulmonary artery. The superior and inferior pulmonary veins collect the oxygenated blood from the lungs and transports it to the left atrium which is pumped to the left ventricle via the bicuspid valve (69). From the ventricle, the oxygenated blood is then supplied to the entire body via the aorta.

Little resistance is provided by the lungs to the blood flow which keeps the right atrium and right ventricle at low pressure. (69).The auricles contract to pump blood into the ventricles. Before the auricles contract, around 75% of the ventricle gets filled with blood. Subsequently, the AV node sends impulses to the auricles to contract and pump blood into the ventricles (71). The final 25% of the ventricle is filled due to this contraction of the atrium. Deregulation of the AV node causes the impulses to be delayed and thus delays the contraction of the auricles. The

valves open to facilitate the flow of blood to the ventricles from the auricles and close to prevent the flow of blood back to the auricles (70). These valves make a sound on opening and closing and analysis of these sounds can be utilized to determine the integrity of the valves. There are two sounds which are made during each heartbeat. The first sound is low pitched and is known as “lubb”, while the other high pitched sound is known as “dub”. These sounds resemble the pulse of the heart. Lubb is internally divided into two parts depending on the frequency: 1) the sound made due to the closure of the tricuspid valve and 2) the sound made due to the closure of the bicuspid valve/mitral valve (72). As the cardiac cycle begins from the right part of the heart, the sound from the tricuspid valve is heard before the bicuspid valve. Dubb is also divided into 2 parts: 1) the sound due to the closure of the aortic valve (A) and 2) the sound due to the closure of the semilunar valves (P). P is louder than A. If the valves do not close properly there would either be a leakage or the narrowing of the valves which could disturb the sound of the pumping (73). Systolic murmur and diastolic murmur occurs when there are any problems in the shutting of the bicuspid/tricuspid valves and aorta/semilunar valves and blood leaks back to the right and the left auricle respectively.

1.4.2 Pacemaker regions of the heart

The normal pumping of the blood from the heart is maintained by pacemaker regions. The action potential which is mediated by several ion channels in the heart are responsible for the electric activity in the myocardium (74).

Action potential basically depicts the sequential activation and inactivation of Na^+ and K^+ ion channels which causes depolarization and repolarization. The sinoatrial (SA) node is the initiator of all the electrical signals in the myocardium (75, 76, 77). From the SA node the signals are then transmitted to the atrioventricular (AV) node which via purkinje fibres spread the

electric signals to the entire heart. Due to the excitation of the myocardial cell, an action potential is generated followed by relaxation and a refractory period until the generation of the next impulse (78, 79, 80, 81). There are different waveforms generated during an action potential. The waveforms of action potentials are different in different types of tissue (82, 83, 84, 85, 86). In the atrial and ventricular cardiomyocytes the upstroke of an action potential is quite rapid due to the opening of Na channels and is thus termed as phase 0. This phase 0 is followed by phase 1 which is the repolarization stage where the Na channels are inactivate and the K current is activated. This repolarization phase occurs for a brief time period in the purkinje fibres and thus effects the duration of phase 2. During phase 2 the voltage gated Ca^{+2} channels are activated and thus there is an influx of calcium ions via the L-type calcium channels (87). The activation of Ca^{+2} channels triggers the excitation mediated contraction of the myocardium. These channels also help in generating action potentials in the SA nodes and AV node cells. Other types of Ca^{+2} channel known as T type calcium channels also occur which plays a role in automaticity and have similar properties to the L type Ca^{+2} channels. During this phase, the force which is required for the efflux of K^{+} is also high (88). As soon as the Ca channels are inactivated, the outward K^{+} currents dominate, causing the membrane to repolarize and resulting in the restoration of the resting potential. There are several voltage gated (K_v) and non-voltage gated (K_{ir}) K^{+} currents (89). There are two types of currents produced by them 1) inward 2) outward. The outward current is then divided into I_{K_r} [I_K (rapid)], I_{K_s} [I_K (slow)], and $\text{I}_{K_{ur}}$ [I_K (ultrarapid)]. Depending upon the type of tissue and any disease condition, the amount of expression and the property of each of these channels varies (250). Several pore forming subunits and channel accessory units have been found to encode Nav, Cav, Kv, and Kir channels.

Any mutations in these encoding genes were found to be responsible for cardiac arrhythmia (89, 90).

1.5 Ischemia-reperfusion injury to the myocardium

Ischemia is defined as a lack of oxygen supply to the tissue but can also be associated with diminished delivery of metabolic substrates to an organ compromising ATP production (91, 92, 93, 94). Depending upon the severity of an ischemic injury, the resulting damage could be reversed by the restoration of blood flow to the tissue which is called reperfusion. Reperfusion not only restores the oxygen and the nutrient levels of the tissue, but also replenishes ATP. However, Hearse et al. in 1973 found that reperfusion after ischemia can also paradoxically induce tissue injury. This re-oxygenation-dependent tissue damage is referred to as “reperfusion injury” (96).

ROS were originally suggested to play a part in reperfusion injury in the 1980s (95, 96). It was found later that this was associated with a burst in ROS production following reintroduction of O₂ overwhelming antioxidant defenses and inducing oxidative distress, cell death, and tissue damage (96). Reperfusion injury has been studied in the heart, brain, skeletal muscle, liver, and kidney (140). Reperfusion injury induces arrhythmia and myocardial infarction, which is associated with necroptosis, apoptosis, and impaired microvascular function (96). Several in vitro models have been designed to study the response of heart cell populations towards simulated ischemia and reperfusion injury (97). These studies demonstrated that reperfusion injury is associated with the over production of ROS by mitochondria. Moreover, mice pre-treated with mitochondria-targeted antioxidants, electron transport chain blockers that limit ROS production, or exposed to ischemia pre-conditioning are protected from IR (ischemic reperfusion) induced injury (97). Other factors that can curtail the reperfusion-mediated

induction of oxidative distress and cell death include cyclosporin A, an inhibitor of mitochondrial permeability transition pore opening (MPTP) (138). Notably, MPTP opening is also associated with the over production of mitochondrial ROS.

The importance of mitochondrial ROS in the induction of reperfusion injury was further demonstrated using experimental models where antioxidant defenses were manipulated through the overexpression or deletion of genes encoding enzymes that eliminate ROS (98). Studies carried out with cell populations challenged with conditions that mimic ischemia-reperfusion also showed enhanced production of ROS (98). The above lines of evidences showed that ROS played a vital role in the injury caused during reperfusion (97, 98). Previous studies utilized SOD (superoxide dismutase), which is a $O_2^{\bullet-}$ scavenger, in the presence/absence of catalase to demonstrate the protective effects towards I/R (ischemic reperfusion) injury (147,148). Several mice models were used where the expression of ROS scavenging enzymes was modulated also demonstrated an association of ROS and I/R induced injury (141,142,143). Experiments carried out with cultured cardiomyocytes treated with H_2O_2 also induced effects that were similar to I/R-induced tissue injury (99). Malondialdehyde, conjugated dienes, and hydroxynonenol which are obtained due to lipid peroxidation are often regarded as the markers for ROS generation in various models (144,145). Oxidative stress and redox imbalance which is mostly created during I/R conditions, is marked by the generation of oxidized glutathione (GSSG) or by the oxidation of sulfhydryl groups. The ROS production was also quantified using several oxidant-sensitive fluorochromes (146). Nowadays proteomic and genomic mapping of the cells which are challenged to I/R injury is done where the responses to oxidative stress is noted (139). Thus, to conclude, the relationship between ROS and I/R induced injury is well studied (100,101).

1.5.1 ROS production during ischemic-reperfusion injury of the heart

During ischemia, the lack of O₂ significantly diminishes the combustion of fuels that drive ATP production by oxidative phosphorylation, including the beta-oxidation of fatty acids. In an effort to meet energy demands, cardiomyocytes increase glucose uptake and enhance the glycolytic production of ATP. Since pyruvate cannot be metabolized by mitochondria, it is diverted towards the production of lactate, acidifying the cellular environment. In addition, glycolysis produces considerably less ATP than oxidative phosphorylation and, therefore, a significant energy debt develops in the myocardium. This also stimulates adenylate kinase, producing ATP by transferring a beta-phosphate from ADP to another ADP molecule. This also generates AMP, prompting its breakdown by the purine degradation pathway (102). The caveat to this mechanism is that it results in the accumulation of hypoxanthine which, following reintroduction of O₂, is metabolized by xanthine oxidase inducing a burst in ROS production.

During ischemia, there is also a slowing of electron transfer through the respiratory chain which results in the over reduction of redox centers in Complexes I-IV (130). There is also a slowing of the Krebs cycle and the accumulation of several intermediates, including succinate which is considered a biomarker for I/R injury (102). Reintroduction of O₂ induces a burst of ROS release by mitochondria which is associated with MPTP opening and the induction of apoptosis and necrosis (Figure 1.5) (102). Recent work by Chouchani *et al* suggests that MPTP opening and the induction of tissue damage is induced by O₂^{•-} release from Complex I and induction of MPTP within 15 seconds of reperfusion (102). The authors demonstrated that succinate accumulation during ischemia due to purine nucleotide metabolism and the slowing of the Krebs cycle is responsible for igniting the massive increase in ROS release by Complex I. The succinate-induced increase in Complex I-mediated ROS release is due to the reverse flow of

electrons from Complex II. Reverse electron transfer (RET) is a natural phenomenon where electrons can flow backwards in the respiratory chain from Complex III or Complex II to Complex I under the right bioenergetic conditions (102). One of the main factors required is a high PMF to promote RET through Complex I and the reduction of NADH. Another important factor that influences RET is the ratio of NADH/NAD⁺ (102). For RET to occur, NAD⁺ needs to be available to accept electrons during reverse flow. In the model proposed by Chouchani *et al*, after ischemia, cardiac mitochondria retain a high PMF and sufficient amounts of NAD⁺ to promote rapid electron flow from succinate to Complex I inducing a massive burst in ROS production and MPTP (Figure 1.5) (102).

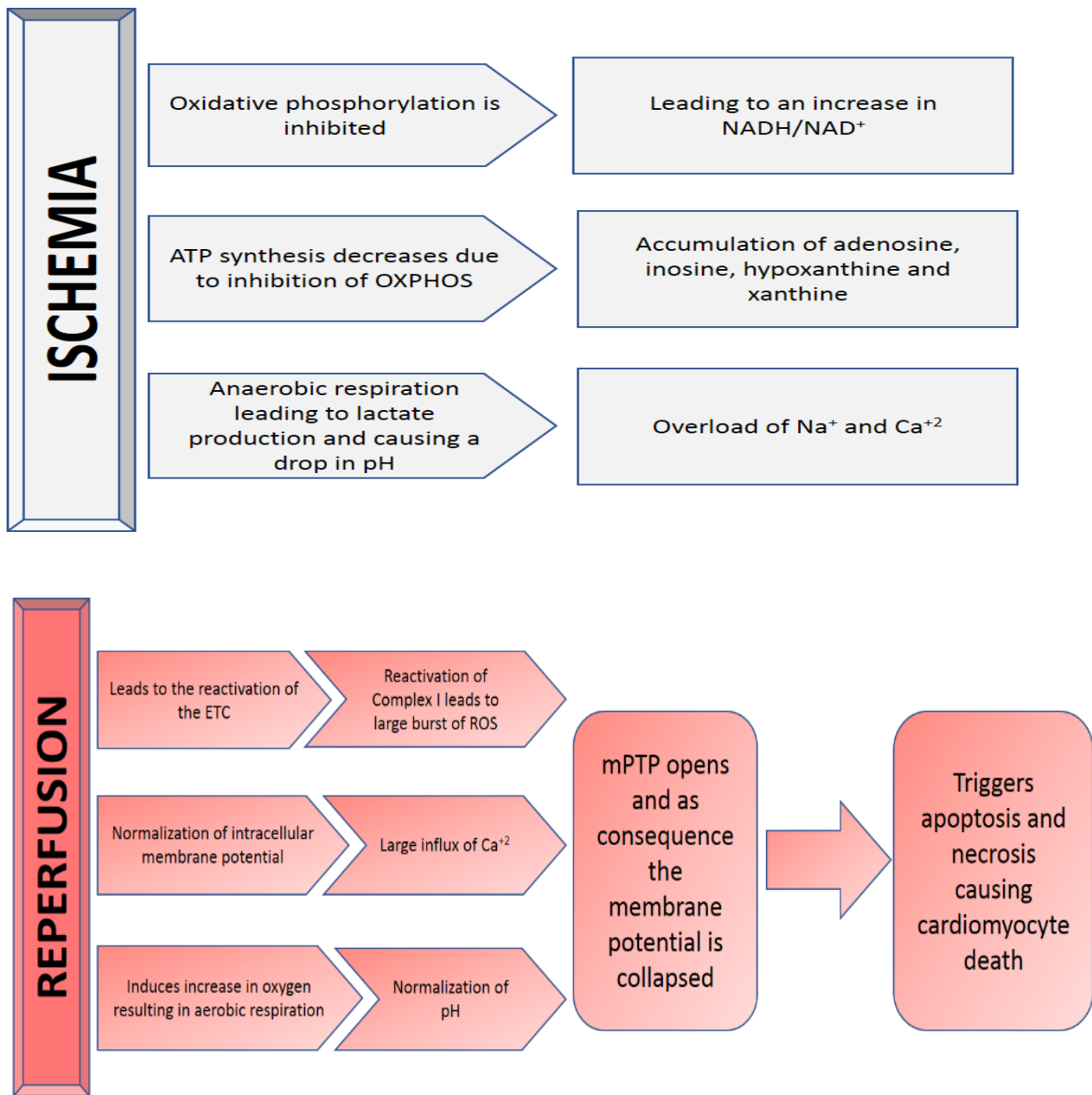


Figure 1.5-The mechanism of IR injury

1..5.2 Problems with the Chouchani model for IR injury to the myocardium

In Chouchani *et al*, it was proposed that Complex I was the only source of the ROS during IR injury (102). However, there are several pitfalls associated with this model. The first is that Complex I adopts a deactivated “D” state during ischemia. The A to D transition occludes the UQ binding site completely suppressing Complex I activity (103). Transition back to an “A” (active) state following re-introduction of oxygen and metabolites takes a few minutes (103,115). Therefore, Complex I cannot engage in RET for the first few minutes after reperfusion. The nicotinamide pool in the matrix of mitochondria is also highly reduced during ischemia which would curtail RET (103,115). Therefore, reverse electron flow through Complex I to FMN, the site for $O_2^{\bullet-}$, may not be possible. The second issue with this model is that it is well known that MPTP opening occurs within seconds following reperfusion and is induced by overloading the mitochondrial matrix with calcium (115). The overproduction of ROS was documented to happen well after MPTP opening (115). In addition, MPTP favors forward electron transfer due to the depolarization of the mitochondrial inner membrane and ADP debt. These conditions would not favor reverse electron flow from succinate to Complex I. The final major issue associated with this model is that it completely ignores the other sites for ROS production in mitochondria. Recent work has shown that mitochondria can contain up to 12 potential ROS forming sites (103). These ROS forming sites can be subcategorized based on the electron donor utilized in the genesis of $O_2^{\bullet-}/H_2O_2$; the NADH/NAD⁺ isopotential group and the UQH₂/UQ isopotential group as shown in Figure 1.6 (103). ROS forming sites associated with the former group including NADH producing and oxidizing enzymes that contain a flavin residue, namely, OGDH, PDH, branched chain amino acid dehydrogenase (BCKDH), 2-oxoadipate dehydrogenase (OADH), and Complex I. The latter group is comprised of enzymes that donate

or accept electrons directly from the UQ pool in the respiratory chain and includes Complexes II and III and various enzymes that adsorb to the outer leaflet of the inner membrane. Several studies have established that the main sites for ROS release in muscle and liver mitochondria are Complex III and OGDH, and to a lesser extent PDH and Complex II (104, 110, 111). This appears to also be the case for cardiac mitochondria. Two recent studies by our group found that Complex I and III both serve as major ROS sources in cardiac mitochondria (110,111). However, OGDH and PDH can also produce a significant amount as well (104). These observations are in line with several studies that have demonstrated Complex III is a major source for ROS during IR injury (132,103). Inhibitors for Complex III ROS release, like stigmatellin and myxothiazol, have been found to curtail IR injury (135). The last issue associated with the Chouchani model is timing for the opening of the MPTP following reperfusion. This occurs within seconds following reperfusion and results in a complete collapse of the mitochondrial membrane potential (115,116). In an effort to restore the PMF, forward electron flow from Complex I and II is augmented resulting in a massive spike in O₂ consumption (115,116). Therefore, it would seem more likely that other mitochondrial ROS producers are involved in IR injury and that the bioenergetics of the cardiac mitochondria do not favor reverse electron flow to Complex I from succinate (115,116).

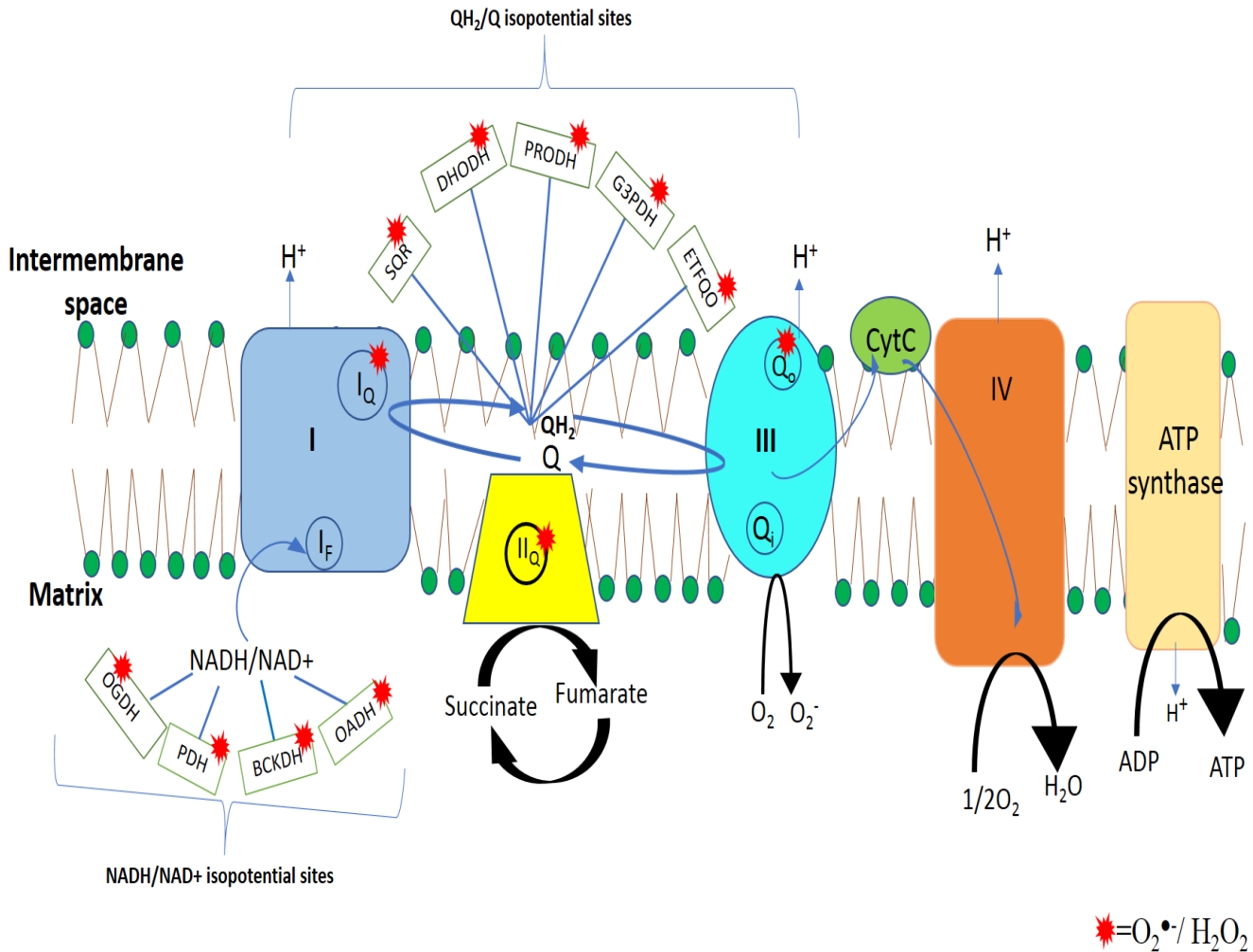


Figure 1.6-Sources of ROS in the ETC

The known sources of ROS production are described in the above diagram. The two major isopotential sites involved in ROS production are 1) NADH/NAD⁺ isopotential site 2) QH₂/Q isopotential sites. The NADH/NAD⁺ isopotential site includes OGDH (2-oxoglutarate dehydrogenase), PDH (pyruvate dehydrogenase), OADH (2-oxoadipate dehydrogenase), and BCKDH (branched chain keto acid dehydrogenase). QH₂/Q isopotential sites are SQR (sulfide:quinone oxidoreductase), DHODH (dihydroorotate dehydrogenase), PRODH (proline dehydrogenase), G3PDH (sn-glycerol-3-phosphate dehydrogenase), ETFQO (electron transfer flavoprotein-ubiquinone oxidoreductase), Complex I, Complex II and Complex III.

1.6 Research objectives

The major objectives of my thesis are as follows:

1. To examine the impact of Complex I deficiency on mitochondrial $O_2^{\bullet-}/H_2O_2$ production and identify high capacity sites in cardiac and liver mitochondria.
2. To determine the impact of partial Complex I deficiency on myocardial reperfusion damage.
3. To ascertain if NADH can drive ROS production by RET in Complex I knockouts.

1.7 Hypothesis

The major hypothesis of my research project are as follows:

1. Complex I is not the sole source of ROS in mitochondria and Complex I deficiency will not alter $O_2^{\bullet-}/H_2O_2$ production by cardiac and liver mitochondria.
2. Partial deletion of Complex I will sensitize the myocardium towards reperfusion injury.
3. NADH will drive ROS production in Complex I knockouts.

2. Materials and Methods

2.1 Breeding and maintaining mice

Male and female mice heterozygous for the *Ndufs4* gene (*Ndufs4*^{+/-}) were purchased from Jackson Laboratory (Bar Harbor, ME, USA). Briefly, mice heterozygous for *Ndufs4* were generated using a 129/sv mouse strain using standard gene eliminating techniques (*Ndufs4* flanked by loxp to remove exon 2 of the gene) (105). 129/sv mice were then backcrossed by several generations with C57Bl/6N mice to facilitate proper phenotypic analyses and increase fertility. Mice were housed in ventilated cages and fed a standard chow diet (44.2% carbohydrate, 6.2% fat, 18.6% crude protein; diet T.2018, Harlan, Indianapolis, IN) *ad libitum* and given free access to water. Mice were housed at room temperature (~23°C, 12 hour (h) dark/12h light cycle, lights on at 0700h). Age-matched male and female mice heterozygous for *Ndufs4* were paired for breeding. Once pregnancy was confirmed, male mice were removed and new litters were weaned at three weeks of age. Female mice were either culled or kept for future breeding. Immediately after weaning, mice were ear notched for genotyping. Ear notches were stored at -20 °C for genotyping. At 10-11 weeks of age, WT or *NDUFS4*^{+/-} mice were either euthanized for the isolation of cardiac and liver mitochondria or hearts extracted for ischemic-reperfusion injury. The capacity of NADH to drive ROS release by reverse electron transfer to OGDH or PDH was examined using mice partially knocked-out for *Ndufs4* (*NDUFS4*^{+/-}). *NDUFS4*^{-/-} mice develop encephalomyopathy, lose motor function, develop blindness, and display retarded growth by ~5-6 weeks of age (105). Therefore, these experiments were conducted on mice no more than 5 weeks of age. WT and *NDUFS4*^{+/-} mice were weighed weekly until euthanasia to compare rate of growth. Breeding of these mice was performed by myself and Danielle Gardiner (Research technician in Dr. Mailloux lab) also helped me during

this procedure. All experiments were approved by Memorial University's Animal Care and Use committee and conducted according to institutional and Federal animal care guidelines.

2.2 Mouse genotyping

2.2.1 DNA isolation

DNA was extracted from ear notch samples using a REDExtract-N-Amp Tissue PCR Kit (Sigma-Aldrich) according to the manufacturer's instructions. One hundred microliters of Extraction Solution and 25 μ L Tissue Prep Solution were pipetted into a 1.5 mL microcentrifuge tube containing an ear notch. Samples were incubated at 55°C for 10 mins followed by an incubation of 95°C for 3 mins. After this, 100 μ L of Neutralization Solution was added to each tube and then samples were vortexed. Samples were used for polymerase chain reaction (PCR) or stored at -20 °C for later use.

2.2.2 Polymerase Chain Reaction (PCR)

Primers for *Ndufs4* were obtained from Integrated DNA Technologies. Table 2.1 shows the detailed primer sequences. The PCR tube contained the following: 0.5 μ M *Ndufs4* wild type forward primer (1 μ L), 0.5 μ M *Ndufs4* reverse primer (1 μ L), 0.5 μ M *Ndufs4* mutant forward (1 μ L), DNA solution (4 μ L), nuclease-free water (3 μ L) and REDExtract-N-Amp Tissue PCR Kit Reaction Mixture (10 μ L). The final volume in the tube was 20 μ L. Eppendorf Mastercycler pro PCR System was used to amplify the DNA. Table 2.2 shows the PCR Protocol for amplification of the *Ndufs4* gene.

Table 2.1-DNA Sequence of primers used for *Ndufs4* genotyping

Primer	Sequence
<i>Ndufs4</i> Wild type Forward	5'-AGT CAG CAA CAT TTT GGC AGT -3'
<i>Ndufs4</i> Reverse primer	5'-GAG CTT GCC TAG GAG GAG GT -3'
<i>Ndufs4</i> Mutant Forward	5'-AGG GGA CTG GAC TAA CAG CA -3'

Table 2.2-Polymerase Chain Reaction (PCR) protocol for Ndufs4 genotyping

Step	Temperature (°C)	Time
1	94	2 min
2 10 cycles	94	20 sec
	65	15 sec
	68	10 sec
3		
4 28 cycles	94	15 sec
	60	15 sec
	72	10 sec
5		
6	72	2 min
Hold	10	

2.2.3 Polyacrylamide gel electrophoresis

PCR samples were electrophoresed in a 1.5% agarose gel which was made by dissolving 0.75 g of agarose powder (Fisher Scientific) in 0.5X Tris-Borate-EDTA (TBE, 10X solution diluted to 0.5X in analytical water) under constant heat. SYBR Safe DNA Gel Stain (Fisher Scientific) was added to the molten agarose at a 1/10,000 dilution. The gel was allowed to solidify in the gel molding of a Fisher Biotech Horizontal Electrophoresis Systems gel box. Trackit 100 bp DNA Ladder (Fisher Scientific) was used as a reference to estimate the DNA fragment size. The samples were loaded into the gel and it was electrophoresed for 40 mins at 90V. *Ndusf4* gene fragments were visualized using an Alpha Innotech ChemiImager Ready System. A single nucleotide sequence produced by the WT mice was 200 base pairs (bp) in length while the *NDUFS4*^{-/-} mice produced a fragment 400 bp in size. The *NDUFS4*^{+/-} mice contained both nucleotide fragments (200 bp and 400 bp). It may seem unusual that the PCR product corresponding to the *Ndusf4* gene lacking the second exon is larger than the WT gene. According to Jackson laboratories, deletion of exon 2 moves the forward primer for *Ndusf4* closer to the common primer, giving a band that is ~400 bp in size. Therefore, the presence of exon 2 generates a PCR product of a smaller size.

2.3 Isolating the mitochondria

Liver and cardiac mitochondria were isolated using protocols established by our group (110,111). Prior to each isolation, 1 liter of MESH buffer (23.95 g sucrose; 70 mM, 40.1 g mannitol; 220 mM, 0.38 g EGTA; 1 mM, 5.2 g HEPES; 20 mM, pH 7.4) was made and stored at 4 °C. On the day of experimentation, mitochondrial isolation buffer was made by adding 0.5% (w/v) fatty acid-free bovine serum albumin (BSA; Sigma-Aldrich) to MESH buffer (abbreviated MESH-B). All mitochondrial isolation steps were performed on ice or at 4 °C. Mice were

deeply anesthetized with isoflurane and then euthanized by cervical islocation. The cardiac and liver tissues of these mice were collected and stored in MESH-B. The cardiac and liver tissues were dabbed dry and weighed. Femur length was also recorded and used to normalize heart weight. Tissues were first cut into small pieces with scissors and rinsed with MESH-B to remove excess blood. Tissue pieces were then minced with a razor on a Teflon watch glass and then placed in a homogenizer with 15 mL MESH-B. For cardiac tissue, MESH-B was also supplemented with 1 unit of subtilisin A (Sigma-Aldrich). Subtilisin A is a protease that was added to release mitochondria from myofibers. The amount added was determined according to equation 2.1.

Equation 2.1-Volume of Subtilisin A to be added

$$\text{Volume of subtilisin A} = \frac{\text{Mass of heart (g)}}{1\text{mg/ml} \times 11.7 \text{ mg/unit}}$$

For liver mitochondria, homogenates were centrifuged at 800 x g for 9 mins at 4 °C to remove nuclei and undisrupted tissue. The supernatant was then collected and centrifuged at 10,000 x g for 9 mins. The supernatant was decanted and the resulting mitochondrial pellet was resuspended in 20 mL of fresh MESH-B and centrifuged again at 10,000 x g. The washing step was carried out to remove any contaminating organelles and fat. The solution was decanted and the resulting mitochondrial pellet was resuspended in 500 µL MESH buffer and stored on ice.

Cardiac mitochondria were isolated by centrifuging the homogenate at 10,000 x g for 9 mins. The supernatant was decanted and the pellet was resuspended in 15 mL MESH-B to remove any residual protease. The homogenate was then centrifuged at 800 x g for 9 mins to remove nuclei and myofibers. After this, the supernatant was centrifuged for 10 mins at 10,000 x

g. The resulting cardiac mitochondrial pellet was resuspended in 100 μ l MESH and stored on ice. Protein equivalents to mitochondrial content were estimated using the Bradford assay.

2.3.1 Bradford assay for protein estimation

Protein equivalents to mitochondria were determined using the Bradford assay. Protein concentration was estimated using a standard curve generated with BSA (Sigma-Aldrich) with a concentration range from 0 to 1.875 μ g/ml (Figure 2.1). For sample quantification, 1 μ L of the mitochondrial suspension was added to 999 μ L of analytical water and then vortex thoroughly in a 1.5 ml microcentrifuge tube. After this, 50 μ L of diluted sample was added to 200 μ L Bradford reagent (Sigma-Aldrich) and the volume was adjusted to 1 ml with analytical water. Samples were then mixed and 200 μ L of sample was pipetted into the wells 96 well plate (Greiner Bio-One) in duplicate. The equation $y = mx+b$ was used to calculate the final concentration of protein equivalents to mitochondria. Samples were then stored on ice for assays. Any additional mitochondria remaining at the end of experiment was stored at -80 $^{\circ}$ C for immunoblot.

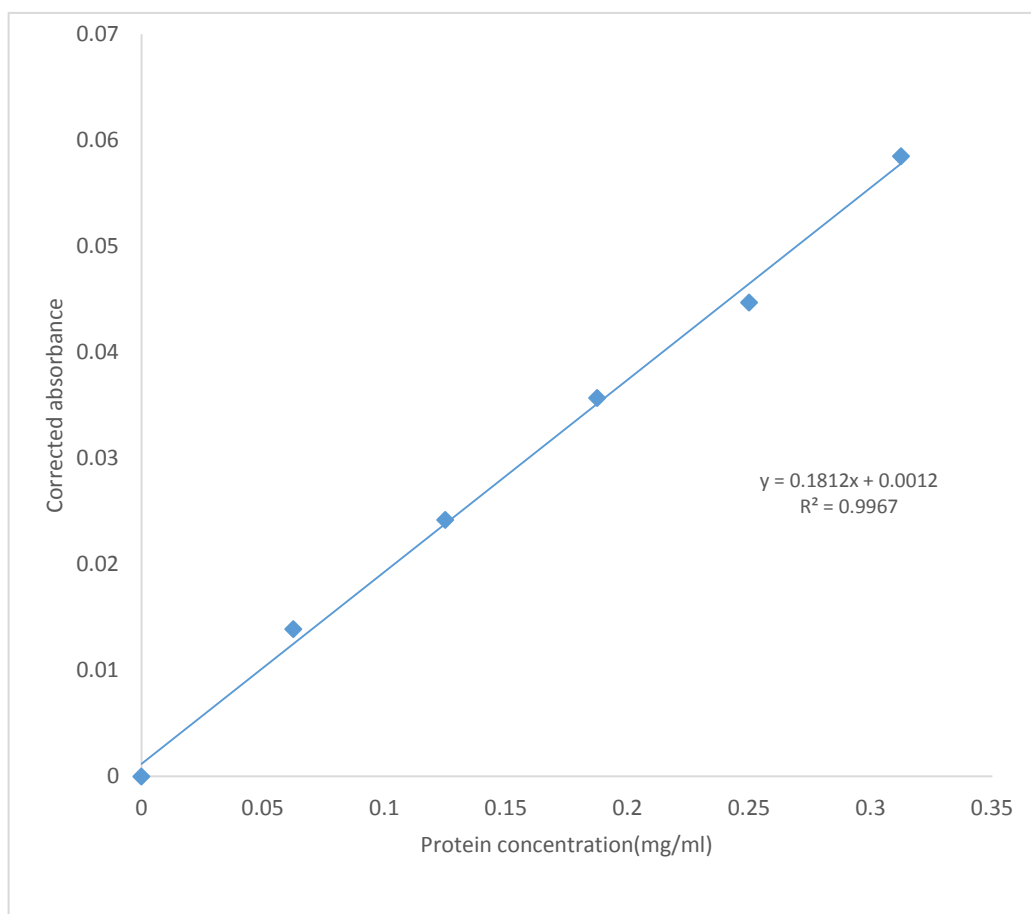


Figure 2.1-Bradford assay standard curve for determination of protein concentration

The absorbance was measured with increasing concentrations of BSA mixed with Bradford reagent. Hence, the unknown concentration of the protein can be determined

2.4 Amplex Ultra Red (AUR) assay

Amplex Ultra Red (AUR) assay was used to selectively measure the rate of $O_2^{\bullet-}/H_2O_2$ production. Although AUR is selective for H_2O_2 , it cannot discriminate between H_2O_2 formed directly by sites of ROS production or by the dismutation of $O_2^{\bullet-}$ by superoxide dismutase (SOD). Indeed, sites of ROS release in mitochondria have been documented to release a mixture of $O_2^{\bullet-}$ and H_2O_2 , a characteristic associated with flavin-based prosthetic groups (6). Therefore, in this thesis, AUR measurements are referred to as the measurement of $O_2^{\bullet-}/H_2O$ to account for 1) H_2O_2 produced directly by sites of production and, 2) H_2O_2 produced due to dismutation of $O_2^{\bullet-}$. In this assay exogenous SOD was added to ensure the full conversion of $O_2^{\bullet-}$ to H_2O_2 .

Before experiments, liver samples were diluted to 3 mg/ml and the cardiac samples to 1 mg/mL in MESH-B (110). These samples were then stored on ice. Twenty microliters of sample were added to the wells of a 96 well plate containing MESH and in the absence or presence of different inhibitors. Experiments with ROS production inhibitors required incubating samples at 25 °C for 10 min in the presence of the inhibitor (110). AUR reagents were then added and reactions initiated by the addition of substrate. The final volume for each reaction was 200 μ L and the final concentration of liver and cardiac mitochondria in each well was 0.3 mg/mL and 0.1 mg/ml, respectively. Changes in fluorescence associated with the conversion of non-fluorescent AUR to fluorescent resorufin were tracked using a SpectraMax M5 plate reader to measure the fluorescence every 30 seconds for a duration of 5 mins at 565/600 nm excitation and emission wavelengths. A standard curve generated by different concentrations of H_2O_2 (30 % stock solution at 12.8 M, Sigma-Aldrich) ranging from 20-400 nM was used for calculating the amount of ROS production (Figure 2.2).

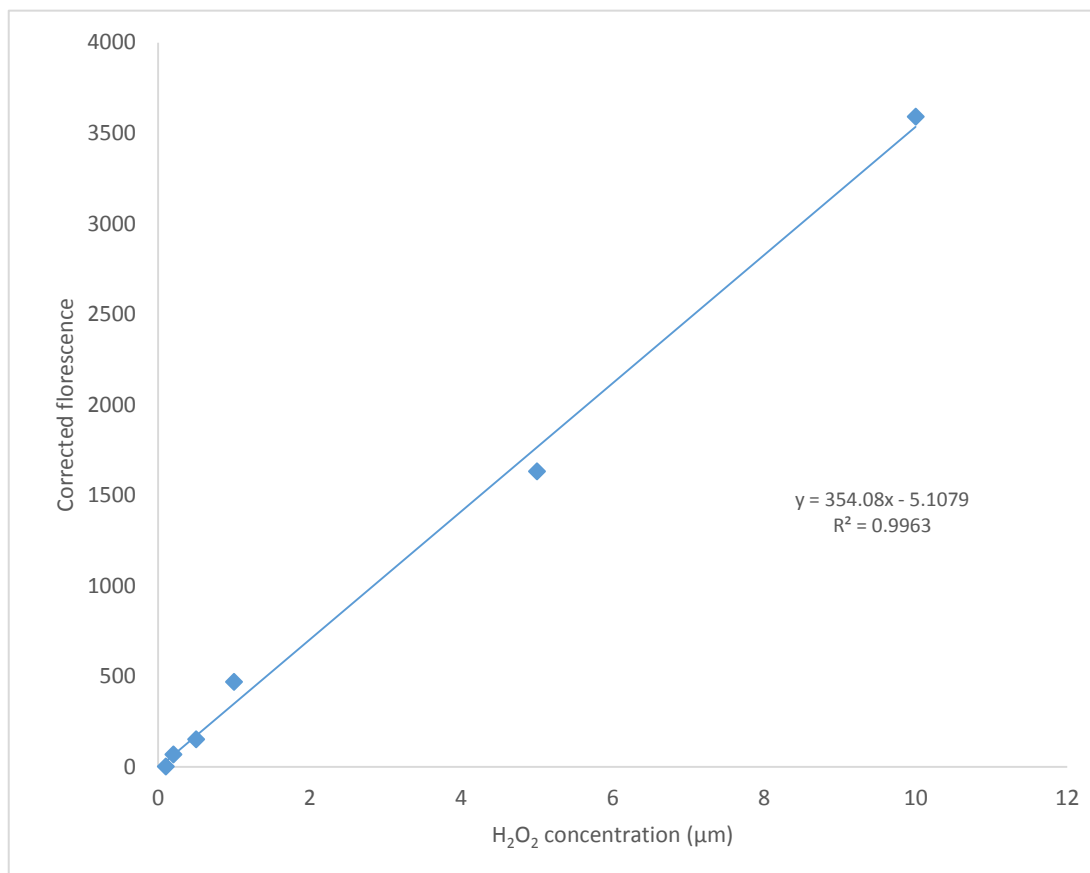


Figure 2.2-AUR Assay standard curve for determination of O₂^{•-}/H₂O₂ concentration

The fluorescence was measured with increasing concentrations of hydrogen peroxide. Hence, the unknown concentration of the O₂^{•-}/H₂O₂ can be determined.

2.4.1 Measuring rate of $O_2^{\bullet-}/H_2O_2$ production during PDH and 2-OGDH oxidation

There can be up to 12 sites of ROS production in mitochondria which includes enzymes that feed electrons directly to the ubiquinone pool, Complex I, Complex II, Complex III and Krebs cycle enzymes (103). In order to determine which enzymes serve as high capacity sites for production and whether or not a deficiency in the NDUFS4 protein influences individual rates of production, mitochondria were treated with different inhibitor and substrate combinations. To examine ROS release associated with the Krebs cycle and electron transport chain, pyruvate and 2-oxoglutarate with malate were utilized as substrates. Malate was included to complete the Krebs cycle ensuring the full oxidation of substrates. OGDH and PDH inhibitors as well as Complex II and III inhibitors were also used to pinpoint which sites formed the most ROS.

Pyruvate (50 μ M) or 2-oxoglutarate (50 μ M) with malate (50 μ M), were used to determine the $O_2^{\bullet-}/H_2O_2$ in the liver and cardiac mitochondria. Our group showed previously that these substrate concentrations (which represent physiological concentrations) induce a measureable rate of $O_2^{\bullet-}/H_2O_2$ production (110). In the individual wells of a 96 well plate, mitochondria were added to MESH buffer containing 10 mM α -keto- β -methyl-n-valeric acid (KMV; OGDH inhibitor) (Sigma-Aldrich), 250 μ M 6,8-bis(benzylsulfanyl) oclanoic acid (CPI-613; OGDH and PDH inhibitor) (Sigma-Aldrich), 40 μ M Atpenin A5 (Santa Cruz; Complex II inhibitor), or 4 μ M myxothiazol (Sigma-Aldrich; Complex III inhibitor) and then incubated at 25 $^{\circ}$ C for 10 min (110). Myxothiazol acts as a selective inhibitor of Complex III. It prevents semiquinone formation by binding to the ubiquinone binding site close to the outer leaflet (Qo) of the mitochondrial inner membrane (Figure 2.3). α -Keto- β -methyl-n-valeric acid (KMV) is a structural analog of 2-oxoglutarate and is thus a site-specific inhibitor for OGDH. Atpenin A5

inhibits Complex II by blocking its ubiquinone binding pocket. Also, CPI-613 effectively inhibits OGDH and PDH by competitively binding the lipoic acid in the E2 subunit. After mitochondria were incubated in the presence or absence of the different inhibitors, 25 U/mL SOD (Sigma-Aldrich), 3 U/mL HRP (Sigma-Aldrich), 10 μ M AUR (Invitrogen), and 50 μ M malate was added in each well. Reactions were initiated by adding 50 μ M pyruvate or 50 μ M 2-oxoglutarate. Changes in fluorescence were tracked as described above.

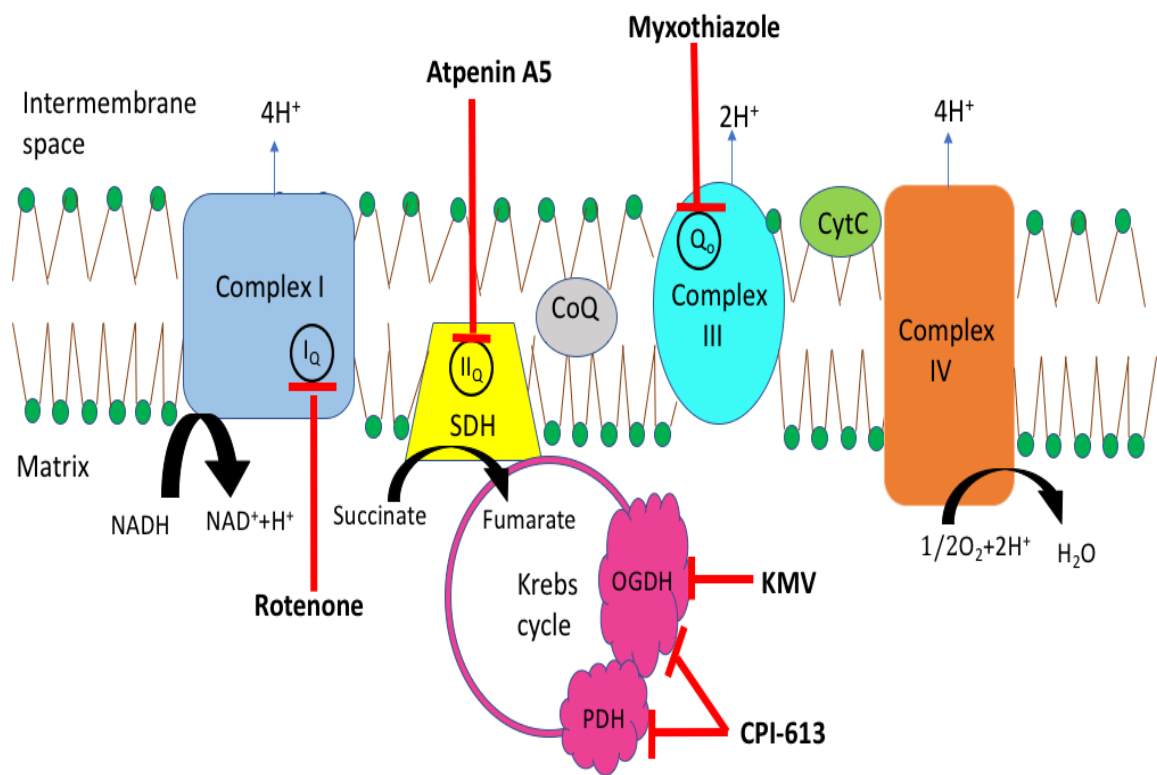


Figure 2.3-Sites of action for the different inhibitors used in the AUR assays

Rotenone and atpenin A5 inhibit Complex I and Complex II respectively by blocking ubiquinone binding sites, I_Q and II_Q, respectively. Myxothiazol blocks the Q_O site of Complex III preventing semiquinone production and ROS release. KMV selectively blocks ROS release from OGDH and CPI-613, a structural analog for liponic acid, inhibits both PDH and OGDH.

2.4.2 *Measuring rate of $O_2^{\bullet-}/H_2O_2$ production during succinate oxidation*

Succinate is oxidized by Complex II of the respiratory chain donating electrons directly to the ubiquinone pool (Figure 2.3). In these reactions, pyruvate was also excluded to prevent the full oxidation of succinate following the production of fumarate. Excluding pyruvate prevents the completion of the Krebs cycle abolishing ROS release from PDH and OGDH. Therefore, these experimental conditions allow for the exclusive measurement of $O_2^{\bullet-}/H_2O_2$ release from the electron transport chain. First, 20 μ l of heart mitochondria was added to individual wells containing MESH with or without different inhibitors and then incubated for 20 min at 25 °C. We used 4 μ M rotenone (Sigma-Aldrich), 40 μ M atpenin A5 (Santa Cruz) or 4 μ M myxothiazol (Sigma-Aldrich), Complex I, II, and III inhibitors, respectively, to pinpoint the site of ROS release during succinate oxidation (Figure 2.3). Sites of action for myxothiazol and atpenin A5 were described in the previous section. Rotenone, a Complex I inhibitor that competitively blocks its ubiquinone binding pocket, was used to ascertain how much ROS was formed during reverse electron flow from succinate (Figure 2.3). After the incubation, 25 U/mL SOD (Sigma-Aldrich), 3 U/mL HRP (Sigma-Aldrich), and 10 μ M AUR (Invitrogen). Reactions were initiated by the addition of 50 μ M succinate. Using a SpectraMax M5 plate reader the rate of ROS production was monitored for every 30 seconds for a duration of 5 mins at 565/600 nm.

2.4.3 *Measuring rate of $O_2^{\bullet-}/H_2O_2$ production during RET from NADH.*

The mitochondrial inner membrane is a selectively permeable barrier that does not allow the free diffusion of solutes between the matrix and intermembrane space. Thus, mitochondria were permeabilized to promote the uptake of exogenously added NADH by the mitochondrial matrix and ascertain if it can contribute to ROS release by reverse electron flow. Note that these

experiments were carried out with mitochondria enriched from *NDUFS4*^{-/-} mice. This ensured that NADH could not be oxidized by Complex I and thus any ROS production could be attributed to PDH or OGDH (or another 2-oxoacid dehydrogenase). Mitochondria were permeabilized using a protocol previously established by our group (112). Liver and heart mitochondria were diluted to 3 mg/mL and 1 mg/mL, respectively, in MESH containing Triton X-100 (0.05% v/v). Samples were then vortexed and incubated on ice for 20 minutes. After permeabilization, 20 µL aliquots of mitochondrial suspension were added to individual wells of a 96-well black plate containing MESH. Twenty-five U/mL SOD (Sigma-Aldrich), 3 U/mL HRP (Sigma-Aldrich), 10 µM AUR (Invitrogen) were then added to each well and then reactions were initiated by the addition of NADH (0.1-10 µM final concentration in each well). Using a SpectraMax M5 plate reader the rate of ROS production was monitored for every 30 seconds for a duration of 5 mins at 565/600 nm.

2.4.4 Immunoblot

Liver and cardiac mitochondria stored at -80 °C were thawed, vortexed vigorously, and then placed on ice. Samples were diluted to 1 mg/ml in analytical water containing Laemmli buffer (2X stock diluted to 1X in water, Bio-Rad) and heated for 10 minutes at 100°C. Proteins were separated in a 12% acrylamide gel to ensure proper immunodetection of the *NDUFS4* protein (~20 kDa in size), glutathione peroxidase-1 (GPX1), or thioredoxin-2 (TRX2). Succinate dehydrogenase subunit A (~70 KDa) served as the loading control for all experiments. The resolving gel solution was made by adding 6 mL of 40% acrylamide solution (36.7% w/v acrylamide /3.3 % w/v bis-acrylamide, Biorad) to a 50 mL conical tube containing 5 mL of 4X Trizma /SDS solution (1.5 M Trizma base +0.4% (w/v) SDS in 100 mL of analytical water, pH 8.8 with HCl) and 10 mL of analytical water. The gel solution was mixed and polymerization

was initiated by adding 75 μ L of TEMED (*N, N, N', N'*-tetramethylethane-1, 2-diamine, Biorad) and 150 μ L 1% (w/v) APS (ammonium persulfate solution, Biorad). Table 2.3 shows a detailed recipe of the gel. The gel solution was then quickly poured into the gel cast (filling the cast by \sim 3/4) and then the gel was overlaid with 100% isopropyl alcohol and allowed to polymerize. After resolving gel polymerization, the isopropyl alcohol was removed and the gel was overlaid with a stacking gel. The stacking gel was prepared in a 15 mL conical tube and contained 1 ml 40% acrylamide (to make a total volume of 4% (v/v)), 2.5 ml 4X Trizma/SDS stacking gel solution (0.5 M Trizma Base + 0.4% (w/v) SDS in 100 mL, pH 6.8). The volume was adjusted to 10 ml with analytical water. Fifty microliters of TEMED and 75 μ L of APS was added to initiate gel polymerization. After the stacking gel was added to the gel cast, a 15 well comb (1 mm) was immediately inserted into the stacking gel. After polymerization, the comb was removed and the wells dabbed dry.

Prior to experiments, a 10X electrophoresis buffer was made and stored at room temperature [1920 mM glycine, 1% (v/v) SDS (sodium dodecyl sulfate) and 25 mM Trizma base]. The electrophoresis buffer was diluted to 1X just before the experiments by adding 100 ml 10X electrophoresis buffer to 900 ml analytical water. Samples were loaded into the individual wells of the gel. PageRuler Plus prestained protein ladder (Fermentas, 15 μ L) was also loaded into the gel to track protein migration and confirm the successful transfer of proteins to the nitrocellulose membrane and the molecular mass of proteins of interest. Samples were initially electrophoresed at 80 V. Once the running front entered the resolving gel and the prestained ladder started to separate, the voltage was increased to 240 V. As soon as the running front reached the bottom of the gel, electrophoresis was stopped. Gels were then removed and equilibrated for 15 min at room temperature under constant agitation in 1X transfer buffer (100

mL of 10X transfer buffer in 800 mL of analytical water and 100 mL methanol), which was made by diluting 100 mL of 10X transfer (500 mM Trizma, 380 mM glycine, 10% w/v SDS) in 900 mL analytical water. One times transfer buffer was also used to equilibrate nitrocellulose membranes (Bio-Rad) and extra thick blotting paper (Bio-Rad). A Mini Trans-Blot Electrophoretic Transfer Cell (Bio-Rad) containing 1X transfer buffer was used to transfer proteins from the resolving gel to the surface of a nitrocellulose membrane. Protein transfer was carried out at 120 V for 1 hr at room temperature. Successful transfer of proteins was confirmed by staining nitrocellulose membranes with Ponceau S (Sigma-Aldrich). Membranes were then rinsed with Trizma-buffered saline (TBS; 1 mM Trizma base, 68 mM NaCl) containing 0.1% (v/v) Tween-20 (Bio-Rad) (TBS-T). Nonspecific binding sites on membranes were then blocked with TBS-T containing 5% w/v non-fat skim milk (Lab Scientific) for 1 hour at room temperature under constant agitation. Membranes were then washed thrice with TBS-T for 5 minutes. Membranes were then probed overnight at 4 °C with constant agitation with anti-SDHA (Santa-cruz, catalogue #sc-377302) and anti-Ndufs4 (Santa-Cruz, catalogue #sc100567) or anti-SDHA (Santa-cruz, catalogue #sc-377302) and anti-GPX1 (Santa-cruz, catalogue #sc-133160) or anti-SDHA (Santa-cruz, catalogue #sc-377302) and anti-TRX2 (Santa-cruz, catalogue #sc-137028) antibodies diluted in TBS-T + 5% (w/v) BSA + 2% (w/v) NaN₃ (Sigma-Aldrich). The primary and secondary antibodies were diluted as per table 2.4. Membranes were washed thrice with TBS-T for 5 mins and then probed with secondary antibodies conjugated to horseradish peroxidase (HRP). Depending on the primary antibody, the secondary antibody (goat antibody conjugated to HRP; anti-mouse or anti-rabbit) was added in the blocking solution containing the membrane. The above solution was agitated for 70 mins at room temperature. WestPico Super Signal Chemiluminescent substrate was added as well. The ImageQuant LAS 4000 system was

utilized for viewing the immunoreactive bands. These immunoblots were performed in duplicates.

Table 2.3-Detailed recipe of the immunoblot gel

	40% Acrylamide/Bis Solution (mL)	4X Tris/SDS 8.8 Buffer (mL)	4X Tris/SDS 6.8 Buffer (mL)	Analytical water (mL)	TEMED (μ L)	APS (μ L)
12% Resolving Gel	6	5	0	9	150	75
4% Stacking Gel	1	0	2.5	6.5	75	50

Table 2.4-Dilution factor for the antibodies

Antibodies		Antibody (μL)	TBS-T (mL)	NaN_3 (μL)	Final concentration (μL)
Loading control	Anti-SDH A (primary Ab)	3.33	10	0.02	1/3000
	Goat anti-mouse (secondary Ab-HRP conjugate)	3.33	10	0.02	1/3000
Ndufs4 antibody	Anti-Ndufs4 (primary Ab)	10	10	0.02	1/1000
	Goat anti-mouse (secondary Ab-HRP conjugate)	3.33	10	0.02	1/3000
GPX1 antibody	Anti-GPX1 (primary Ab)	5	10	0.02	1/2000
	Goat anti-mouse (secondary Ab-HRP conjugate)	3.33	10	0.02	1/3000
TRX2 antibody	Anti-TRX2 (primary Ab)	5	10	0.02	1/2000
	Goat anti-mouse (secondary Ab-HRP conjugate)	3.33	10	0.02	1/3000

2.5 Isolated heart perfusions

This experiment was conducted as described previously (112). Briefly, the Krebs-Henseleit (K-H) buffer including 7 mmol/l glucose, 0.4 mmol/l oleate, 1% BSA, and 10 ϵ U/ml insulin was prepared and oxygenated (95% O₂; 5% CO₂ gas). A peristaltic pump connected with silicon tubing was used to pump the KH buffer into the Langendorff perfusion system at a flow rate of 4 ml/min (Figure 2.4). The flow rate at 4 ml/min maintains a normal mouse coronary pressure *in vivo*.

The WT and NDUFS4^{+/-} mice (n=10) aged 10-11 weeks were initially heparinized (100 U i.p) in order to prevent blood coagulation prior to anesthesia They were then anesthetized with pentobarbital sodium (60 mg/kg i.p). Hearts were excised and cannulated with aorta. A balloon was inserted into the left ventricle to measure the hemodynamic function of the heart. . During the baseline perfusion, the balloon was inflated to 5mm Hg diastolic pressure and the left ventricular developed pressure (LVDP) and heart rate (HR) were recorded by the Lab Chart software (AD heart perfusion instruments). Every heart underwent a normal perfusion at a flow rate of 4 ml/min for 30 min followed with 15 min no-flow global ischemia. The hearts were then reperfused with K-H buffer at a recovered flow rate (4 ml/min).

At the end of the reperfusion, hearts were collected and either put in MESH buffer for mitochondrial isolation and AUR assays or subjected to triphenyltetrazolium chloride (TTC) staining for estimation of infarct size. ROS release assays were performed as described in sections 2.4.1 and 2.4.2. The TTC staining is used to measure the infarct size. The TTC staining buffer was firstly prepared. The detailed recipe is as given below in table 2.5. The heart was taken and 5ml of the TTC stain was injected into the heart at 37° C. Then the heart was stored in formalin. For the infarct size determinations, the sections of the heart were taken and were

visualized under a microscope. Image-J software was used to determine the area of the infarct size

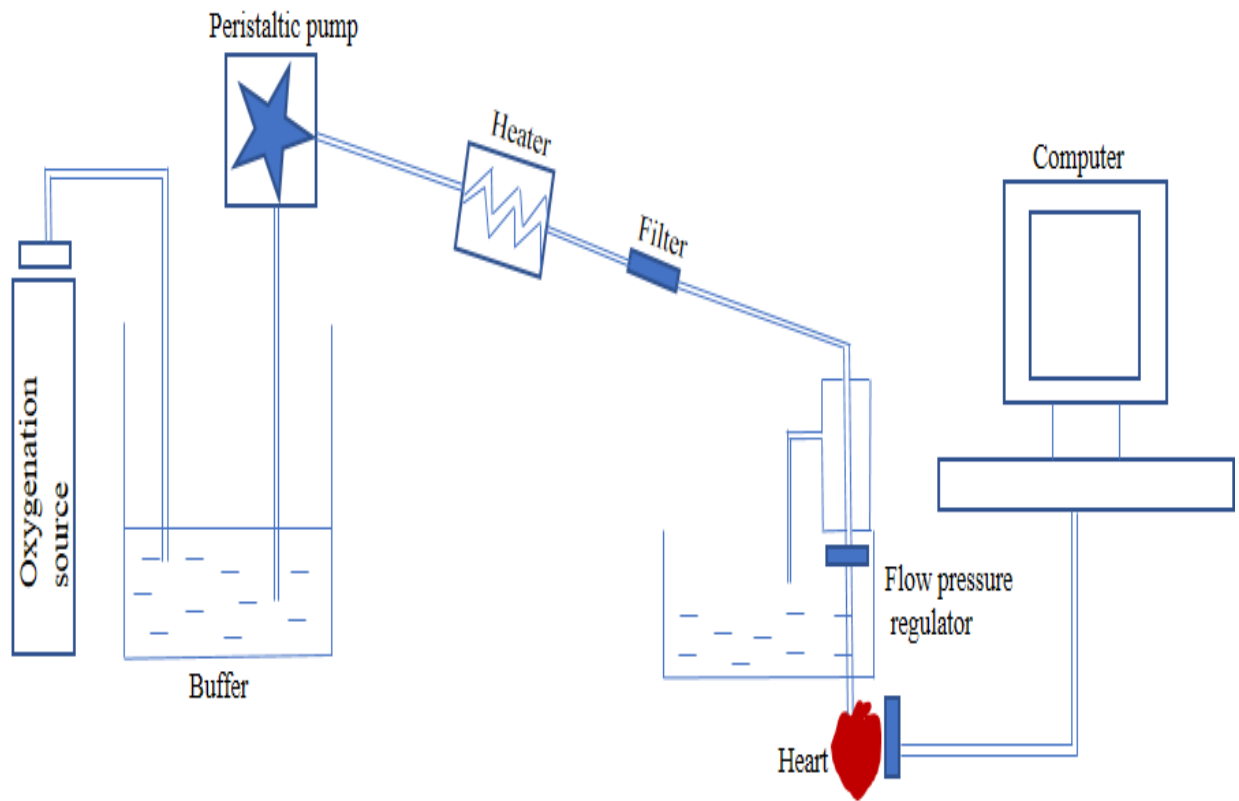


Figure 2.4-The Langendorff heart perfusion system.

This system was used to perform ex vivo heart perfusion and conduct cardiac global ischemia-reperfusion. Cardiac function was evaluated by heart rate and left ventricular developed pressure.

Table 2.5-Detailed recipe of the TTC stain

	Ingredients	Quantity
Buffer 1	NaPO ₄ Dibasic	12.4 g/l
	Dextran	76.5 g/l
Buffer 2	NaPO ₄ Monobasic	12.4 g/l
	Dextran	76.5 g/l
Buffer 3	Buffer 1	800 ml
	Buffer 2	200 ml
Working buffer	Buffer 3	100 ml
	TTC	1g

2.5.1 Measurement of mitochondrial NAD(P)H levels following IR injury

Mitochondrial NAD(P)H levels following IR injury was tracked by measuring the autofluorescence of the nicotinamide group. Following IR injury, hearts were quickly placed in ice-cold MESH buffer and the mitochondria were isolated as described above. Mitochondria were then diluted to 1 mg/mL in MESH and 20 μ L aliquots were added to wells of a 96-welled black plate containing 180 μ L of MESH. NAD(P)H autofluorescence was tracked using a SpectraMax M5 plate reader operating at 376 nm/420 nm excitation and emission wavelengths. A standard curve generated by different concentrations of NAD(P)H (1mM in 1ml MESH stock solution, Sigma-Aldrich) was used for calculating the amount of NAD(P)H as discussed above in Figure 2.5

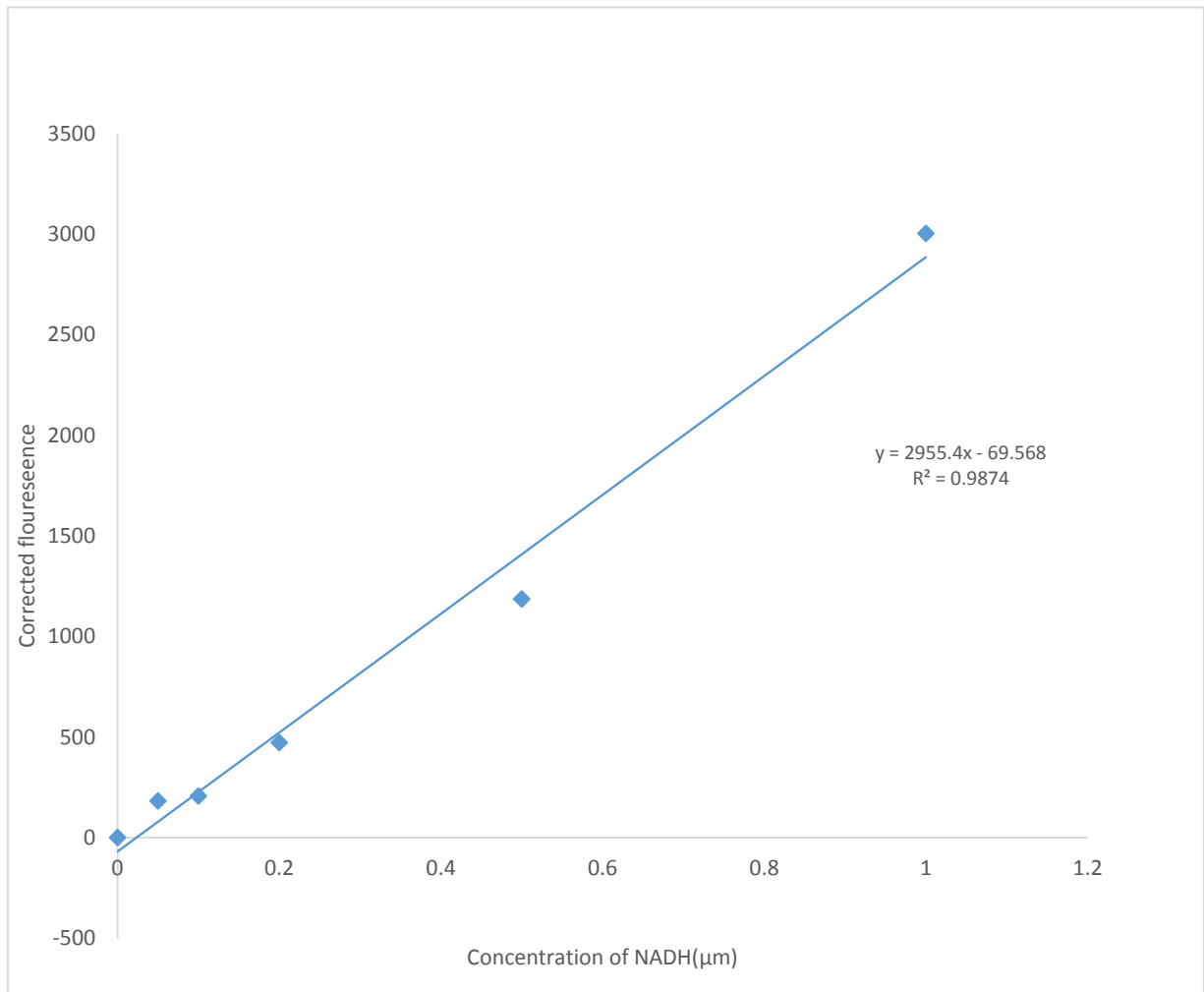


Figure 2.5 NAD(P)H standard curve for measuring NAD(P)H levels after IR injury

The fluorescence was measured by increasing the amount of NAD(P)H. Hence, the unknown concentration of NAD(P)H was determined.

2.6 Data Analysis

All experiments were performed in duplicate and the average of duplicates taken. Data was analyzed in Microsoft Excel 2013. Absolute rate data was expressed as a percent change to control. GraphPad Prism 6 software was used to perform statistical analyses. Two-tailed paired Student T-Test and one-way or two-way analysis of variance (ANOVA) with Tukey's post-hoc test were used for statistical analysis. All values are shown as mean +/- SEM (standard error mean). (* or # < 0.05, ** or ## < 0.01, *** or ### P < 0.001, **** or #### P < 0.0001).

3. Results

3.1 Mouse genotyping and immunoblotting for NDUFS4

Successful knockout of the NDUFS4 was achieved by the removal of exon 2 in the gene encoding this protein. Mice heterozygous (NDUFS4^{+/-}) or homozygous (NDUFS4^{-/-}) and WT littermates were identified by amplifying the *Ndufs4* gene by PCR and agarose gel electrophoresis (Figure 3.1). Ear notch samples from NDUFS4^{+/-} mice contained two PCR products at ~200 and 400 bp, respectively. By contrast, the WT PCR product had a mass of ~200 bp and the NDUFS4^{-/-} samples contained a ~400 bp fragment. To confirm successful knockout the absence or presence of the NDUFS4 protein by immunoblot was examined. Figure 3.2 demonstrates that mice that were identified as homozygous for the *Ndufs4* gene did not contain any detectable protein whereas heterozygotes displayed a ~50% decrease relative to the WT samples.

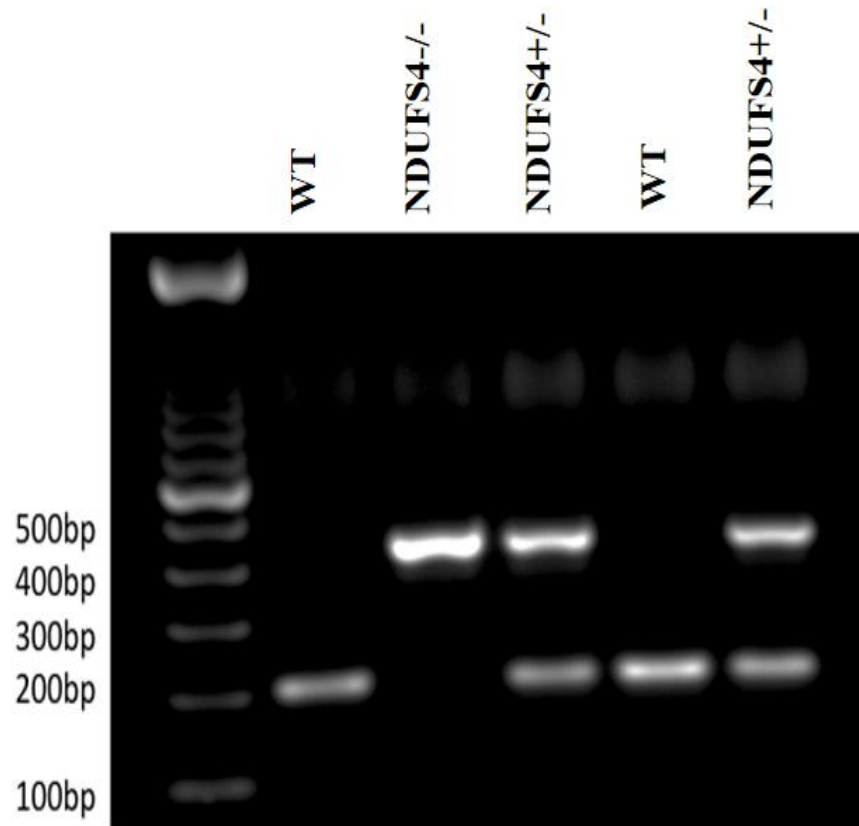


Figure 3.1- Identification of mice heterozygous or homozygous for the *Ndufs4* gene by PCR and agarose gel electrophoresis

Genetic material was extracted from ear notches and subjected to PCR amplification and then the relative size of the product was assessed by agarose gel electrophoresis. A band at 200 bp or 400 bp band corresponded to samples collected from WT or NDUFS4^{-/-} mice. NDUFS4^{+/-} samples contained both 200 bp and 400 bp.

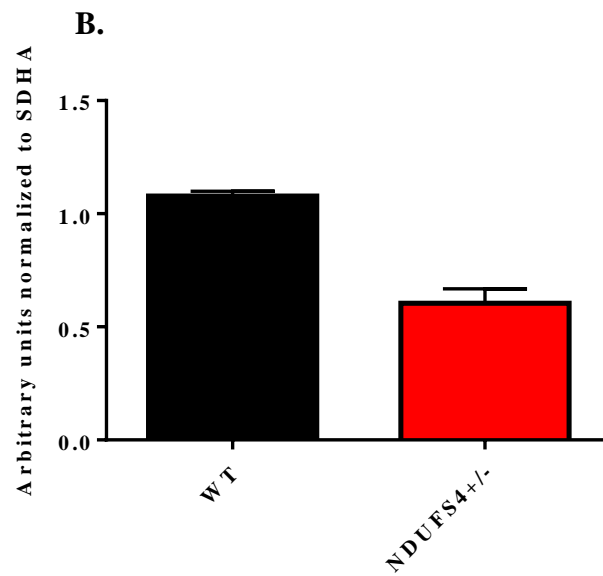
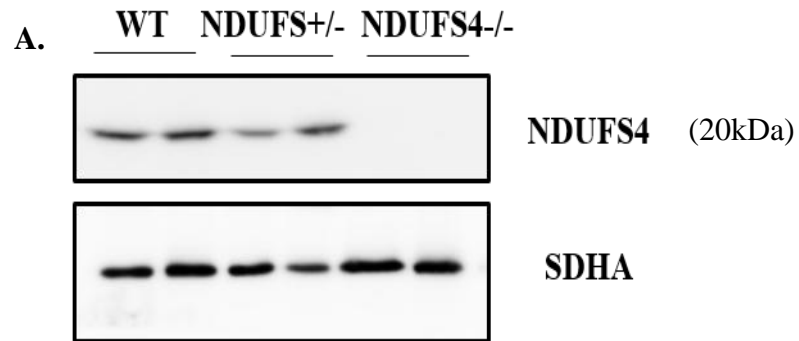


Figure 3.2- Confirmation of partial or full ablation of NDUFS4 protein expression

- A) Western blot analysis of NDUFS4 protein levels in liver mitochondria. Succinate dehydrogenase subunit A (SDHA) was used as the loading control B) Densitometric analysis of NDUFS4 normalized to SDHA. N=2.

3.2 Impact of NDUF54 deficiency on organ and body weight

Mice homozygous for the *Ndufs4* gene rapidly develop severe encephalomyopathy and heart disease by 5-6 weeks of age, which is associated with deficiencies in linear growth (105,106). Thus, before proceeding, we wanted to ensure that the partial deletion of the *Ndufs4* gene did not alter linear growth. Changes in body weight were monitored once a week from 4 to 8 weeks of age. WT and NDUF54+/- mice displayed no difference in overall body weight over the 5-week period, an observation that is consistent with previous publications (105,107) (Figure 3.3). We also weighed heart and liver tissue to ascertain if NDUF54+/- mice displayed any abnormal changes in these organs. It was observed that the partial deletion of the *Ndufs4* gene induced no changes in cardiac (Figure 3.4) or liver weight (Figure 3.5).

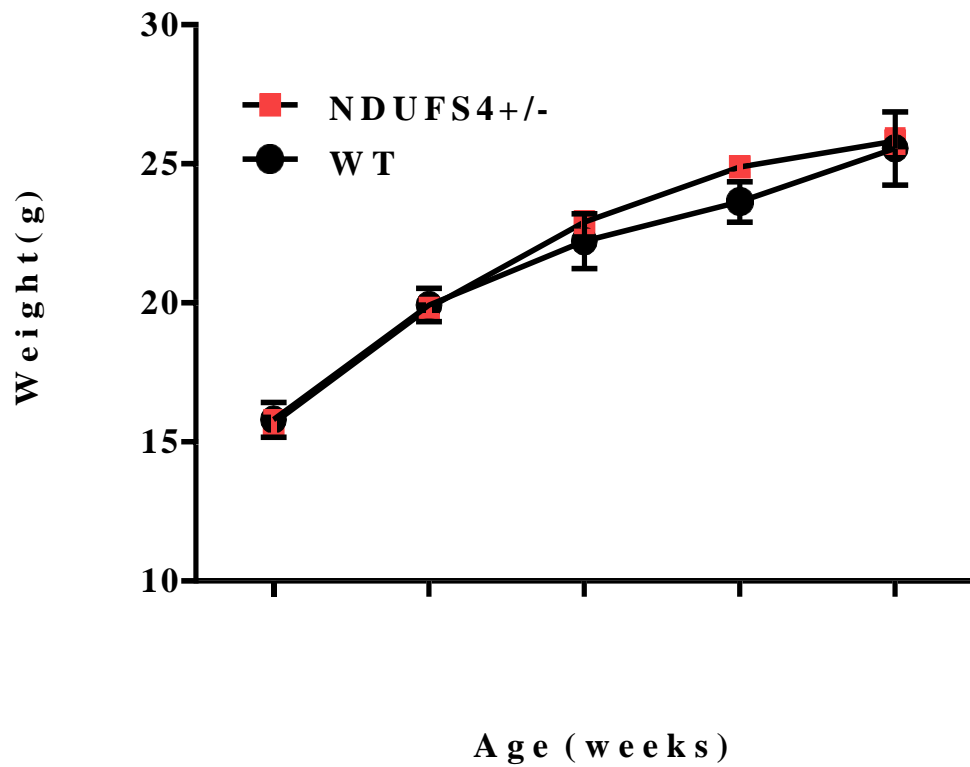


Figure 3.3-Body weight profile for WT and NDUFS4^{+/-} mice

Overall body weight of mice in grams measured weekly from 4-8 weeks. Data are mean \pm SEM, N= 5-6, Two-way ANOVA with a Tukey's post-hoc test.

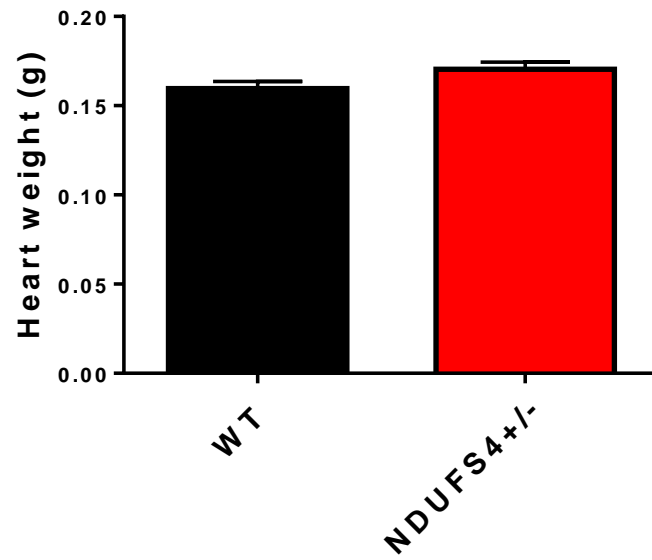


Figure 3.4- Heart weight profile for WT and NDUFS4^{+/-} mice

Cardiac weight in grams was measured. Data are mean \pm SEM, N=5-6, paired two-tailed Student T-Test.

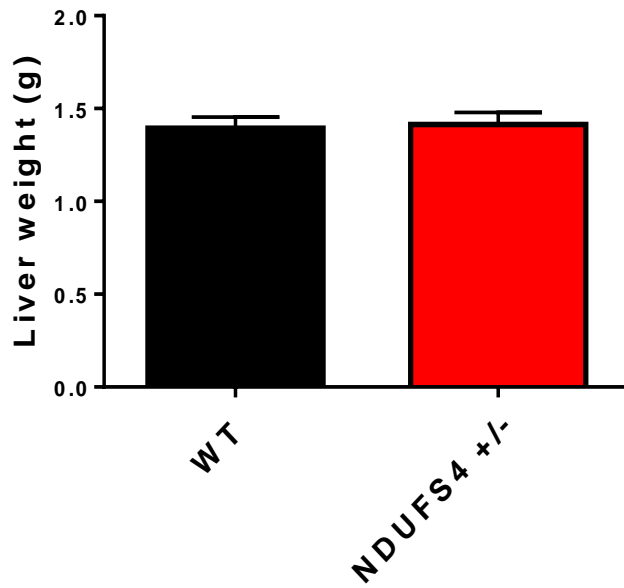


Figure 3.5-Liver weight profile for WT and NDUFS4^{+/-} mice

Mass of the liver (g) was measured. Data are mean \pm SEM, N=5–6, paired two-tailed Student T-Test.

3.3. Examination of the $O_2^{\bullet-}/H_2O_2$ release potential of NDUFS4 deficient mitochondria

It has been proposed by Chouchani *et al.* that Complex I is the only source of $O_2^{\bullet-}/H_2O_2$ following IR injury (102). Therefore, we postulated that if this were true then a ~50% decrease in Complex I levels would lower ROS release from mitochondria. First, we examined if liver mitochondria from NDUFS4^{+/-} mice displayed any changes in ROS release. Mitochondria were supplemented with pyruvate, 2-oxoglutarate, or succinate in the absence of ADP to induce state 4 respiratory conditions. We chose these respiratory conditions since state 4 respiration hyperpolarizes the mitochondrial inner membrane allowing for a more robust measure of the velocity of ROS production. In addition, state 4 conditions favor reverse electron flow to Complex I in the respiratory chain, allowing us to ascertain if partial loss of NDUFS4 affects the rate of ROS production. Liver mitochondria from NDUFS4^{+/-} mice oxidizing pyruvate (50 μ M) and malate (50 μ M) displayed no change in $O_2^{\bullet-}/H_2O_2$ production when compared to samples from WT littermates (Figure 3.6). To confirm this observation, we conducted a similar experiment using 2-oxoglutarate, another Krebs cycle substrate. No change in the rate of $O_2^{\bullet-}/H_2O_2$ production was observed in NDUFS4^{+/-} mitochondria (Figure 3.6). Next, we tried succinate, which by-passes the Krebs cycle feeding electrons directly into the respiratory chain at the level of Complex II. In addition, succinate was reported to be a potent inducer of mitochondrial ROS release (109). Liver mitochondria oxidizing succinate (50 μ M) displayed no change in the rate of ROS production (Figure 3.6). Similar studies were carried out using cardiac mitochondria from WT and NDUFS4^{+/-} mice. Mitochondria were supplemented with

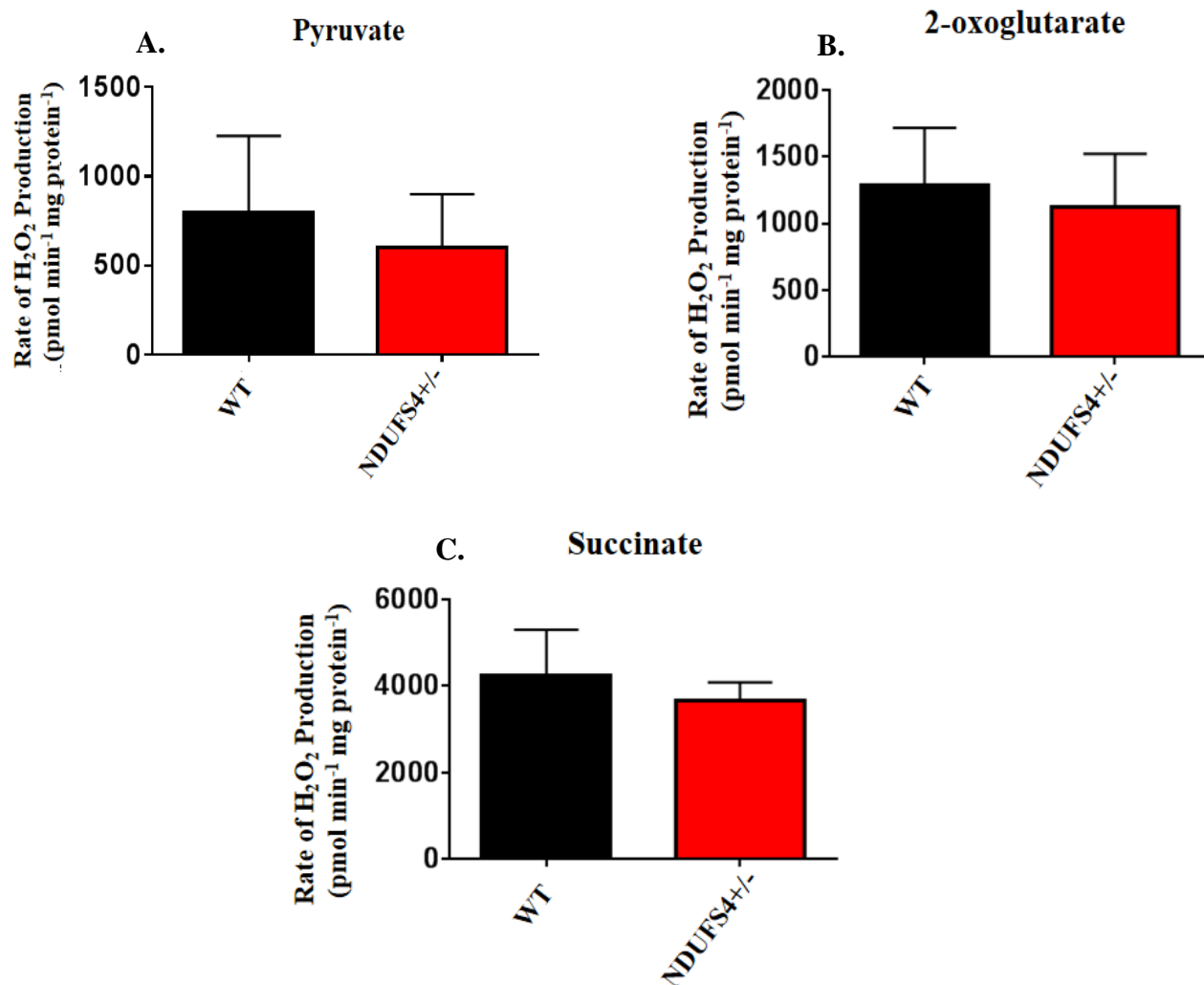


Figure 3.6-Partial loss of the *Ndufs4* gene does not alter O₂[•]/H₂O₂ release from liver mitochondria

The rate of O₂[•]/H₂O₂ production by liver mitochondria supplemented with A) 50 μM pyruvate and 50 μM malate, B) 50 μM 2-oxoglutarate and 50 μM malate, or C) 50 μM succinate was estimated using the AUR assay. Changes in fluorescence were measured at 565/600 nm. Data are mean ± SEM, N = 5, paired two-tailed Student T-Test.

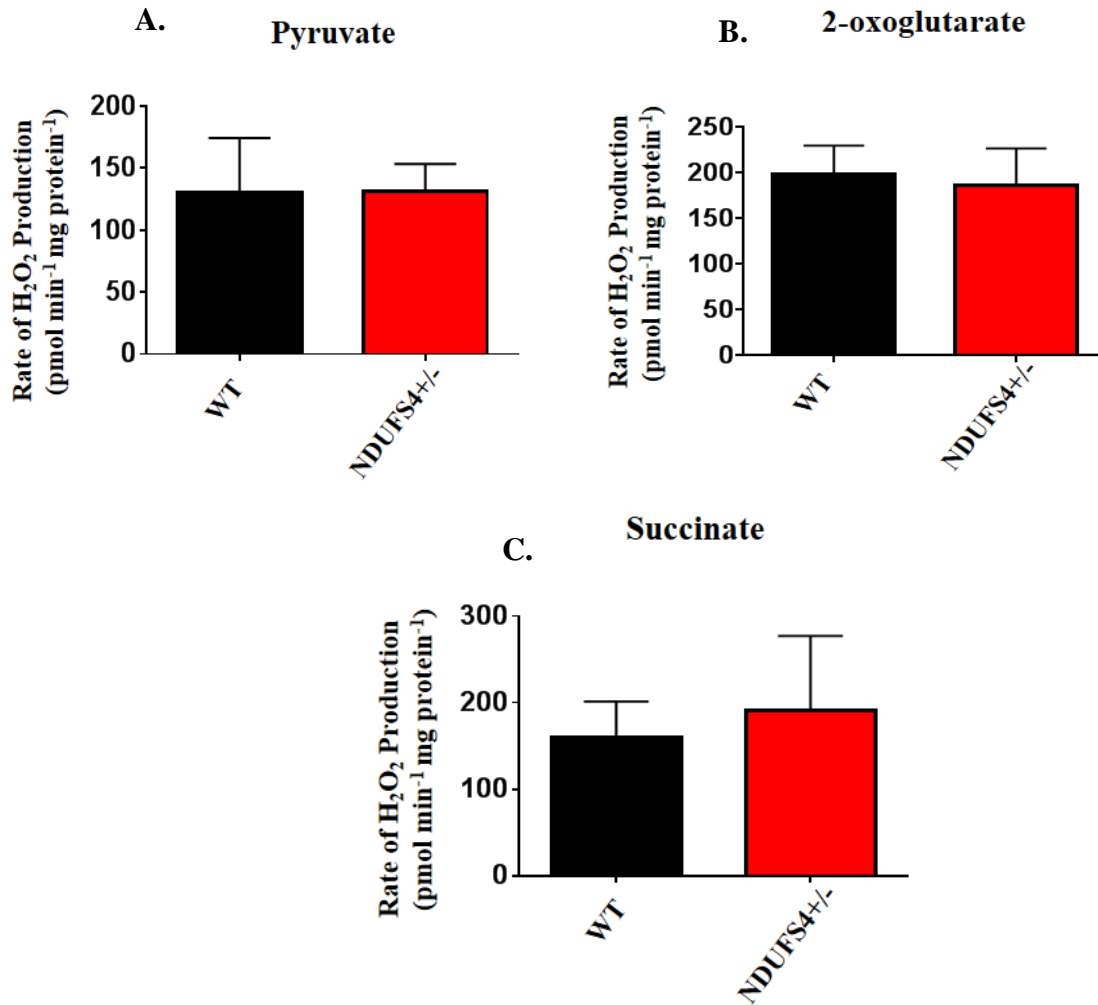


Figure 3.7- Partial loss of the *Ndufs4* gene does not alter O₂[•]/H₂O₂ release from cardiac mitochondria

The rate of O₂[•]/H₂O₂ production by cardiac mitochondria supplemented with A) 50 μM pyruvate and 50 μM malate, B) 50 μM 2-oxoglutarate and 50 μM malate, or C) 50 μM succinate was estimated using the AUR assay. Changes in fluorescence were measured at 565/600 nm. Data are mean ± SEM, N = 5, paired two-tailed Student T-Test .

pyruvate, 2-oxoglutarate, or succinate as described above and then rates for ROS release were recorded. No changes were observed in the rate of $O_2^{\bullet-}/H_2O_2$ production (Figure 3.7). Collectively, these findings indicate that partial loss of NDUFS4 does not alter $O_2^{\bullet-}/H_2O_2$ production under state 4 respiratory conditions.

3.4 Identification of the high capacity sites for $O_2^{\bullet-}/H_2O_2$ production in liver and heart mitochondria

As indicated above, Chouchani *et al* indicated that Complex I was the sole ROS source in cardiac tissue subjected to IR injury (102). However, our group and others have demonstrated that mitochondria in liver, heart and muscle can contain up to 12 sites for ROS production (103,110,111). In addition, our group has found that Complex I makes a negligible contribution to overall ROS production in liver mitochondria and Complex III is the major producer in cardiac mitochondria (110,111). Therefore, whether or not Complex I was 1) a major ROS generator and 2) the only ROS source of production, was tested in liver and cardiac mitochondria. To do so, different site-specific ROS release inhibitors were used (Figure 2.3).

First, which sites served as major ROS producers in liver mitochondria was examined with pyruvate or 2-oxoglutarate (Figure 3.8). Malate was also included in the reaction mixtures to prime the Krebs cycle. We chose to examine ROS release from liver mitochondria from WT or NDUFS4^{+/-} first since we had previously established that OGDH, PDH, and Complex III were the chief producers in liver mitochondria from C57Bl6N mice (110). All the inhibitors significantly decreased ROS production by liver mitochondria supplemented with either pyruvate or 2-oxoglutarate in comparison to the control (no inhibitor added). KMV and CPI-613 decreased ROS production by $\geq 90\%$ in liver mitochondria collected from WT and NDUFS4 mice. It is important to note that both inhibitors can also impede mitochondrial NADH

production, an important factor for ROS release from the respiratory chain. Therefore, inhibitors for Complex II and III were utilized to ascertain how much ROS was released from either site. Myxothiazol lowered ROS production by ~50% in WT and NDUFS4^{+/-} liver mitochondria (Figure 3.8). In addition, atpenin A5 decreased production by ~80% relative to control (no inhibitors) (Figure 3.8). It is worthy to note as well that we observed no statistical differences in the rates of ROS release between WT and NDUFS4^{+/-} liver mitochondria treated with or without the different inhibitors except in mitochondria treated with myxothiazol. In that particular case, a small but significant increase in ROS release was observed in the NDUFS4^{+/-} mitochondria when compared to WT samples treated with myxothiazol (Figure 3.8). Based on these findings, Complexes II and III serve as the major sources of ROS release in liver mitochondria when Krebs cycle-linked metabolites serve as substrates. It is also likely that PDH and OGDH make minor contributions as well and Complex I makes a negligible contribution.

Next, the high velocity sites for ROS release were examined in heart mitochondria. Experiments were initially designed as described above, utilizing pyruvate or 2-oxoglutarate and malate as substrates (Figure 3.9). It was found that KMV and CPI-613 augmented ROS release, but only when pyruvate served as the substrate (Figure 3.9). Inclusion of KMV or CPI-613 did not change ROS production when 2-oxoglutarate served as the substrate. This could be attributed to the inhibition of NADH production which would limit the production of ROS by the electron transport chain. when pyruvate was the substrate (Figure 3.9).

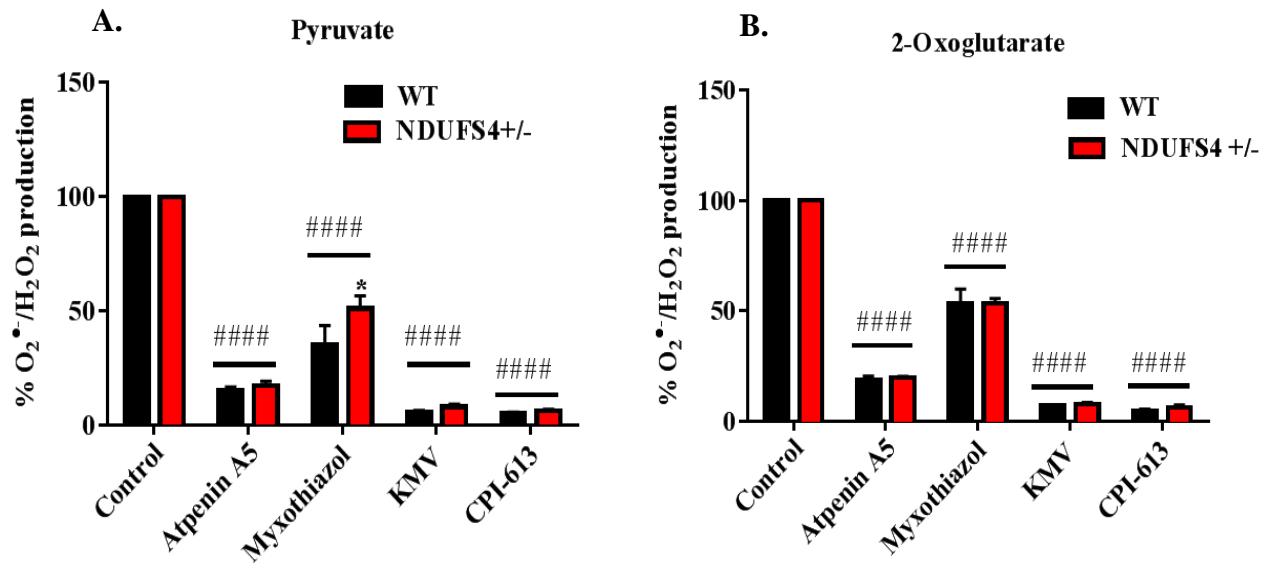


Figure 3.8- Assessment of which enzymes serve as high velocity ROS producers in liver mitochondria

Liver mitochondria were supplemented with (A) 50 μ M pyruvate or (B) 50 μ M 2-oxoglutarate and treated with or without 10 mM KMV, 250 μ M CPI-613, 4 μ M myxothiazol, or 40 μ M atpenin A5 and then ROS release rates were tracked with AUR reagent. All samples were also supplemented with 50 μ M malate. Changes in fluorescence were measured at 565/600 nm. Results were normalized to control ROS release rates to estimate the individual contributes of the different sites towards overall production. Data are mean \pm SEM, N = 5, Two-way ANOVA with Tukey's post hoc test, *P < 0.05, #####P < 0.001. * corresponds to statistical comparisons between genotypes for mitochondria treated with or without inhibitors and # corresponds to statistical comparisons of inhibitor effect relative to control.

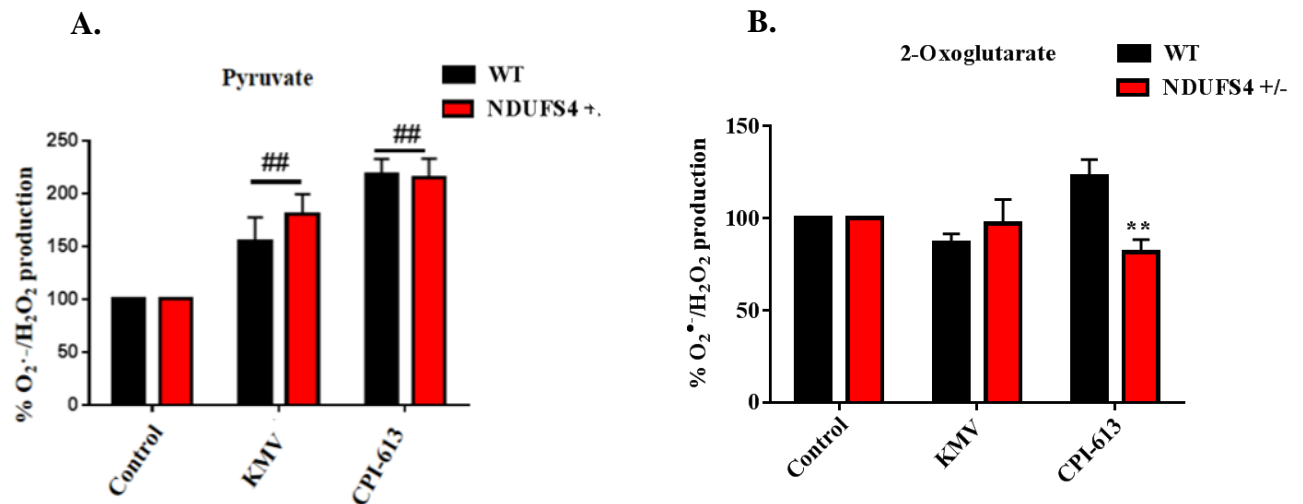


Figure 3.9-The electron transport is the major source for ROS release in cardiac mitochondria

Cardiac mitochondria were supplemented with (A) 50 μ M pyruvate or (B) 50 μ M 2-oxoglutarate and treated with or without 10 mM KMV or 250 μ M CPI-613 and then ROS release rates were tracked with AUR reagent. All samples were also supplemented with 50 μ M malate. Changes in fluorescence were measured at 565/600 nm. Results were normalized to control ROS release rates to estimate the individual contributes of the different sites towards overall production. Data are mean \pm SEM, N = 5, Two-way ANOVA with Tukey's post hoc test, **P<0.01, ## P<0.01. * corresponds to statistical comparisons between genotypes for mitochondria treated with or without inhibitors and # corresponds to statistical comparisons of inhibitor effect relative to control.

Few differences in the ROS release profile were observed between WT and NDUFS4^{+/-} cardiac mitochondria (Figure 3.9). However, it was noted that NDUFS4^{+/-} mitochondria treated with KMV displayed a higher rate of ROS release when compared to WT mitochondria

3.5 O₂^{•-}/H₂O₂ production by cardiac tissue supplemented with succinate

The results collected in Figure 3.9 indicate that the electron transport chain may be the chief site for ROS release in cardiac mitochondria. Succinate does induce high rates of ROS release in cardiac mitochondria and our group has found that Complex I and III are the main generators in heart tissue (111). In addition, other groups have found that succinate does accumulate in cardiac tissue following reperfusion injury, driving high rates of ROS release from the respiratory chain (111). Therefore, mitochondria oxidizing only succinate was used to identify which complex in the electron transport chain produced the most ROS. No genotype effect was observed indicating WT and NDUFS4^{+/-} display similar rates of ROS release in the absence or presence of the different inhibitors and when succinate served as the sole source of electrons (Figure 3.10). However, it was found that Complex III was the major source of ROS in cardiac mitochondria oxidizing succinate under state 4 respiratory conditions. Indeed, myxothiazol induced a ~50% decrease in ROS release relative to control in WT and NDUFS4^{+/-} cardiac mitochondria (Figure 3.10). It was also observed that rotenone, which inhibits reverse electron flow to Complex I, thereby curtailing ROS release, also decreased O₂^{•-}/H₂O₂ production by ~30%. Finally, atpenin A5, which also blocks flow from Complex II to the rest of the chain, decreased ROS production by almost 80% (Figure 3.10). Therefore, the hierarchy for ROS release from highest to lowest in cardiac mitochondria is Complex III (~50% production) > Complex I (~30% production) > Complex II (~20% production) when succinate is the substrate.

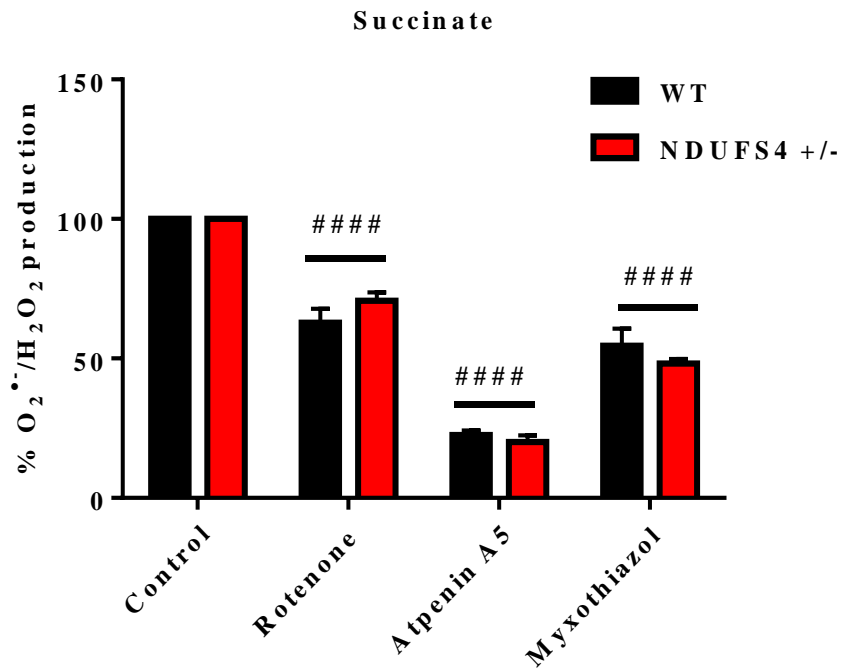


Figure 3.10- Complex III is the major ROS source in cardiac mitochondria

Cardiac mitochondria were supplemented with 50 μ M succinate and treated with 4 μ M rotenone, 4 μ M myxothiazol, or 40 μ M atpenin A5 and then ROS release rates were tracked using the AUR assay. Changes in fluorescence were measured at 565/600 nm. Results were normalized to control ROS release rates to estimate the individual contributes of the different sites towards overall production. Data are mean \pm SEM, N = 5, Two-way ANOVA with Tukey's post hoc test, #####P <0.001. * corresponds to statistical comparisons between genotypes for mitochondria treated with or without inhibitors and # corresponds to statistical comparisons of inhibitor effect relative to control.

3.6 Assessment of the induction of electrophilic cell signaling pathways

It is possible that increased expression of H₂O₂ clearing enzymes could account for the lack of difference in ROS release between cardiac mitochondria isolated from WT and NDUFS4^{+/-} mice. Therefore, we conducted immunoblot analyses to determine if mitochondrial H₂O₂ clearing enzymes, GPX1 and TRX2, displayed any changes in protein levels. It was found that partial deletion of the *Ndufs4* gene increased the protein levels of both GPX1 and TRX2, two crucial enzymes involved in eliminating ROS (Figure 3.11). Collectively, these results demonstrate that the lack of difference in ROS release between WT and NDUFS4^{+/-} mice was related to an increase in antioxidant defenses.

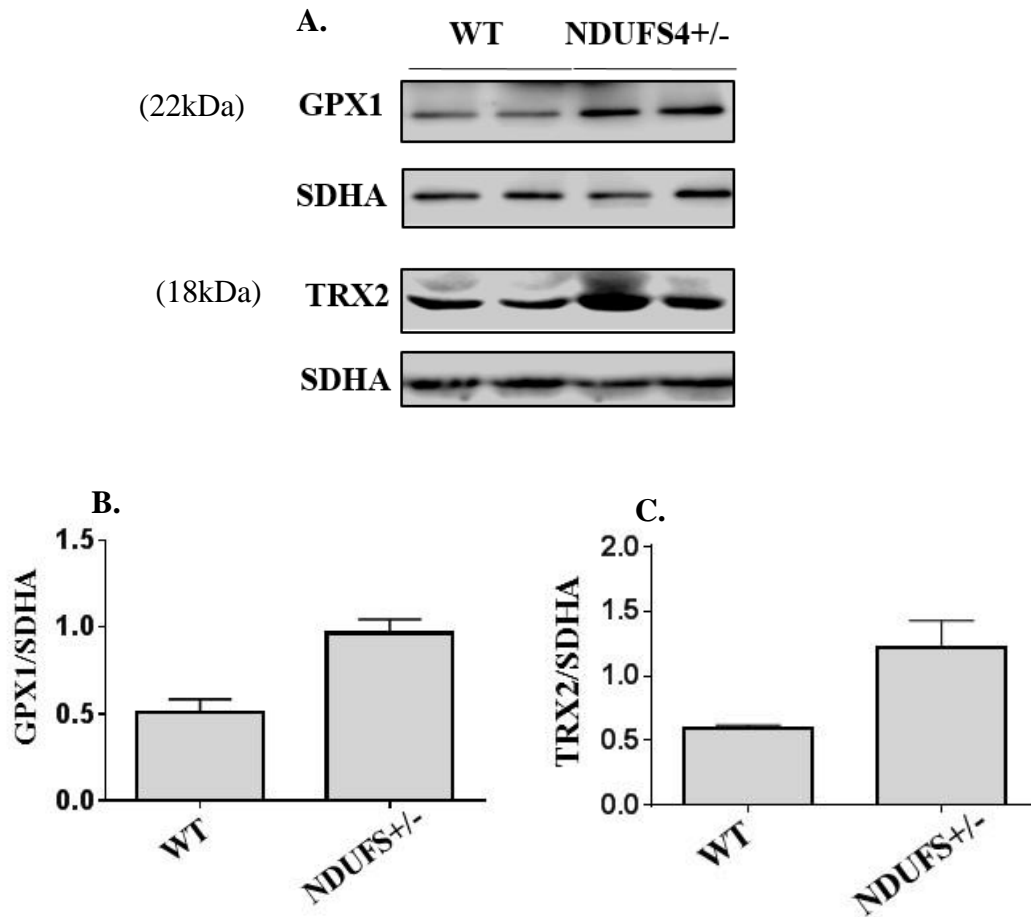


Figure 3.11- Partial deletion of the *Ndufs4* gene increases GPX1 and TRX2 levels

NDUFS4 deficiency increased the induction of electrophilic stress signaling pathways. A) Western blot with 10 μ g protein using anti-GPX1 and anti-TRX2 wherein SDHA was used as a loading control. B) Densitometry analysis of GPX1/SDHA. C) Densitometry analysis of TRX2/SDHA. Data are mean \pm SEM, n=2.

3.7 Examination of the effect of IR injury on NDUFS4-deficient mice

3.7.1 Impact of NDUFS4 deficiency on contractile recovery from reperfusion injury

The results collected above indicate that there is no difference in the ROS release profile in cardiac mitochondria collected from mice with a partial deficiency in the *Ndufs4* gene, which could be related to an increase in electrophilic stress signaling and the increased expression of antioxidant defense enzymes. It was also observed that Complex III is the major ROS source, not Complex I. Next, the response of NDUFS4^{+/-} mice towards reperfusion injury was assessed. During the normal perfusion period, the WT and NDUFS4^{+/-} mice displayed a similar cardiac output (LVDP*HR index) (Figure 3.12). However, after 15 minutes of ischemia, the functional recovery of the WT hearts are much better than NDUFS4^{+/-} hearts (Figure 3.12). Following a 30 minute full reperfusion, both WT and NDUFS4^{+/-} hearts were subsequently sectioned and subjected to TTC staining to evaluate cardiac post-ischemic injury (infarct size). It was found that infarct size comprised ~60% of the total myocardial area in NDUFS4^{+/-} hearts whereas it made up ~39% of the area in WT samples (Figure 3.13). Taken together, partial loss of Complex I sensitizes the myocardium to ischemia-reperfusion injury leading to cardiac dysfunction.

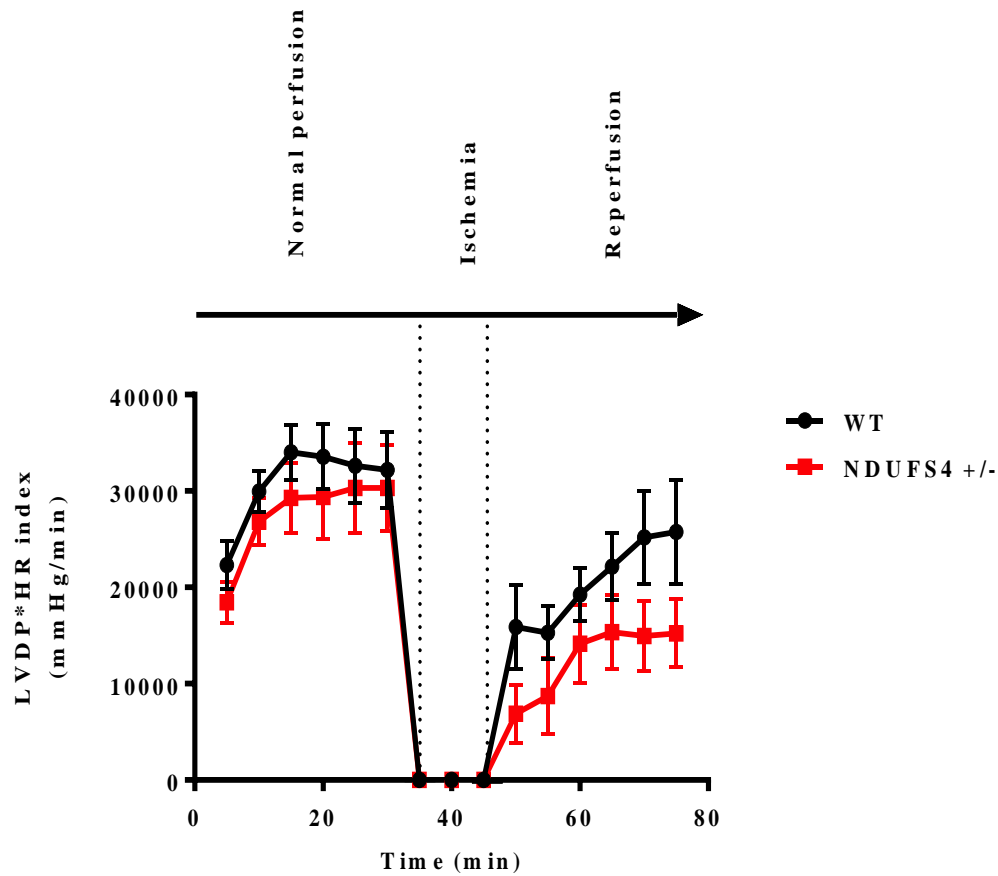


Figure 3.12-Comparison of the contractile status between the genotypes

The cardiac output of the NDUFS4^{+/-} and the WT mice was compared using a Langendorff assembly at several stages. Data are mean ± SEM, N=5, paired two-tailed Student T-Test.

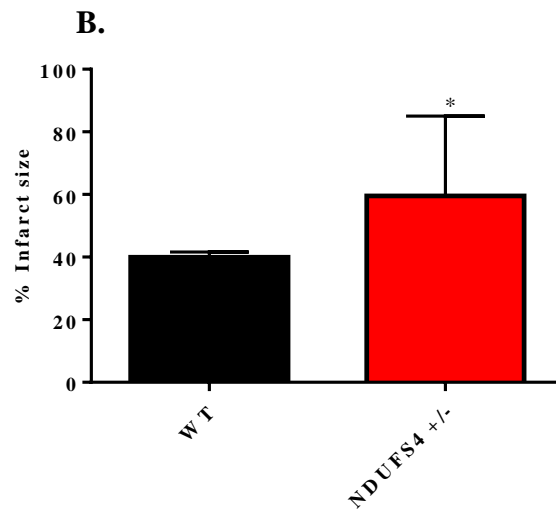
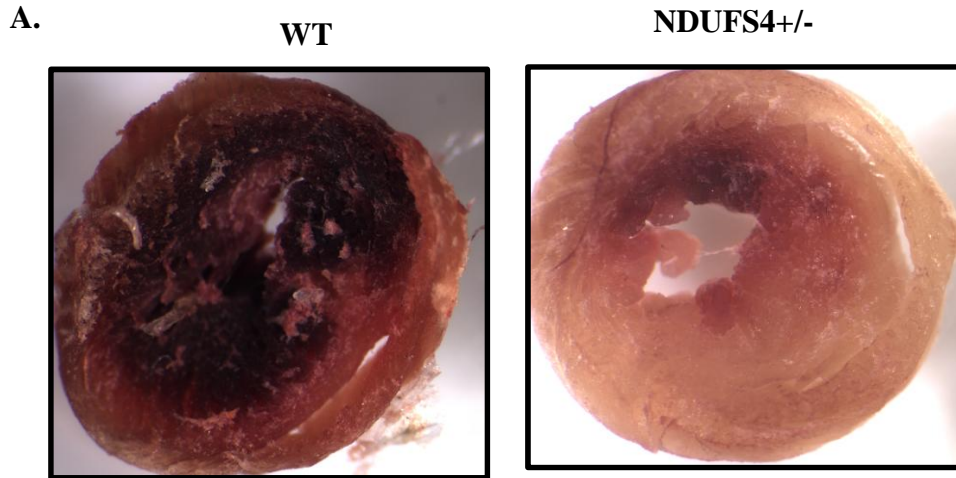


Figure 3.13-Comparison of the infarct size in WT and NDUFS4^{+/-} hearts following an IR challenge.

Myocardial necrosis determined by (A) TTC staining and (B) quantification of the affected area. Data are mean ± SEM, N = 9, paired two-tailed Student T-Test, *P < 0.05.

3.7.2. Partial loss of Complex I augments ROS release from NDUFS4^{+/-} mitochondria following reperfusion injury.

Our finding that NDUFS4^{+/-} cardiac mitochondria contain higher amounts of H₂O₂ eliminating enzymes led to the genesis of the hypothesis that the increased sensitivity of the myocardium towards IR injury in Complex I deficient mice is related to increased mitochondrial ROS production. Therefore, we tested the ROS forming potential of cardiac mitochondria isolated from WT and NDUFS4^{+/-} mice subjected to IR injury. It was found that NDUFS4^{+/-} mitochondria produced significantly more ROS than WT samples regardless of substrate (Figure 3.14). Indeed, oxidation of pyruvate, 2-oxoglutarate, or succinate induced between a ~50-100% increase in ROS production by NDUFS4^{+/-} mitochondria following IR injury (Figure 3.14). We wanted to determine if these affects were related to changes in the redox potential of the mitochondrial nicotinamide pools. No changes in mitochondrial NAD(P)H levels were observed indicating the changes in ROS release were not associated with the capacity to generate NADH or NAD(P)H (Figure 3.15).

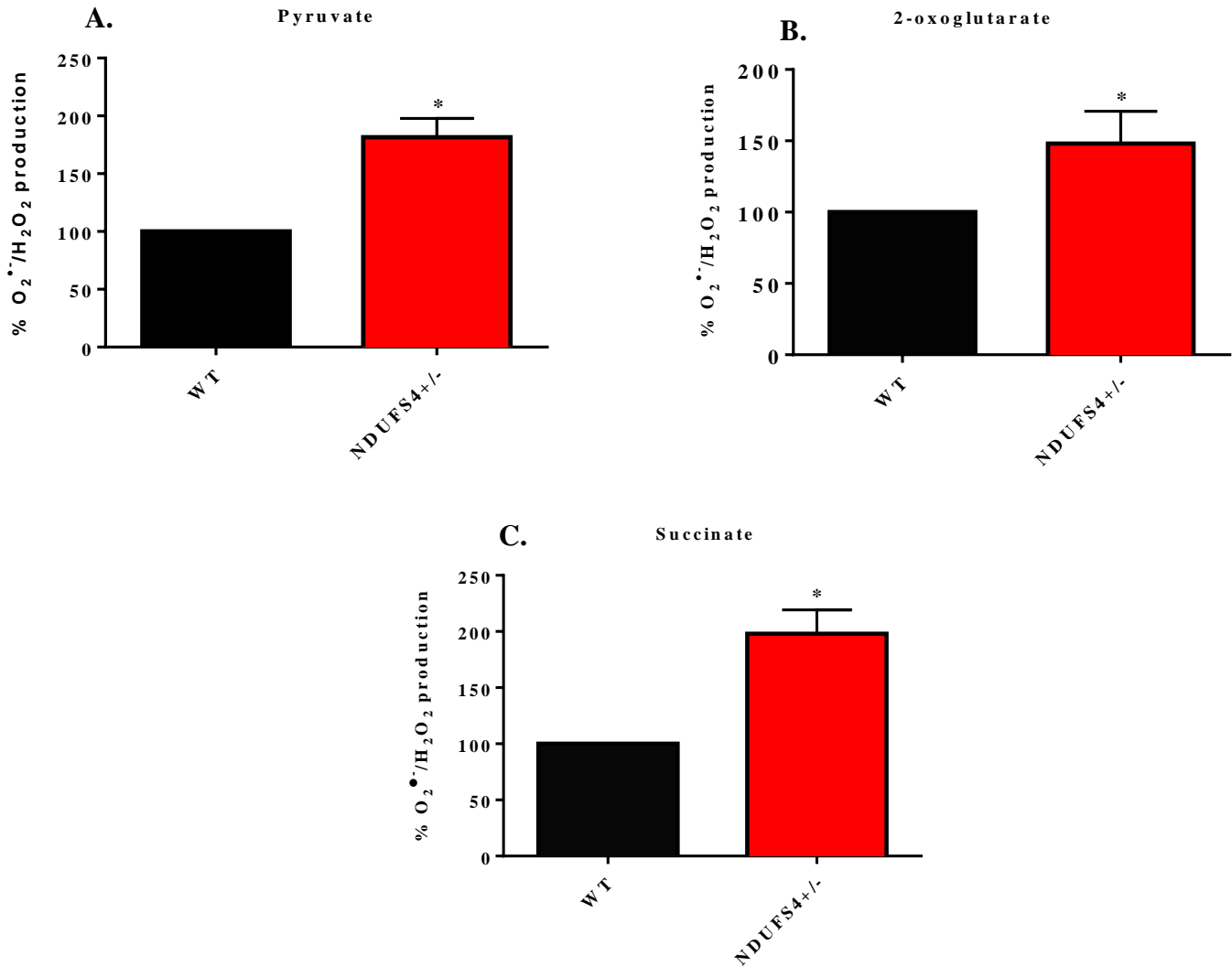


Figure 3.14-Assessment of the % O₂^{•-}/H₂O₂ production between the genotypes in IR challenged cardiac tissues

Comparing the % ROS production between the NDUFS4^{+/-} and the NDUFS4^{+/+} mice supplemented with 50 μM malate with either 50 μM (A) pyruvate or (B) 2-oxoglutarate or (C) succinate. AUR fluorescence was measured at 565/600 nm. Data are mean ± SEM, N = 5, paired two-tailed Student T-test, *P < 0.05.

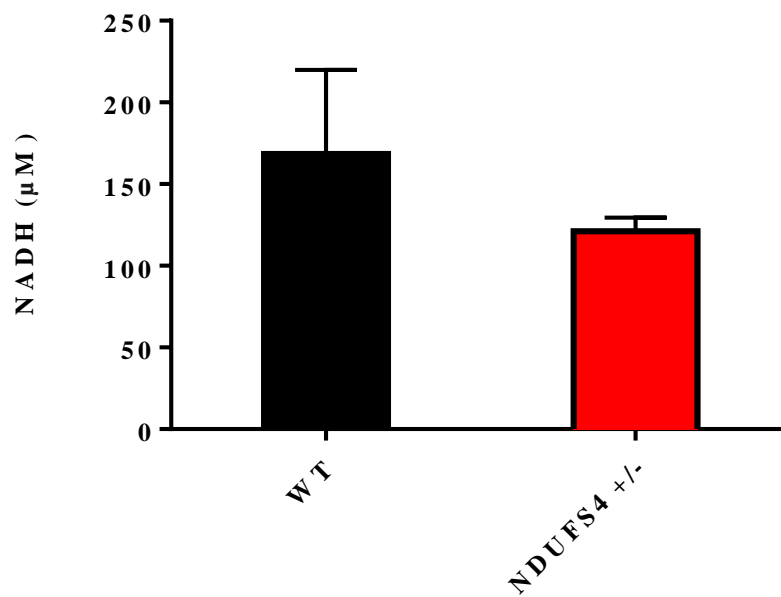


Figure 3.15-Comparison of the NADH driven ROS production between the genotypes

AUR fluorescence was measured at 376-420 nm. Data are mean \pm SEM, N =4- 5, paired two-tailed Student T-Test.

3.8 Utilization of Complex I knockout mitochondria to assess NADH-driven ROS release by OGDH and PDH

It has been known for some time that Complex I can generate high amounts of ROS by reverse electron flow from Complex II when the mitochondrial inner membrane is highly polarized (e.g. under state 4 respiratory conditions). It has also been documented that OGDH and PDH can also produce ROS by reverse electron flow from NADH (110,112). In this scenario, accumulation of NADH due to defective Complex I activity results in its re-oxidation by OGDH and PDH, inducing ROS release from the E3 subunit of either enzyme complex. However, all studies demonstrating that OGDH and PDH can form ROS by reverse electron flow have been conducted with purified enzymes (112). Therefore, the physiological relevance of ROS production from either enzyme by reverse flow has always been questioned. Since we possessed a Complex I deficient mouse model, we decided to test if ROS could be produced by liver and cardiac mitochondria treated with different concentrations of NADH. For these assays, we isolated mitochondria from 5-week old mice homozygous for *Ndufs4* to ensure that there would be no Complex I to turn over NADH. Mitochondria were permeabilized to allow NADH uptake which also depolarized mitochondria inhibiting transhydrogenase activity and preventing reverse electron flow in the ETC. As demonstrated in Figure 3.16, a robust increase in ROS release was observed with increasing NADH levels. As per the results obtained by our experiments we could see a concentration dependent increase in the $O_2^{\bullet-}/H_2O_2$ production in the liver tissue with the increasing concentration of NADH (Figure 3.16). A significant increase in the % $O_2^{\bullet-}/H_2O_2$ production was seen when 5 μ M and 10 μ M NADH was used in the liver tissue. Similarly, the cardiac tissue was also supplemented with various concentrations of NADH. The results obtained in the cardiac tissues were similar to that obtained in the liver tissues. A concentration

dependent increase was seen in the % $O_2^{\bullet-}/H_2O_2$ production with the increasing NADH concentrations. A significant increase in the % $O_2^{\bullet-}/H_2O_2$ production was seen when 5 μM NADH was used (Figure 3.16). Thus, these results prove NADH to be responsible for the increase in ROS production. These preliminary results show that NADH can induce ROS release potentially by OGDH and PDH by RET.

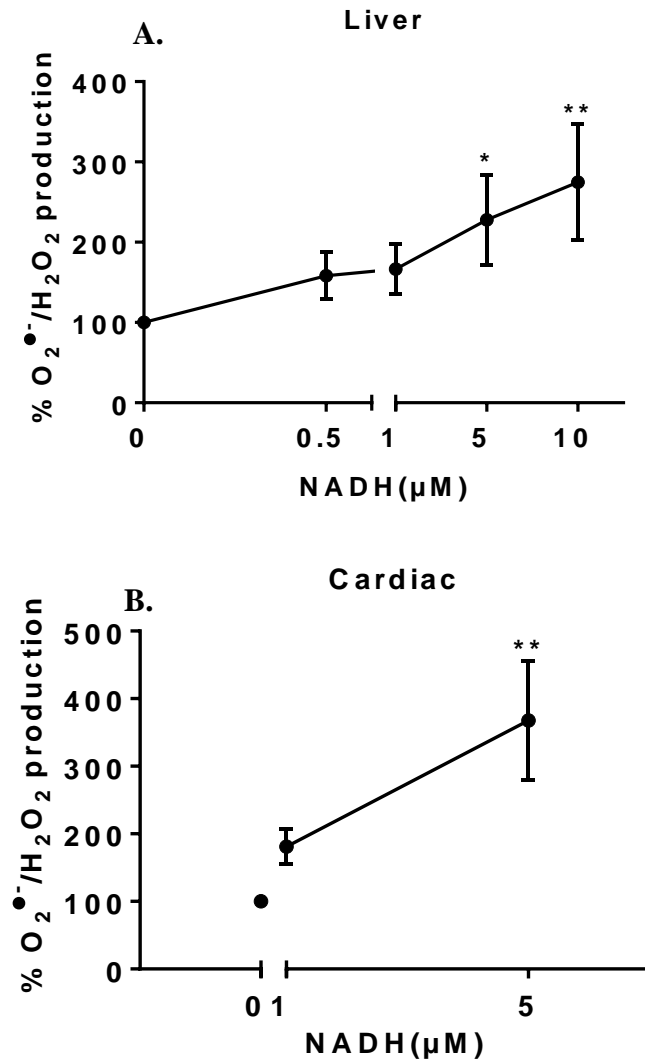


Figure 3.16-Assessment of % $\text{O}_2^{\bullet-}/\text{H}_2\text{O}_2$ production in mitochondria supplemented with NADH

A) 0.3 mg/ml liver mitochondria was supplemented with 0 μM - 10 μM NADH or (B) 0.1 mg/ml cardiac mitochondria was supplemented with 0 μM - 5 μM NADH. AUR fluorescence was measured at 565/600 nm. N = 4, One-way ANOVA with a Tukey's post-hoc test, *P < 0.05 and **P < 0.01.

4. Discussion

4.1 Summary

ROS are oxygen-containing free radicals formed due to the premature leaking of the electrons from the flavin-containing dehydrogenases or electron carriers in the ETC to oxygen. ROS have a dual nature; at higher concentrations, they can be harmful but can serve as signaling molecules at low levels (114). ROS can be produced by various sites in the electron transport chain or by flavin-containing enzymes that combust carbon. For the past decade, Dr. Martin Brand's group has been characterizing the velocity of ROS release from these individual sites in permeabilized muscle mitochondria (103). OGDH and PDH were found to produce 8x and 4x more ROS, respectively, when compared to Complex I and Complexes II and III served as high capacity sites for release as well (103). Complex I can be a critical source but only during reverse electron flow from the UQ pool. Chouchani *et al* proposed that Complex I is the sole ROS source in mitochondria from hearts subjected to IR injury. This is unlikely considering it is well known that mitochondria can contain a number of ROS sources. Therefore, the goal of this thesis was to ascertain if Complex I was the sole ROS source in hearts subjected to IR injury. This was tested using a mouse model that had a 50% decrease in Complex I availability due to partial removal of the *Ndufs4* gene. The findings from my thesis indicate that Complex II and III are major sources in liver mitochondria with OGDH and PDH making minor contributions (109). In cardiac mitochondria on the other hand, it was demonstrated that the hierarchy of production, from highest to lowest capacity site, was Complex III > Complex I > Complex II with OGDH and PDH making negligible contributions (109). Thus, Complex I was not the sole producer of ROS in heart mitochondria (109). Moreover, it was found that mice heterozygous for the *Ndufs4* gene displayed increased sensitivity towards reperfusion injury. These results not only contradict the

findings by Chouchani *et al.*, but also show that fully active Complex I may be vital for protecting the heart from ischemic damage. Indeed, loss of Complex I sensitized hearts towards reperfusion injury which was associated with diminished heart performance recovery. These results correlated strongly with an increase in mitochondrial ROS release indicating that Complex I may play a critical role in preserving electron transfer efficiency in the respiratory chain (109). It is important to point out that there were no differences in ROS release from WT or NDUFS4^{+/-} mitochondria isolated from hearts and liver tissue not subjected to IR challenge. However, this may be associated with an increase in the protein levels of the ROS clearing enzymes, GPX1 and TRX2 (109).

4.2 Complex I is not the sole ROS source during myocardial reperfusion injury

Complex I is often considered the most important ROS source in cells, including cardiac tissue (102). In addition, it was recently reported that Complex I is the sole ROS source in cardiac tissue, accounting for 100% of the damage associated with reperfusion injury (102). Ischemia followed by reperfusion can cause considerable damage to the myocardium and is still considered the number one contributor to heart disease (102). Ischemia cuts off the supply of oxygen and nutrient rich blood to the myocardium. As noted in the introduction, this can have a number of effects including acidification of the myocardium and the accumulation of purine nucleotides. In mitochondria, ischemia results in the over-reduction of the respiratory chain and the accumulation of several metabolites, including NADH and succinate. NADH accumulates due to the absence of O₂ and electron flow in the respiratory chain and subsequent return of protons to the matrix by Complex V (or other solute transporters). According to Chouchani *et al.*, the accumulation of succinate occurs due to the reduction of fumarate by the reversal of Complex II (102). Fumarate is generated by the purine nucleotide chain (PNC) or malate

aspartate shunt (MAS) which is then taken up by mitochondria and converted to succinate through reverse electron flow from the UQ pool to the active site of Complex II (102).

Subsequent reperfusion of the myocardial tissue restores oxygen and nutrient levels which is vital for the recovery of viable tissue. However, it paradoxically induces heart damage and can account for $\geq 50\%$ of the injury associated with ischemia-reperfusion (122). Although a clear picture for the mechanism of reperfusion injury has started to develop, the role of mitochondria in this process still remains poorly understood. According to Chouchani *et al*, succinate accumulation during ischemia is responsible for reperfusion injury and ignition of ROS production under these conditions is mediated solely by reverse electron flow to Complex I (102). However, as noted in Section 1.4.2 in the Introduction, problems with this model arise when one starts to carefully consider the bioenergetics required to drive RET from succinate to Complex I to induce this massive burst in ROS production. Another important consideration is the fact that mitochondria can contain up to 12 sites for production and that the results from Chouchani *et al* completely ignore studies demonstrating that Complex II and III also serve as high capacity sites for production following IR injury (124,103,115).

In the present study, three critical observations were made that refute the claim that Complex I is the sole source of ROS during IR injury. The first stems from inhibitor studies that showed that Complex III was the highest capacity site for ROS release from cardiac mitochondria isolated from WT and NDUFS4^{+/-} mice. Using myxothiazol, which inhibits the production of semiquinone radicals in the Q_O site in the complex, it was demonstrated that Complex III accounted for ~50% of the ROS produced when succinate was the substrate. Complex I produced ~30% of the ROS when succinate was being oxidized and Complex II generated the rest (~20%). OGDH and PDH made negligible contributions to mitochondrial ROS

production. These observations fall in line with a previous study published by our group that showed that Complexes III and I were the major ROS sources in cardiac mitochondria isolated from C57Bl6N mice (111). What is also note-worthy about this observation as well is that these results were collected with mitochondria respiring under state 4 conditions (absence of ADP), which would favor the hyperpolarizing of the electrochemical potential of protons across the inner membrane. Therefore, even under conditions that favor RET from succinate to Complex I, Complex III is still the highest capacity site. The second major observation demonstrating that Complex I is not the sole source is the finding that partial ablation of the *Ndufs4* gene actually augmented ROS production from mitochondria isolated from hearts subjected to reperfusion injury. If Complex I is the sole source, then even its partial loss should at the very least have some protective effect against IR injury. However, this was not the case in this study. The final observation is associated with results collected in Figure 3.7 where it was found that the loss of NDUFS4 did not alter ROS release from mitochondria respiring under state 4 conditions. Again, if Complex I was the sole supplier of ROS in heart tissue then its partial loss should have diminished the rate of production. Moreover, we did not see any change in the rate of ROS production in the WT and the NDUFS4^{-/-} mice which shows that the NDUFS4 deficiency did not alter the O₂⁻/H₂O₂ production. Also, as per the previous research in our lab, Complex I was found to be a negligible source of ROS in the liver and Complex III was shown to be a major source of ROS in the cardiac tissue (110,111). In fact, we found that heart mitochondria actually contained higher amounts of GPX1 and TRX2, two key factors involved in the clearance of H₂O₂. Therefore, it may be that mitochondria in the myocardium of NDUFS4^{+/-} mice may initially produce more ROS which is then offset over its lifespan by the induction of electrophilic stress signaling pathways and the stabilization of NRF2, a transcription factor that induces the

expression of genes encoding antioxidant enzymes. However, no studies have shown that loss of complex I alters NRF2 expression.

One critical factor that was not measured in this study was MPTP opening following reperfusion and the timing of its opening relative to the ignition of ROS production. Chouchani *et al* found that the initial burst in ROS production occurred within a few seconds and was found to be responsible for MPTP opening and the induction of cell death and tissue damage (102). By contrast, several studies published by Dr. Andrew Halestrap's group over the past two decades consistently showed that MPTP opening occurs within seconds due to calcium overloading (115,149,150,151,152). The burst in ROS release and subsequent myocardial damage occurs 30 seconds to 1 minute after opening (115). Intriguingly, cyclosporin A can prevent the immediate opening of the MPTP after reperfusion (136,138). Likewise, ROS production blockers and mitochondria-targeted antioxidants or ischemic precondition, which bolsters endogenous antioxidant defenses, have been found to protect from damage (137). Taken together, although we did not measure the timing for ROS release and MPTP opening following reperfusion, it is clear that both ROS from mitochondria and MPTP are involved in myocardial damage.

4.3 Can Complex I protect from ischemia-reperfusion injury?

In the present study, it was found that the partial deletion of the *Ndufs4* gene sensitizes the myocardium towards reperfusion injury. This was associated with poor contractile recovery following a bout of stop-flow ischemia, which correlated strongly with a significant increase in ROS production (109). These results are in line with another study that found that the complete ablation of *Ndufs4* accelerates the induction of heart disease in mice (125). In addition, selective loss of Complex I due to NDUF54 deficiency was also found to induce severe hypertrophic cardiomyopathy (102). Collectively, this would suggest that fully functional Complex I can

protect the myocardium from heart disease. Indeed, loss of Complex I function is associated with the development of a number of disorders, including Leigh's syndrome, which is associated with defects in the expression of *NDUFS4* (105). In fact, Leigh's syndrome is characterized by the over production of mitochondrial ROS and oxidative distress (105). In this thesis, it was found that even a ~50% decrease in Complex I can significantly increase the sensitivity of the myocardium towards heart damage. Although speculative, this could be due to the re-distribution of electrons in the respiratory chain, prompting increased ROS release from more potent sites of production like Complex III. Indeed, it has been found that inhibitors for ROS production by Complex III, like myxothiazol and stigmatellin, can be protective against reperfusion injury (124).

Temporary inhibition of Complex I followed by the full recovery of its activity has been found to protect heart tissue and other organs from reperfusion injury. Indeed, Complex I adopts a fully deactivated "D" confirmation for up to 12 minutes after reperfusion (132). Complex I deactivation can be prolonged by the modification of Cys39 in ND3 subunit of the complex. The ND3 subunit forms a critical part of the UQ binding pocket. S-nitrosylation of the ND3 subunit in the D state can prolong Complex I deactivation which can protect from damage (123). In addition, similar results have been collected with iodoacetamide and N-ethylmaleimide (133). It has even been postulated that ND3 can be S-glutathionylated to afford prolonged protection from IR injury (130). However, it should be noted that this deactivation needs to be temporary since chronic Complex I inhibition can exacerbate heart damage.

4.4 Impact of the deletion of the *Ndufs4* gene on mouse and cell physiology

The observation that the partial deletion of the *Ndufs4* gene sensitizes the myocardium to reperfusion-induced heart disease is in line with studies that found that the total ablation of

NDUFS4 accelerates heart failure and induces fatal encephalomyopathy, blindness, and lethargy (125,105). In fact, we made similar observations where mice completely lacking NDUFS4 develop alopecia, blindness, and display stunted growth and lethargy. However, linear growth rate and organ weights of mice heterozygous for the *Ndufs4* gene were similar to the WT littermates demonstrating that its partial loss does not affect overall mouse physiology, an observation that is consistent with previously published studies (109,105). Variations in the gene encoding *Ndufs4* has also been linked to the development of Leigh's syndrome in humans and has been speculated to contribute to the development of heart disease (127). Therefore, understanding the molecular and biochemical consequences of the partial loss of *Ndufs4* is crucial for delineating how defects in Complex I assembly contribute to the pathogenesis of heart diseases and neurological disorders. Karamanlidis *et al* observed that the complete ablation of the *Ndufs4* gene actually diminished mitochondrial H₂O₂ production, but only when mitochondria were metabolizing succinate (125). However, the decrease in ROS release was very small. By contrast, when pyruvate and malate served as the substrates, no difference in ROS release was recorded (125). Furthermore, no changes in H₂O₂ release from heart mitochondria were observed when antimycin A or ADP were added to reaction mixtures, experimental conditions that promote and prevent ROS production, respectively (125). Finally, there is only a very small, but significant, decrease in ROS produced by mitochondria in isolated cardiomyocytes. The findings in this thesis confirm some of the results reported by Karamanlidis *et al* since no difference in ROS release was observed in our system unless hearts were subjected to reperfusion injury (125). It should be noted, however, that we did not observe any decrease in ROS release when succinate was being oxidized. This contrasts with results reported by Karamanlidis *et al* where it was found that total ablation of *Ndufs4* leads to ~25% decrease in

ROS release (125). This discrepancy can be explained by the fact that ROS release assays in this study were conducted on mice heterozygous for NDUFS4 (109). Therefore, it is likely that we observed no differences in ROS release when succinate was the substrate simply because Complex I was still present, even though its expression was diminished by ~50%, in our system (109).

In another study, Valsecchi *et al* found that the elimination of the *Ndusf4* also does not alter ROS release in cultured mouse embryonic fibroblasts (MEF) (120). However, removal of the *Ndusf4* gene did decrease O₂ consumption in intact MEF cells, even though ROS production was unaltered (120). It should be emphasized dihydroethidine was utilized to measure ROS releases in this study (120). This is problematic for several reasons. First, dihydroethidine, although specific for O₂^{•-}, only reacts with it at a rate of $2 \times 10^7 \text{ M}^{-1}\text{s}^{-1}$, which is two orders of magnitude lower than the activity of SOD (114). Therefore, although it is specific for O₂^{•-} it is not that sensitive. Another issue with using dihydroethidine is the fact that it is a cytosolic probe and does not specifically measure ROS formed in the matrix of mitochondria (114). This is important since most of the ROS generating enzymes in the mitochondria make contact with the matrix. Finally, dihydroethidine does not measure H₂O₂, the main ROS generated by mitochondria and found throughout the cell (114). However, despite these shortcomings, the results generated with cultured cells by Valsecchi *et al* confirm, to a certain degree, the findings generated in this thesis; 1) that partial loss of NDUFS4 does not alter ROS production and 2) ROS production by cardiac mitochondria lacking NDUFS4 can increase only when the heart is subjected to a reperfusion challenge (120).

Another important observation made in this thesis was that the partial deletion of the *Ndusf4* gene increased the protein expression levels of GPX1 and TRX2, two important H₂O₂

eliminating enzymes found in the matrix of mitochondria (109). It is therefore entirely possible that the absence of a difference in ROS release from WT and *NDUFS4*^{+/-} cardiac mitochondria was due to the increased availability of H₂O₂ removing enzymes in the hearts collected from heterozygous mice. This effect is likely due to the activation of stress signaling pathways such as the NRF2 cascade which augments the expression of genes involved in the adaptation of cells towards oxidative distress. Unfortunately, the impact of the loss of *NDUFS4* on the NRF2 pathway has never been investigated. However, the results collected here would suggest that defects in Complex I assembly can trigger a stress response that allows the adaptation of cells towards increased ROS levels.

4.5 OGDH and PDH as a source of ROS in liver mitochondria

In 2004, it was shown for the first time that OGDH can produce ROS in synaptosomes (128). This finding demonstrated that Complex I and III were not the sole ROS sources in mitochondria and that other flavin-containing enzymes could serve as generators as well. A full decade later, it was established that OGDH and PDH can generate ~8x and ~4x more ROS than Complex I in muscle mitochondria (126). Similar results were collected with permeabilized muscle fibers where it was found that PDH is a major source of ROS (129). A few years later, Slade *et al* showed for the first time that OGDH can account for up to ~30% of the ROS released by liver mitochondria (110). In the same study, Complex III made up ~50% of the total production and PDH only accounted for 7-12% (110). Complex I made a negligible contribution. These observations were confirmed in a second study published by the Mailloux group, where it was demonstrated that PDH and OGDH are not only significant sources of ROS, but also important sites for regulation by redox signals (112). Overall, these findings have provided

conclusive evidence that OGDH and PDH can serve as major ROS sources in muscle and liver tissue.

In Figure 3.8 of this thesis, different inhibitors were employed to ascertain 1) the impact of partial loss of Complex I on ROS release from several major sites of production and 2) which ROS source produces the most ROS. KMV, a highly specific inhibitor for ROS release from OGDH, and CPI-613, which inhibits ROS production by PDH and OGDH and other 2-oxoacid dehydrogenases, almost completely abolished ROS production from liver mitochondria oxidizing pyruvate or 2-oxoglutarate in the presence of malate. However, to our surprise, atpenin A5 also induced a similar effect and myxothiazol lowered ROS release by ~50%. This would suggest that the major sites for production are Complex II and III and not OGDH and PDH. Atpenin A5 blocks the UQ binding site in Complex II, which is found in the SDHD subunit and donates electrons from succinate to the UQ pool. In addition, the site for ROS release in Complex II is the FAD associated with the SDHA where succinate is oxidized to form fumarate as shown in Figure 1.6. In Figure 3.8, pyruvate and 2-oxoglutarate are serving as substrates meaning that electrons are entering at the level of Complex I through NADH oxidation. Therefore, atpenin A5 is blocking ROS release from Complex II by preventing the reverse flow of electrons originating from Complex I to the FAD in the SDHA subunit. In regards to the myxothiazol effect, it is simply preventing semiquinone production during forward electron flow from the UQ pool. In addition, KMV and CPI-613 prevent ROS release from OGDH and PDH by blocking the E2 subunit which would simultaneously inhibit NADH production (112). Taken together, Complex II and III are the major sites for production in liver mitochondria isolated from 129/Sv X C57BL/6N mice. It is now crucial to emphasize that these findings are in contrast to previous publications generated in our lab (110, 126). For instance, in Slade *et al* and O'Brien *et al*, it was

shown that OGDH and PDH are major sources in liver mitochondria collected from C57Bl6N mice (110,112). It is possible that there is a strain-dependent effect on the ROS release profiles of liver mitochondria collected from C57Bl6N and 129/Sv X C57BL/6N mice. ROS release profiles differ greatly between Sprague-Dawley rat, C57Bl6N mouse, and human muscle tissue (129). To our knowledge, whether or not there is a true strain effect on which site(s) serve as major suppliers of ROS in mitochondria has never been investigated. However, based on our findings and previously published observations, it is likely that there is a strain-dependent effect in terms of which sites serve as major ROS generators in liver mitochondria. This was also demonstrated with 6N and 6J mice where it was found that 6J and 6N mice produced different amounts of ROS (153), which is similar to the observations made in our lab recently (*unpublished results*).

4.6 Reverse electron transfer from NADH to OGDH and PDH

In 2004, it was not only observed that OGDH can produce ROS by forward electron flow from 2-oxoglutarate to NAD^+ (128), but it was also found that it can also emit $\text{O}_2^{\bullet-}/\text{H}_2\text{O}_2$ by reverse transfer from NADH (119). Using purified OGDH, Starkov *et al* demonstrated that production by reverse flow depended on the ratio of NADH to NAD^+ (119). A higher NADH/ NAD^+ induced an exponential increase in ROS production. These findings led to the genesis of the hypothesis that defects in Complex I activity could potentially contribute to the development of neurological disorders through the NADH-induced production of ROS by RET to OGDH (119). Studies conducted by the Mailloux lab also demonstrated that OGDH purified from porcine heart can display a high rate for ROS release during reverse electron flow from NADH (104). The rate for ROS release was dependent on the concentration of NADH and

OGDH was a higher capacity site for production when compared to PDH (104). Furthermore, it was also found in two separate studies that protein S-glutathionylation could alter ROS release during reverse flow from NADH to PDH and OGDH (104, 112). This would indicate that reverse electron flow from NADH to PDH and OGDH is an important ROS source that can be subjected to regulation by redox signals.

The drawback associated with these studies is that purified enzymes were used to examine OGDH and PDH ROS release due to reverse electron flow. This brings into question the physiological relevance of the production of ROS by OGDH and PDH during reverse electron flow. Indeed, it is possible that defects in Complex I could prompt the accumulation of NADH leading to increased ROS production by PDH and OGDH. In addition, it was found that as little as 1 μM NADH (which is a low physiological concentration) could induce ROS production by OGDH and PDH (104). Since I had access to a mouse line deficient in Complex I, I decided to test if NADH could stimulate mitochondrial ROS release. The logic here was that total ablation of *Ndufs4* would prevent the turnover of NADH by Complex I promoting RET to OGDH and PDH in isolated mitochondria. We also decided to permeabilize mitochondria with Triton X-100 to promote NADH uptake but also hinder the establishment of a proton motive force. Indeed, the second major NADH consuming enzyme in mitochondria is transhydrogenase which uses the proton motive force to transfer the hydride from NADH to NADP^+ . Therefore, depolarizing the mitochondrial inner membrane would also inhibit transhydrogenase. Using permeabilized mitochondria, we were able to show for the first time that NADH can promote ROS release from 2-oxoacid dehydrogenases (PDH and OGDH and potentially other 2-oxoacid dehydrogenases). This was demonstrated in permeabilized liver and cardiac mitochondria isolated from *NDUFS4*^{-/-} mice. In addition, the rate for ROS release was dependent on the

concentration of NADH. Although preliminary, these findings do suggest that RET from NADH to 2-oxoacid dehydrogenases can produce ROS in mitochondria, pointing to the possibility that it may be a physiologically relevant phenomenon.

4.7 Conclusion

This thesis demonstrates that Complex I is not the sole source of ROS during ischemic reperfusion injury to cardiac tissue. According to this study, Complex III was found to be the major source while Complex I accounted for only ~30% of the ROS release. Complex II was found to be a minor source and OGDH and PDH were low capacity sites of production. In the liver tissue, Complex II and Complex III were found to be the major sources of ROS. The partial loss of Complex I did not alter ROS release from mitochondria oxidizing pyruvate, 2-oxoglutarate, or succinate, which is attributed to the increase in GPX1 and TRX2 expression. Subjecting hearts from WT and Complex I deficient mice to IR injury revealed that the partial deletion of NDUFS4 sensitized the myocardium to damage. Mice heterozygous for NDUFS4 displayed diminished recovery from ischemia, increased myocardial infarct size, and a significant increase in ROS production by isolated mitochondria following IR injury. Finally, it was found that production of ROS by 2-oxoacid dehydrogenases through reverse electron transfer from NADH may be of physiological relevance. This is based on our findings that demonstrated that liver and cardiac mitochondria displayed robust rates for ROS production in the presence of NADH and in the absence of Complex I.

4.8 Future directions

Based upon the results obtained in this thesis, following work could be done for the future:

Based upon the results obtained in this thesis, following work could be done for the future:

1. Testing if myxothiazol can impede IR injury in mouse hearts deficient in Complex I. The

observation from our present study showed Complex III to be a major source of ROS during I/R injury. Hence, it would be really interesting to see if myxothiazol which inhibits Complex III could delay IR injury..

2. Fully examining the ROS forming potential of different sites of production in heart and liver.

3. Investigating the major sources of ROS production in various strains of mice. Various strains of mice like C129 and C57B/6N showed differences in the sources of ROS as per an observation made during our experiments. Hence, comparing the sources between these mice could suggest us about the strain effects on the sources of ROS.

4. Investigating if OGDH and PDH were sources of ROS production in cell lines devoid of a functional ETC. This was done in order to know more about RET and thus, evaluating the exact amount of ROS produced from OGDH and PDH.

REFERENCE

1. Arora, K. K., Filburn, C. R., and Pedersen, P. L. (1991) Glucose phosphorylation. Site-directed mutations which impair the catalytic function of hexokinase. *J. Biol. Chem.* **266**, 5359–5362
2. Nelson, D. L., and Cox, M. M. (2013) *Lehninger Principles of Biochemistry 6th ed.*, 10.1016/j.jse.2011.03.016
3. Massa, M. L., Gagliardino, J. J., and Francini, F. (2011) Liver glucokinase: An overview on the regulatory mechanisms of its activity. *IUBMB Life.* **63**, 1–6
4. Achari, A., Marshall, S. E., Muirhead, H., Palmieri, R. H., and Noltmann, E. a (1981) Glucose-6-phosphate isomerase. *Philos. Trans. R. Soc. Lond. B. Biol. Sci.* **293**, 145– 157
5. Evans, P. R., Farrants, G. W., and Hudson, P. J. (1981) Phosphofructokinase: structure and control. *Philos. Trans. R. Soc. Lond. B. Biol. Sci.* **293**, 53–62
6. Harris, J. leuan, and M. W. (1976) 1 glyceraldehyde-3-phosphate dehydrogenase. *Enzym.* **13**, 1–49
7. Banks R, Blake C, Evans P, Haser R, and Rice D (1979) Sequence, structure and activity of phosphoglycerate kinase: a possible hinge-bending enzyme. *Nature.* **279**, 773–777
8. Jurica, M. S., Mesecar, A., Heath, P. J., Shi, W., Nowak, T., and

- Stoddard, B. L. (1998) The allosteric regulation of pyruvate kinase by fructose-1,6-bisphosphate. *Structure*. **6**, 195–210
9. Rich, P. R. (2003) The molecular machinery of Keilin's respiratory chain. *Biochem. Soc. Trans.* **31**, 1095–1105
10. Mailloux, R., Treberg, J., Protein S-glutathionylation links energy metabolism to redox signaling in mitochondria, Volume 8, August 2016, Pages 110- 118
11. Violante, S., Ijst, L., Te Brinke, H., De Almeida, I. T., Wanders, R. J. A., Ventura, F. V., and Houten, S. M. (2013) Carnitine palmitoyltransferase 2 and carnitine/acylcarnitine translocase are involved in the mitochondrial synthesis and export of acylcarnitines. *FASEB J.* **27**, 2039–2044
- 12 Ghisla, S., and Thorpe, C. (2004) Acyl-CoA dehydrogenases: A mechanistic overview. *Eur. J. Biochem.* **271**, 494–508
- 13 Agnihotri, G., and Liu, H. W. (2003) Enoyl-CoA hydratase: Reaction, mechanism, and inhibition. *Bioorganic Med. Chem.* **11**, 9–20
14. Fisher, H. F. (1985) [3] L-Glutamate dehydrogenase from bovine Liver. *Methods Enzymol.* **113**, 16–27
15. Patel, M. S., Nemeria, N. S., Furey, W., and Jordan, F. (2014) The pyruvate dehydrogenase complexes: Structure-based

- function and regulation. *J. Biol. Chem.* **289**, 16615–16623
16. Wiegand, G., and Remington, S. J. (1986) Citrate Synthase: structure, control, and mechanism. *Annu. Rev. Biophys. Biophys. Chem.* **15**, 97–117
 17. Beinert, H., Kennedy, M. C., and Stout, C. D. (1996) Aconitase as Iron–Sulfur Protein, Enzyme, and Iron-Regulatory Protein. *Chem. Rev.* **96**, 2335–2374
 18. McLain, A. L., Szweda, P. A., and Szweda, L. I. (2011) α -Ketoglutarate dehydrogenase: a mitochondrial redox sensor. *Free Radic. Res.* **45**, 29–36
 19. Zickermann, V., Kerscher, S., Zwicker, K., Tocilescu, M. A., Radermacher, M., and Brandt, U. (2009) Architecture of complex I and its implications for electron transfer and proton pumping. *Biochim. Biophys. Acta - Bioenerg.* **1787**, 574–583
 20. Dröse, S., Stepanova, A., and Galkin, A. (2016) Ischemic A/D transition of mitochondrial complex I and its role in ROS generation. *Biochim. Biophys. Acta - Bioenerg.* **1857**, 946–957
 21. Sun, F., Huo, X., Zhai, Y., Wang, A., Xu, J., Su, D., Bartlam, M., and Rao, Z. (2005) Crystal structure of mitochondrial respiratory membrane protein Complex II. *Cell.* **121**, 1043–1057
 22. Yankovskaya, V., Horsefield, R., Tornroth, S., Luna-Chavez, C., Miyoshi, H., Leger, C., Byrne, B., Cecchini, G., and Iwata, S. (2003) Architecture of succinate dehydrogenase and reactive oxygen species generation. *Science (80-.).* **299**, 700–704
 23. Cecchini, G., Schröder, I., Gunsalus, R. P., and Maklashina, E. (2002) Succinate dehydrogenase and fumarate reductase from escherichia coli. *Biochim. Biophys.*

Acta. **1553**, 140–157

24. Iwata, S. (1998) Complete structure of the 11-subunit bovine mitochondrial cytochrome bc₁ complex. *Science* . **281**, 64–71
25. Mitchell, P. (1975) The protonmotive Q cycle: a general formulation. *FEBS Lett.* **59**, 137–139
26. Balsa, E., Marco, R., Perales-Clemente, E., Szklarczyk, R., Calvo, E., Landázuri, M. O., and Enríquez, J. A. (2012) NDUFA4 is a subunit of complex IV of the mammalian electron transport chain. *Cell Metab.* **16**, 378–386
27. Yamashita, T., and Voth, G. A. (2012) Insights into the mechanism of proton transport in cytochrome c oxidase. *J. Am. Chem. Soc.* **134**, 1147–1152
28. Sazanov, L. A. (2015) A giant molecular proton pump: structure and mechanism of respiratory complex I. *Nat. Rev. Mol. Cell Biol.* **16**, 375–388
29. Mitchell, P., and Moyle, J. (1967) Chemiosmotic hypothesis of oxidative phosphorylation. *Nature.* **213**, 137–139
30. Mitchell, P. (2011) Chemiosmotic coupling in oxidative and photosynthetic phosphorylation. *Biochim. Biophys. Acta - Bioenerg.* **1807**, 1507–1538
31. Mailloux, R., Willmore, W. G. (2014) S-glutathionylation reactions in mitochondrial function and disease. *Front Cell Dev Biol.* **2**: 61-68.
32. Yoshida, M., Muneyuki, E., and Hisabori, T. (2001) ATP synthase--a marvellous rotary engine of the cell. *Nat. Rev. Mol. Cell Biol.* **2**, 669–77
33. Murphy, M. P. (2009) How mitochondria produce reactive oxygen species. *Biochem. J.* **417**, 1–13
34. Murphy, M. P. (2009) How mitochondria produce reactive oxygen species.

Biochem. J. **417**, 1–13

35. St-Pierre, J., Buckingham, J. A., Roebuck, S. J., and Brand, M. D. (2002) Topology of superoxide production from different sites in the mitochondrial electron transport chain. *J. Biol. Chem.* **277**, 44784–90
36. Staniek, K., and Nohl, H. (2000) Are mitochondria a permanent source of reactive oxygen species? *Biochim. Biophys. Acta - Bioenerg.* **1460**, 268–275
37. Bienert, G. P., and Chaumont, F. (2014) Aquaporin-facilitated transmembrane diffusion of hydrogen peroxide. *Biochim. Biophys. Acta - Gen. Subj.* **1840**, 1596–1604
38. Gardner, P. R., Raineri, I., Epstein, L. B., and White, C. W. (1995) Superoxide radical and iron modulate aconitase activity in mammalian cells. *J. Biol. Chem.* **270**, 13399–13405
39. Nulton-Persson, A. C., and Szweda, L. I. (2001) Modulation of mitochondrial function by hydrogen peroxide. *J. Biol. Chem.* **276**, 23357–23361
40. Kehrer, J. P. (2000) The Haber-Weiss reaction and mechanisms of toxicity. *Toxicology.* **149**, 43–50
41. Finkel, T. (2011) Signal transduction by reactive oxygen species. *J. Cell Biol.* **194**, 7–15
42. Helmut, S. et al. (2015) Oxidative stress: a concept in redox biology and medicine. *Redox Biol.* **4**, 180–183
43. Tormos, K. V., Anso, E., Hamanaka, R. B., Eisenbart, J., Joseph, J., Kalyanaraman, B., and Chandel, N. S. (2011) Mitochondrial complex III ROS regulate adipocyte

differentiation. *Cell Metab.* **14**, 537–544

44. Kil, I. S., Lee, S. K., Ryu, K. W., Woo, H. A., Hu, M. C., Bae, S. H., and Rhee, S. G. (2012) Feedback control of adrenal steroidogenesis via H₂O₂-dependent, reversible inactivation of peroxiredoxin III in mitochondria. *Mol. Cell.* **46**, 584–594
45. Leloup, C., Turrel-Cuzin, C., Magnan, C., Karaca, M., Castel, J., Carneiro, L., Colombani, A. L., Ktorza, A., Casteilla, L., and Pénicaud, L. (2009) Mitochondrial reactive oxygen species are obligatory signals for glucose-induced insulin secretion. *Diabetes.* **58**, 673–68
46. Slade, L., Chalker, J., Kuksal, N., Young, A., Gardiner, D., and Mailloux, R. J. (2017) Examination of the superoxide/hydrogen peroxide forming and quenching potential of mouse liver mitochondria. *Biochim. Biophys. Acta - Gen. Subj.* 10.1016/j.bbagen.2017.05.010
47. Mailloux, R. J., McBride, S. L., and Harper, M. (2013) Unearthing the secrets of mitochondrial ROS and glutathione in bioenergetics. *Trends Biochem. Sci.* **38**, 592–602
48. Fernandez-Checa, J. C., Kaplowitz, N., Garcia-Ruiz, C., and Colell, A. (1998) Mitochondrial glutathione: importance and transport. *Semin Liver Dis.* **18**, 389–401
49. Booty, L. M., King, M. S., Thangaratnarajah, C., Majd, H., James, A. M., Kunji, E. R. S., and Murphy, M. P. (2015) The mitochondrial dicarboxylate and 2-oxoglutarate carriers do not transport glutathione. *FEBS Lett.* **589**, 621–628

50. Garcia, J., Han, D., Sancheti, H., Yap, L. P., Kaplowitz, N., and Cadenas, E. (2010) Regulation of mitochondrial glutathione redox status and protein glutathionylation by respiratory substrates. *J. Biol. Chem.* **285**, 39646–39654
51. Johansson, C., Lillig, C. H., and Holmgren, A. (2004) Human mitochondrial glutaredoxin reduces S-glutathionylated proteins with high affinity accepting electrons from either glutathione or thioredoxin reductase. *J. Biol. Chem.* **279**, 7537–7543
52. Lundberg, M., Johansson, C., Chandra, J., Enoksson, M., Jacobsson, G., Ljung, J., Johansson, M., and Holmgren, A. (2001) Cloning and expression of a novel human glutaredoxin (Grx2) with mitochondrial and nuclear isoforms. *J. Biol. Chem.* **276**, 26269–26275
53. Cox, A. G., Winterbourn, C. C., and Hampton, M. B. (2010) Mitochondrial peroxiredoxin involvement in antioxidant defence and redox signalling. *Biochem. J.* **425**, 313–325
54. Trujillo, M., Clippe, A., Manta, B., Ferrer-Sueta, G., Smeets, A., Declercq, J. P., Knoop, B., and Radi, R. (2007) Pre-steady state kinetic characterization of human peroxiredoxin 5: taking advantage of Trp84 fluorescence increase upon oxidation. *Arch. Biochem. Biophys.* **467**, 95–106
55. Jastroch, M., Divakaruni, A. S., Mookerjee, S., Treberg, J. R., and Brand, M. D. (2010) Mitochondrial proton and electron leaks. *Essays Biochem.* **47**, 53–67

56. Trenker, M., Malli, R., Fertschai, I., Levak-Frank, S., and Graier, W. F. (2007) Uncoupling proteins 2 and 3 are fundamental for mitochondrial Ca²⁺ uniport. *Nat. Cell Biol.* **9**, 445–452
57. Schrauwen, P., Hoeks, J., Schaart, G., Kornips, E., Binas, B., Van De Vusse, G. J., Van Bilsen, M., Luiken, J. J., Coort, S. L., Glatz, J. F., Saris, W. H., and Hesselink, M. K. (2003) Uncoupling protein 3 as a mitochondrial fatty acid anion exporter. *FASEB J.* **17**, 2272–2274
58. Korshunov, S. S., Skulachev, V. P., and Starkov, A. A. (1997) High protonic potential actuates a mechanism of production of reactive oxygen species in mitochondria. *FEBS Lett.* **416**, 15–18
59. Mailloux, R. J., and Harper, M. (2011) Uncoupling proteins and the control of mitochondrial reactive oxygen species production. *Free Radic. Biol. Med.* **51**, 1106–1115
60. Brand, M. D., Buckingham, J. A., Esteves, T. C., Green, K., Lambert, A. J., Miwa, S., Murphy, M. P., Pakay, J. L., Talbot, D. A., and Echtay, K. S. (2004) Mitochondrial superoxide and aging: uncoupling-protein activity and superoxide production. *Biochem Soc Symp.* **71**, 203–213
61. Toime, L. J., and Brand, M. D. (2010) Uncoupling protein-3 lowers reactive oxygen species production in isolated mitochondria. *Free Radic. Biol. Med.* **49**, 606–11
62. Salvayre, A. N., Troly, M., and Upresa, C. (2017) A role for uncoupling protein-2 as a regulator of mitochondrial hydrogen peroxide generation. *FASEB Journal.* **11**,

809–815

63. Dmitry, B., Zorov, M. J., Sollott S. J., (2006) Mitochondrial ROS-induced ROS release: an update and review. **1757**, 509-517
64. Kuksal, N., Chalker, J., Mailloux, R. J., (2017) Progress in understanding the molecular oxygen paradox - function of mitochondrial reactive oxygen species in cell signaling. *Biol Chem.* **398**, 1209-1227.
65. Rehder, D. S., and Borges, C. R. (2010) Cysteine sulfenic acid as an intermediate in disulfide bond formation and nonenzymatic protein folding. *Biochemistry.* **49**, 7748– 7755
66. Jensen, K. S., Pedersen, J. T., Winther, J. R., and Teilum, K. (2014) The pKa value and accessibility of cysteine residues are key determinants for protein substrate discrimination by glutaredoxin. *Biochemistry.* **53**, 2533–2540
67. Klaus, A., Zorman, S., Berthier, A., Polge, C., Ramirez, S., Michelland, S., Sève, M., Vertommen, D., Rider, M., Lentze, N., Auerbach, D., and Schlattner, U. (2013) Glutathione S-Transferases interact with AMP-activated protein kinase: evidence for S-glutathionylation and activation in vitro. *PLoS ONE.* **8(5)**, 1-13
68. Mailloux, R. J., Skye, L., Bride, M., Harper, M. E. (2013) Unearthing the secrets of mitochondrial ROS and glutathione in bioenergetics. *Biochem Sci.* **38**, 592-602

69. Turner, J.R., (1994) Reurativity orirl Stress: Patterns of phvsiological response. *New York: Plenum Press*.**9**, 22-21.
70. A Farb, A P Burke, R Virmanl, (1992) "Anatomy and pathology of the right ventricle (including acquired tricuspid and pulmonic valve disease)," *Cardiology Clinics*.**20**, 1-21
71. B F Walker, R C Schlant et al. (1994) "Anatomy of the heart," in Hurst's the heart . *New York: McGraw-Hill, Inc*.**8**, 64.
72. McCance A., Huether, (2014) Pathophysiology: The Biologic basis, for disease in adults and children .**2**, 950.
- 73 Lee, F.A., (1992) "Hemodynamics of the right ventricle in normal and disease states," *Cardiobgy Clinics*.**10**, 59-67.
74. Jeck, N., Derst, C., Wischmeyer, E., Ott, H., Weber, S., Rudin, C., Seyberth, H. W., Daut, J., Karschin, A., and Konrad, M., (2001) Functional heterogeneity of ROMK mutations linked to hyperprostaglandin E syndrome. *Kidney Int.* **59**, 1803–1811,.
75. Jerng, H.H., Qian, Y., and Pfaffinger, P.J. (2004) Modulation of Kv4.2 channel expression and gating by dipeptidyl peptidase 10 (DPP10). *Biophys J.* **87**, 2380–2396.
76. Jiang, M., Tseng-Crank, J., and Tseng, G.N., (1997) Suppression of slow delayed rectifier current by a truncated isoform of KvLQT1 cloned from normal human heart. *J Biol Chem.* **272**, 24109–24112.
77. Jing, J., Peretz, T., Singer-Lahat, D., Chikvashvili, D., Thornhill, W. B., and Lotan,

- I. (1997) Inactivation of a voltage-dependent K channel by subunit: modulation by a phosphorylation-dependent interaction between the distal C terminus of subunit and cytoskeleton. *J Biol Chem.* **272**, 14021–14024.
78. Johns, D.C., Nuss, H.B., and Marban, E. (1997) Suppression of neuronal and cardiac transient outward currents by viral gene transfer of dominant- negative Kv4.2 constructs. *J Biol Chem.* **272**, 31598-31603.
79. Johnson, B.D. and Byerly, L., (1994) Ca⁺² channel Ca⁺²-dependent inactivation in a mammalian central neuron involves the cytoskeleton. *Pflügers Arch.* **429**, 14–21.
80. Jones, E., Roti, E. C., Wang, J., Delfosse, S. A., and Robertson, G. A. (2004) Cardiac IKr channels minimally comprise hERG 1a and 1b subunits. *J Biol Chem.* **279**, 44690–44694.
81. Jones, J.M., Meisler, M.H., and Isom, L.L., (1996) SCN2B, a voltage-gated sodium channel beta2 gene on mouse chromosome 9. *Genomics.***34**, 258–259.
82. Jones, L. P., Wei, S. K., and Yue, D. T., (1998) Mechanism of auxiliary subunit modulation of neuronal alpha1E calcium channels. *J Gen Physiol.* **112**, 125–143.
83. Jongasma, H. J. and Wilders, R., (2001) Channelopathies: Kir2.1 mutations jeopardize many cell functions. *Curr Biol.* **11**, 747–750.
84. Josephson, I. R. and Brown, A. M., (1986) Inwardly rectifying single channel and whole cell K currents in rat ventricular myocytes. *J Membr Biol.* **94**, 19–35.
85. Jouvenceau, A., Eunson, L. H., Spauschus, A., Ramesh, V., Zuberi, S. M., Kullmann, D. M., and Hanna, M. G., (2001) Human epilepsy associated with dysfunction of the brain P/Q-type calcium channel. *Lance*, **358**, 801–807.

86. Kagan, A., Yu, Z., Fishman, G. I., and McDonald, T. V., (2000) The dominant negative LQT2 mutation A561V reduces wild-type HERG expression. *J Biol Chem*, **275**, 11241–11248.
87. Kakulas, B. A., (1996) The differential diagnosis of the human dystrophinopathies and related disorders. *Curr Opin Neurol*. **9**, 380–388.
88. Kambouris, N.G., Nuss, H.B., Johns, D.C., Marban. E., Tomaselli, G., and Balsler, J. R., (2000) A revised view of cardiac sodium channel “blockade” in the long QT syndrome. *J Clin Invest*.**105**, 1133–1140.
89. Kamiya, K., Kaneda, M., Sugawara, T., Mazaki, E., Okamura, N., Montal, M., Makita, N., Tanaka, M., Fukushima, K., Fujwara, T., Inoue, Y., and Yamakawa, K. (2004) A nonsense mutation of the sodium channel gene SCN2A in a patient with intractable epilepsy and mental decline. *J Neurosci*.**24**, 2690–2698.
90. Kang, M. G. and Campbell, K. P., (2003) Subunit of voltage-activated calcium channels. *J Biol Chem*, **278**: 21315–21318.
91. Carden, D.L., (2000) Granger D.N. Pathophysiology of ischaemia-reperfusion injury. *J. Pathol*. **190**, 255–266.
- 92 Raedschelders, K., Ansley, D.M., Chen, D.D., (2012), The cellular and molecular origin of reactive oxygen species generation during myocardial ischemia and reperfusion. *Pharmacol. Ther.* **133**, 230–255.
93. Costantino, C., Corday, E., Lang, T.W., Meerbaum, S., Brasch, J., Kaplan, L., Rubins, S., Gold, H., Osher, J., (1975) Revascularization after 3 h of coronary arterial occlusion: effects on regional cardiac metabolic function and infarct size. *Am. J.*

Cardiol. **36**, 368–384.

94. Kloner, R.A., Ganote, C.E., Whalen, D.A., Jr., Jennings, R.B., (1974) Effect of a transient period of ischemia on myocardial cells. II. Fine structure during the first few minutes of reflow. *Am. J. Pathol.* **74**, 399–422.
95. Reimer, K.A., Lowe, J.E., Rasmussen, M.M., Jennings, R.B. (1977) The wavefront phenomenon of ischemic cell death. 1. Myocardial infarct size vs duration of coronary occlusion in dogs. *Circulation.* **56**, 786–794.
96. Hearse, D.J., Humphrey, S.M., Chain, E.B., (1973) Abrupt reoxygenation of the anoxic potassium-arrested perfused rat heart: a study of myocardial enzyme release. *J. Mol. Cell. Cardiol.* **5**, 395–407.
97. Gonzalez, L.M., Moeser, A.J., Blikslager, A.T., (2015) Animal models of ischemia-reperfusion-induced intestinal injury: progress and promise for translational research. *Am. J. Physiol. Gastrointest. Liver Physiol.* **308**, G63–G75.
98. Moore, R.M., (1997) Clinical relevance of intestinal reperfusion injury in horses. *J. Am. Vet. Med. Assoc.* **211**, 1362–1366
99. Sanderson, T.H., Reynolds, C.A., Kumar, R., Przyklenk, K., Huttemann, M., (2013) Molecular mechanisms of ischemia-reperfusion injury in brain: pivotal role of the mitochondrial membrane potential in reactive oxygen species generation. *Mol. Neurobiol.* **47**, 97-100.
100. Guarnieri, C., Flamigni, F., Caldarera, C.M., (1980) Role of oxygen in the cellular

damage induced by re-oxygenation of hypoxic heart. *J. Mol. Cell. Cardiol.* **12**, 797–808

101. Granger, D.N., Rutili, G., McCord, J.M., (1981) Superoxide radicals in feline intestinal ischemia. *Gastroenterology.* **81**, 22–29
102. Chouchani, E. T., Pell V. R., et al., (2014) Ischaemic accumulation of succinate controls reperfusion injury through mitochondrial ROS. **515**, 431–435
103. Brand, M.D., (2016) Mitochondrial generation of superoxide and hydrogen peroxide as the source of mitochondrial redox signaling. *Free Radical Biology and Medicine.* **100**, 14–18
104. Mailloux, R. J, Gardiner, D., O'Brien, M, (2016) 2-Oxoglutarate dehydrogenase is a more significant source of $O^2 (-\cdot)/H_2O_2$ than pyruvate dehydrogenase in cardiac and liver tissue. *Free Radical Biol.Med.* **97**:501-512.
105. Kruse, S. E. Watt, W. E. et al., (2008) Mice with mitochondrial complex I deficiency develop a fatal encephalomyopathy, *Cell Metab.* **4**:312-320
106. Kayser, E.B., Sedensky, M.M., Morgan, P. G., (2016) Region-specific defects of respiratory capacities in the *Ndufs4* (KO) mouse brain. *PLoS One.***11**, e0148219.
107. Dillon, W., Leong, Jasper, C., Komen, Chelsee, A. et al, (2012) Proteomic and metabolomic analyses of mitochondrial complex I-deficient mouse model generated by spontaneous B2 short interspersed nuclear element (SINE) insertion into NADH dehydrogenase (Ubiquinone) Fe-S protein 4 (*Ndufs4*) gene. *The Journal of Biological Chemistry*, **287**, 20652-20663.

108. Chouchani, E. T., Pell V. R., et al., (2016) Succinate metabolism: a new therapeutic target for myocardial reperfusion injury. *Cardiovascular Research*. **111**, 134–141
109. Kuksal.N., Gardiner, D., Qi, D., Mailloux, R.J.,(2018) Partial loss of complex I due to NDUFS4 deficiency augments myocardial reperfusion damage by increasing mitochondrial superoxide/hydrogen peroxide production. *Biochem Biophys Res Commun*.**498**, 214-220
110. Slade,L.,Chalker,J.,Kuksal,N.,Young,A.,Gardiner,D.,Mailloux,R.J.,(2017) Examination of the superoxide/hydrogen peroxide forming and quenching potential of mouse liver mitochondria. *Biochimica et. Biophysica Acta (BBA)* .**8**, 1960-1969
111. Chalker, J., Gardiner, D., Kuksal, N., Mailloux, R.J., (2018) Characterization of the impact of glutaredoxin-2 (GRX2) deficiency on superoxide/hydrogen peroxide release from cardiac and liver mitochondria. *Redox Biol.* **15**, 216-227
112. O'Brien, M., Chalker, J., Slade, L., Gardiner, D., Mailloux, R. J. (2017) Protein S-glutathionylation alters superoxide/hydrogen peroxide emission from pyruvate dehydrogenase complex. *Free Radic Biol Med.* **106**,302-314
- 113 Bjoem, S. et al, (2009) Optical mapping of Langendorff-perfused rat hearts, *J Vis Exp*.**30**,1138.
114. Mailloux, R. J., (2015) Teaching the fundamentals of electron transfer reactions in mitochondria and the production and detection of reactive oxygen species. *Redox Biol.* **4**,381-98

115. Andrienko, T., Pasdois P., Rossbach, A., Halestrap,A.P.,(2016) Real-time fluorescence measurements of ROS and [Ca²⁺] in ischemic/reperfused rat hearts:
detectable increases occur only after mitochondrial pore opening and are attenuated by ischemic preconditioning. *PLoS One*.**11**, 22-35
116. Andrienko, T., Pasdois P., Halestrap,A.P., (2017) The role of succinate and ROS in reperfusion injury - a critical appraisal. *J. Mol. Cell. Cardiol.* **110**, 1-14
117. David, F. S., et al. (2012) Damage to mitochondrial complex I during cardiac ischemia reperfusion injury is reduced indirectly by anti-anginal drug ranolazine, (*BBA*).**3**, 419-429
118. Lenaz, G. (2001) The mitochondrial production of reactive oxygen species: mechanisms and implications in human pathology. *IUBMB Life* .**52**, 159-164
119. Starkov, A. A., Fiskum, G., Chinopoulos, C., Lorenzo, B. J., Browne, S. E., Patel, M.S., Beal, M. F.,(2004) Mitochondrial alpha-ketoglutarate dehydrogenase complex generates reactive oxygen species. *Neurosci*.**24**, 7779-7788
120. Valsecchi, F., Grefte, S., Roestenberg, P., Joosten-Wagenaars. J., Smeitink, J.A., Willems, P.H., Koopman, W.J., (2013) Primary fibroblasts of NDUFS4(-/-) mice display increased ROS levels and aberrant mitochondrial morphology. *Mitochondrion*.**5**,436-438
121. Jagannathan. L., Cuddapah, S., Costa, M., (2016) Oxidative stress under ambient and physiological oxygen tension in tissue culture. *Curr Pharmacol Rep.* **2**, 64-72

122. Truyen, N., Paul, N. and Cecil, B., (2009) The Nrf2-antioxidant response element signaling pathway and its activation by oxidative stress*. *The Journal of Biological Chemistry*.**284**, 13291-13295.
123. Pell, V. R., Chouchani E.T., Murphy M.P., Brookes P.S., Krieg T., (2016) Moving forwards by blocking back-flow: the Yin and Yang of MI therapy. *Circ. Res.***118**, 898-906
124. Lesnefsky, E. J., Chen, Q., Tandler, B., Hoppel, C. L. (2017) Mitochondrial dysfunction and myocardial ischemia-reperfusion: implications for novel therapies. *Annu. Rev. Pharmacol. Toxicol.* **57**,535-565
125. Karamanlidis, G.et al. (2013) Mitochondrial complex I deficiency increases protein acetylation and accelerates heart failure. *Cell Metab.* **18**,239-250
126. Treberg, J.R., Quinlan, C.L., Brand, M. D. (2011) Evidence for two sites of superoxide production by mitochondrial NADH-ubiquinone oxidoreductase (complex I). *J. Biol. Chem.***286**, 27103-27110
127. Scacco, S., Petruzzella, V., Budde, S., Vergari, R. Tamborra, R. Panelli, D. van den Heuvel, L.P. Smeitink, J. PapaS., (2003) Pathological mutations of the human NDUFS4 gene of the 18-kDa (AQDQ) subunit of complex I affect the expression of the protein and the assembly and function of the complex, *J. Biol. Chem.***278**,44161-44167
128. Tretter, L., Adam-Vizi, V, (2004) Generation of reactive oxygen species in the reaction catalyzed by alpha-ketoglutarate dehydrogenase, *J Neurosci.***36**, 7771-8.

129. Fisher-Wellman, K.H., Gilliam, L.A., Lin, C.T., Cathey, B.L., Lark, D.S., Neuffer, P.D., (2013) Mitochondrial glutathione depletion reveals a novel role for the pyruvate dehydrogenase complex as a key H₂O₂-emitting source under conditions of nutrient overload., *Free Radic Biol Med.* **65**,1201-8.
130. Dröse, S., Stepanova., A., Galkin, A. (2016) Ischemic A/D transition of mitochondrial complex I and its role in ROS generation. *Biochim Biophys Acta.* **7**, 946-57.
131. Babot, M., Birch,A., Labarbuta,P. and Galkin,A., (2014) Characterisation of the active/de-active transition of mitochondrial complex I.*Biochim Biophys Acta.***7**,1083–1092.
132. Galkin, A., Abramov, A.Y., Frakich, N., Duchen, M.R., and Moncada, S. (2009). Lack of oxygen deactivates mitochondrial complex I: implications for ischemic injury? *J. Biol. Chem.***284**, 36055–36061
133. Babot M.,Birch, A., Labarbuta,P. and Galkin,A., et al.,(2014) ND3, ND1 and 39 kDa subunits are more exposed in the de-active form of bovine mitochondrial complex I, *Biochimica et Biophysica Acta (BBA) - Bioenergetics* ;**1837** :929-939
134. Bleier, L., Dröse, S. (2013) Superoxide generation by complex III: From mechanistic rationales to functional consequences mice. *Biophysica Acta (BBA).***1827**, 1300-1320
135. Lesnefsky, E.J. and Hoppel, C. L., (2003) Ischemia–reperfusion injury in the aged heart: role of mitochondria. *Archives of Biochemistry and Biophysics.* **420**, 287–297

136. Hausenloy, H D.J. and Yellon, D.M. (2013) Myocardial ischemia-reperfusion injury: a neglected therapeutic target. *J Clin Invest.***123**, 92-100
137. Wang, Y., Mendoza-Elias J.E., et al., (2012) Implication of mitochondrial cytoprotection in human islet isolation and transplantation. *Biochemistry Research International.***2012**, 1-16
138. Victor, G., Sharov, et al. (2006) Cyclosporin A attenuates mitochondrial permeability transition and improves mitochondrial respiratory function in cardiomyocytes isolated from dogs with heart failure. *J Mol Cell Cardiol.***42**, 150-158
139. Binek, A., Fernandez, J. et al. (2017) Proteomic footprint of myocardial ischemia/reperfusion injury: longitudinal study of the at risk and remote regions in the pig model. *Nature.***7**, 1-15
140. Gillot, M., et al. (2014) Oxidative stress precedes skeletal muscle mitochondrial dysfunction during experimental aortic cross-clamping but is not associated with early lung, heart, brain, liver or kidney mitochondrial impairment. *Journal of vascular surgery.***60**, 1043-1051
141. Yuan, G.J., Gong Z.J. et al. (2005) Modulation of liver oxidant-antioxidant system by ischemic preconditioning during ischemia/reperfusion injury in rats. *World Journal of Gastroenterology.***11**, 1825-1828

142. Granger, N.D. Kvietys, P.R. (2015) Reperfusion injury and reactive oxygen species: the evolution of a concept. *Redox Biol.* **6**, 524-551
143. Zhan, K.Y. Yu, P. et al. (2016) Detrimental or beneficial: the role of TRPM2 in ischemia/reperfusion injury. **37**, 4-12
144. Ho, E. Galougahi, K.K. LU C. C, Bhindi, R. Figtree, G. (2013) Biological markers of oxidative stress: applications to cardiovascular research and practice. *Redox Biology.* **1**, 483-491
145. Ayala, A. Munoz, M. Arguelles, S. (2014) Lipid peroxidation: Production, metabolism and signalling mechanisms of malondialdehyde and 4-hydroxy 2-noneal. *Oxidative Medicine and cellular longevity.* **2014**, 1-31
146. Polster, B., Nicholls, D., Shealina, G. and Roelofs, B. (2014) Use of potentiometric fluorophores in the measurement of mitochondrial reactive oxygen species. *Methods Enzymol.* **547**, 225–250.
147. Schneider, M. Sullivan, J. Wach, P. et al. (2010) Protective role of extracellular superoxide dismutase in renal ischemia/reperfusion injury. *Kidney Int.* **78**, 374–381
148. Wang, T., Tian, Y., Xu, W.X. Cui, L.H. Xiang, S.Y. Lü, S.C. (2015) Protective effects of modeled superoxide dismutase coordination compound (MSODa) against ischemia/reperfusion injury in rat skeletal muscle. *Cell Physiol Biochem.* **37**, 465-476

149. Halestrap, A.P. et al. (1999) The Mitochondrial permeability transition: its molecular mechanism and role in reperfusion injury. *Bio-chemical Society Symposia*. **66**, 181–203.
150. Halestrap, A.P., McStay, G.P., Clarke, S.J. (2002) The permeability transition pore complex: another view. *Biochimie*. **84**, 153–66.
151. Halestrap, A.P., Kerr, P.M., Javadov, S., Woodfield, K.Y. (1998) Elucidating the molecular mechanism of the permeability transition pore and its role in reperfusion injury of the heart. *Biochim Biophys Acta* .**1366**, 79–94.
152. Halestrap, A.P., Brenner, C. (2003) The adenine nucleotide translocase: a central component of the mitochondrial permeability transition pore and key player in cell death. *Curr Med Chem*. **10**, 1507–25.
153. Nickel, A.G., Hardenberg, A. et al. (2015) Reversal of mitochondrial transhydrogenase causes oxidative stress in heart failure. *Cell metabolism*. **22**, 363-365.
154. Robinson, B.H., (1998) Human complex I deficiency: clinical spectrum and involvement of oxygen free radicals in the pathogenicity of the defect. *Biochimica et Biophysica Acta*. **1364** (2): 271–86

